UCLouvain

École polytechnique de Louvain

Multi-objective optimization of an urban canopy

Author: **Léon DE SÉJOURNET**
Supervisors: **Luca SGAMBI, Maider LLAGUNO-MUNITXA**
Readers: **Pierre LATTEUR, Martin STEINMETZ**
Academic year 2022–2023
Master [120] in Civil Engineering

Multi-objective optimization of an urban canopy

Léon de Séjournet

Acknowledgement

I would like to thank my supervisors Professor Luca Sgambi for the weekly advise and follow up of the advancements of my thesis, and Professor Maider Llaguno-Munitxa for the precious advises and the help in the use of Rhino3D, Grasshopper and its plugins.

I would also like to thank Professor Pierre Latteur and Martin Steinmetz for agreeing to be readers of this master thesis.

And lastly I would like to thank my sister Alice de Séjournet, my uncle Juan van Wassenhove, and my father Antoine de Séjournet for the great help provided for the form of this thesis and the proofreading.

Contents

1 Introduction **1**

2 Urban Canopy **4**

3 Multi-objective optimization **19**
3.1 Optimization 19
3.2 Multi-Objective Optimization 21
3.2.1 Classification of multi-objective optimization algorithms . . 21
3.2.2 Evolutionary algorithms 22
3.2.3 Genetic algorithms 24
3.2.4 Applications of multi-objective optimization in engineering . 31

4 What are the different tools used **33**
4.1 Rhinoceros3D 33
4.2 Grasshopper3D 33
4.3 Karamba3D 34
4.3.1 Getting familiar 34
4.4 Ladybug Tools 45
4.5 Wallacei 49
4.5.1 IPE Beam 59
4.5.2 Rectangular beam 66

5 Optimization of an urban canopy **74**
5.1 Modelization of an urban canopy 74
5.1.1 Geometry 76
5.1.2 Cross-section 79
5.1.3 Shaded area 80
5.1.4 Stress 80
5.1.5 Genes 83
5.1.6 Fitness objectives 83
5.2 Optimization of an urban canopy 84

5.2.1 Structural analysis 84
5.2.2 Shade and population based analysis 87
5.2.3 Shade and dimension based analysis 105

6 Conclusion **120**
6.1 Encountered difficulties & further developments 122

A **i**
A.1 Structural analysis i
A.2 Shade and population based analysis vii
A.3 Shade and size based analysis xv

Chapter 1

Introduction

With urbanization, an ever increasing number of people moved to cities with the hope of a better life. The development of cities induced a change from natural areas to urban areas provoking changes in the thermal properties of the local environment. The pavements building and other surfaces increasing the quantity of heat retained compared to the surrounding rural areas. This phenomenon is called the heat island effect. This effect results in a significant increase in city temperatures inducing an increase in energy cost to cool down the cities, air pollution levels, and heat-related illnesses.[1][2]

A solution to limit the heat island effect is by providing shade to allow the shaded surfaces to retain less heat. This shade can be provided either by natural or structural elements.

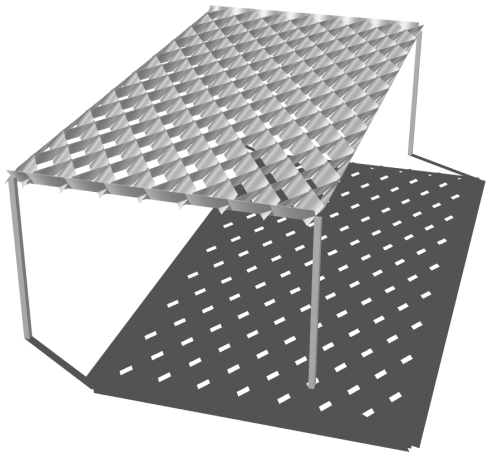


Figure 1.1: Urban canopy model

In this thesis, we will propose a structural solution to provide shade, see figure 1.1. This solution will be modeled using digital tools and multi-objective optimization with a genetic algorithm called NSGA-II. This solution is called an urban canopy.

The thesis has the following structure:

Chapter 2 is the state of the art of urban canopies, we define the term and show what as been done around the world on the subject of urban canopies.

Chapter 3 is a state of the art about multi-objective optimization. We start by defining optimization, then continue with multi-objective optimization explaining different methods and algorithms. And finally selecting the algorithm that we will use for the multi-objective optimization of our urban canopy.

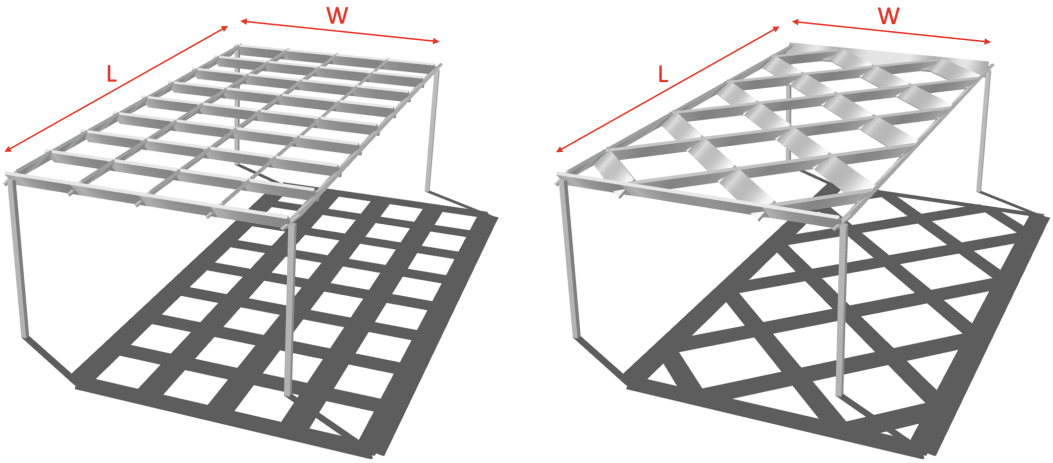
In chapter 4, we describe all the tools that are needed for the modelization and optimization of our urban canopy model. These tools are:

- Rhinoceros3D: for the interface of the modelization and visual renderings
- Grasshopper: for the parametric modelization
- Karamba3D: for the structural modelization
- Ladybug: for sun path simulations for the shade analysis
- Wallacei: for the multi-objective optimization

We also made verification in order to make sure that we use the tools properly and that they give us the correct results.

In chapter 5, we start by modeling our urban canopy see figure 1.2. We chose to model a rectangular steel canopy, its dimension can be adapted to the requirement of the environment. Its shape however is fixed but the model could be adapted to have a shape more adequate to different environment. To model our urban canopy, we start with a rectangular structure to which we add beams in the vertical and horizontal directions. These beams can either follow a rectangular pattern or a diamond pattern. We will then optimize the structure using Wallacei by modifying the beam pattern, the number of beam in the vertical and horizontal direction, the height and width of the cross-section and the angle of inclination of the beams. By modifying these parameters, we will do three optimization analysis types:

- A structural optimization analysis: we will be minimizing the mass of the canopy while respecting a deflection constraint for different canopy dimensions.



(a) Rectangular grid (b) Diamond grid

Figure 1.2: Perspective view of our canopy model

- A population based analysis for a shade optimization: we will be maximizing the shaded area of a canopy of fixed length and width while minimizing its mass and respecting a deflection constraint. We will be doing this with different population parameters in order to analyse the impact of these parameters on the simulation.
- A dimension based analysis for a shade optimization: we will be maximizing the shaded area of different canopy dimensions while minimizing their masses and respecting a deflection constraint. This will permit us to analyse the impact of the dimension of the canopy on its parameters.

Chapter 2

Urban Canopy

When we are looking for the term “urban canopy” online we discover that it covers a large range of topics. We can find a company doing thermal imaging of urban areas, another doing an urban farming, or still another one planting trees in urban areas. The list goes on with still different definitions of the urban canopy. However, there are no clear definitions on the type of urban canopies that this thesis is about.

It is therefore important to clarify what we mean by "urban canopy". The Collins dictionary describes a canopy as "a layer of something that spreads out and covers an area, for example the branches and leaves that spread out at the top of trees in a forest"[3] and describes urban as "belonging to, or relating to, a town or city"[4]. Based on those definitions and on the following examples of urban canopies, we will define an urban canopy as a structure designed to provide shade and shelter in an urban area.

Urban canopies can be made from a variety of materials, such as steel, wood, glass, or fabric, and can take on a variety of shapes and sizes depending on the specific needs and design of the space. They can be freestanding or attached to buildings, and may be used for different purposes, including providing shade for pedestrians, protecting against the elements, and creating a visual barrier or division between different areas. Urban canopies are an important feature of many modern cities, as they can help to create comfortable and attractive public spaces that are more inviting to people and can help to enhance the overall livability of the city. We can find in several cities covered streets with simple fabrics as in Granada in Spain[5](figure 2.1a), or even umbrellas as in Agueda in Portugal[6](figure 2.1b), to create shade and make the city walk more pleasant in warm weather. The use of fabric to produce shade over is however not new, it has even been around since ancient Egypt (figure 2.2).



(a) Granada's covered street - image by Peter Xu[5]



(b) Agueda's umbrella sky project - image by Adam Rifkin[6]

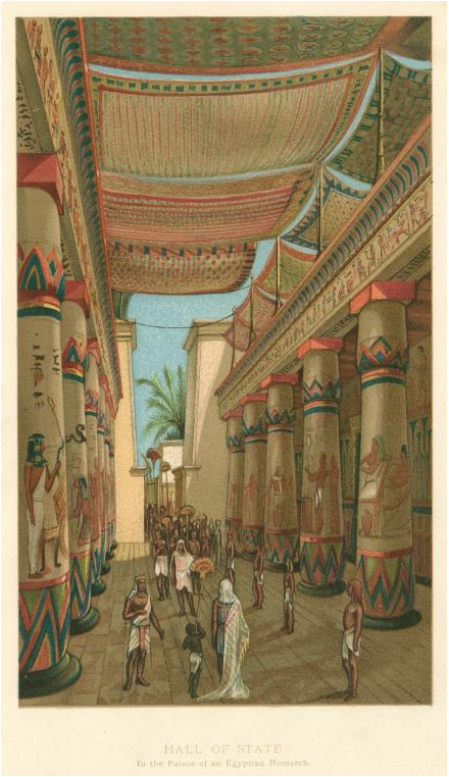


Figure 2.2: Canopy of ancient Egypt[7]

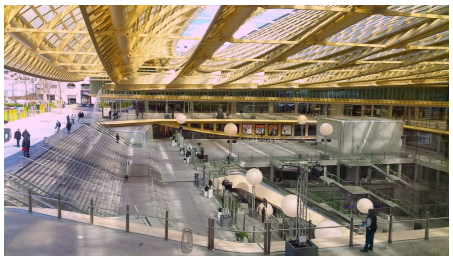
However, for this thesis, we will concentrate on more complex structures and explore different urban canopies that can be found around the world.

Canopy of "Les Halles" - Paris, France

The canopy of the "Forum des Halles"[8][9][10][11] (figure 2.3) in Paris was designed by the architects Patrick Berger and Jacques Anziutti. The canopy is a 17 metres high and 2,5 hectares undulating glass roof inaugurated on the 5th of April 2016. "Les halles", a market building build in the 1850s, was a wrought-iron and glass designed by the architect Victor Baltard but was destroyed in the 1970s and replaced by an underground shopping centre. It was nicknamed "the hole of les Halles" and has been a national embarrassment ever since. The canopy was therefore constructed to recall some of the spirit of Baltard's market. The canopy with its 18,000 glass shingles held in the air by 7000 tonnes of steel and a cost of over €200m was said to be one of the most ambitious architectural projects of the decade. The canopy is now stretched above a station that serves 750,000 passengers daily, the second most visited shopping mall of Paris with 42 million visitors in 2018, gardens, a library, and a music and arts conservatory.



(a)



(b)



(c)

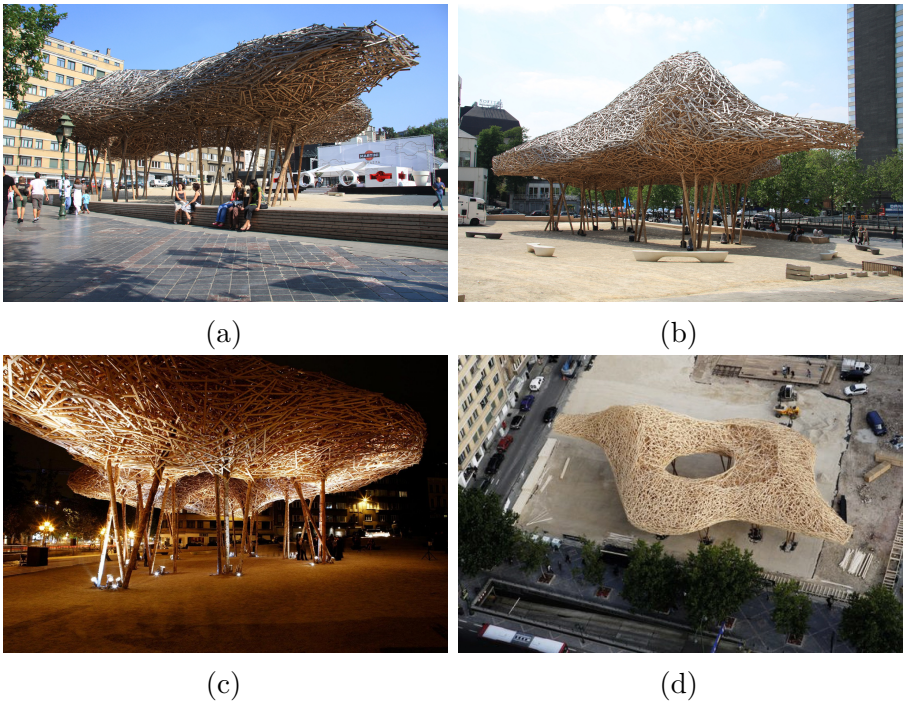


(d)

Figure 2.3: The canopy - images by Sergio Grazia[11]

Cityscape - Brussels, Belgium

Cityscape[12][13](figure 2.4) was a wooden sculpture designed by Arne Quinze in Brussels. It was planned to be displayed from September 2007 to September 2009 to bring life to the Louisa neighbourhood but stayed up a bit longer thanks to its success. The artwork was an 18 metres high structure supported on 12 metres high posts and was 65 metres long and 25 metres wide. After the demolition, 'Cityscape' literally and figuratively left a feeling of emptiness in the neighbourhood.



(a) (b)

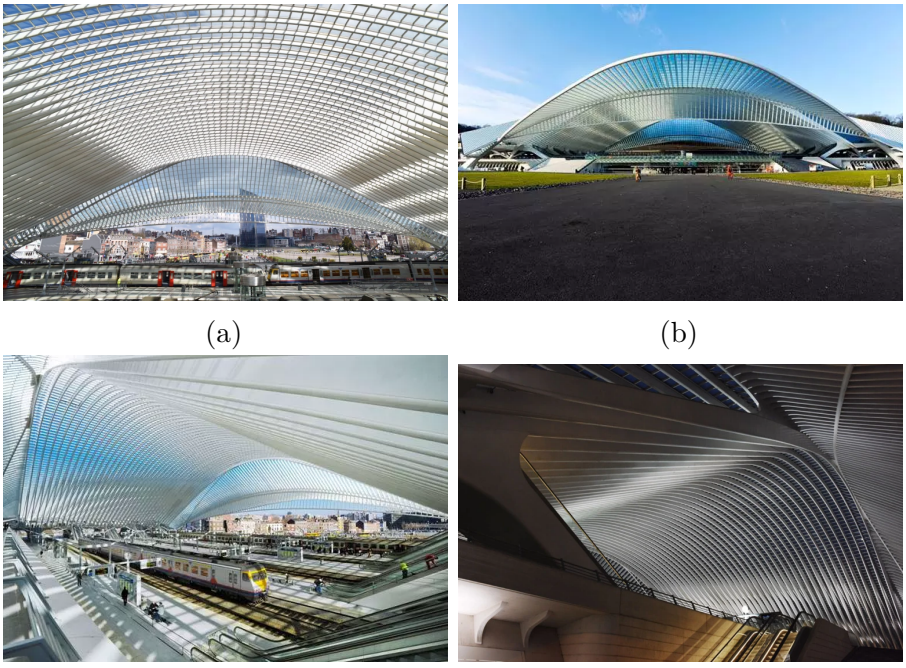
(c) (d)

Figure 2.4: Cityscape[12]

Guillemins station - Liège, Belgium

The Guillemins station[14][15](figure 2.5) in Liège was designed by the architect Santiago Calatrava. He won the commission to design the new Guillemins station after Eurogare issued a request for design proposals from architects all over Europe to replace the former station due to increasing demands for the high-speed rail travel. The station was conceived as a link between two areas of the city of Liège. The dome is composed of 32,200 m^2 of glass and 39 arcs going up to 40 metres above ground level. The vault above the station is 200 metres long, 73 metres wide and has a surface of 29,000 m^2. The structure is composed of 10,000 tonnes of steel

and required 67,000 m^3 of concrete to hold the structure. The construction lasted from 2001 to 2009 and was mainly achieved by Franki Foundations and Wust.



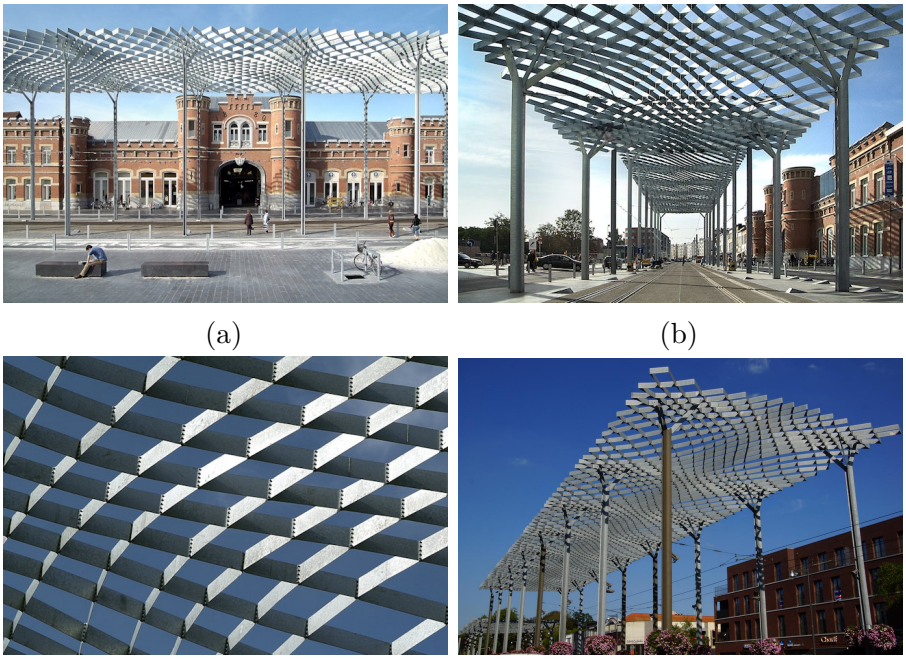
(a) (b)

(c) (d)

Figure 2.5: Guillemins station - images by fredlarebiere (a,b,d)[16] and (c)[15]

Kiel Canopy - Antwerp, Belgium

The Kiel Canopy[17](figure 2.6) was designed by B-architecten to provide a landmark for commercial plaza in Antwerp. The structure is a 12 metres high 92 by 13 metres grid composed of continuous steel strips of 6mm by 250mm. The grid's geometry was structurally optimized with variation in the grid's density instead of variations in the grid's height. The same structural principle has been used on smaller canopies providing glazed shelters. The engineering designs were done by Ney & Partners in 2004 for the construction in 2005. The cost of the project was of €1M.



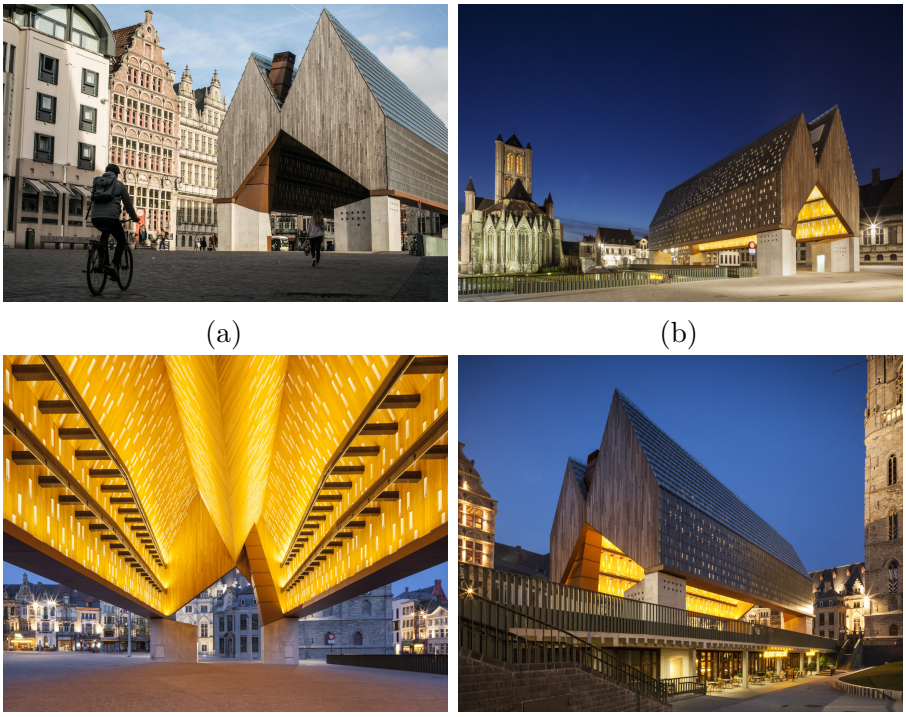
(a) (b)

(c) (d)

Figure 2.6: Kiel canopy - images by Filip Dujardin (a,b,c)[18] and Nicolas Janberg (d)[19]

Market Hall - Ghent, Belgium

The Market Hall[20][21][22][23](figure 2.7) designed in 2012 by Robbrecht & Daem and Marie-José Van Hee is a concrete and timber structure, with gabled forms inspired by a nearby town hall, that provides shelter in the center of the city of Ghent. The Market Hall is 40 metres long and opened on all sides. It is composed of four concrete feet on the four corners that support an asymmetric roof made out of timber protected by glass squares. The glass squares reflects the light giving a chameleon-like appearance to the Hall with constant changing colors. The roofs has hundreds of rectangular slits lighting the interior by day and shining out by night when the hall is internally lit. With the concrete piers containing a great fireplace and a lift to the level below, they give great support for the various events, such as concerts, dance performances, and markets.



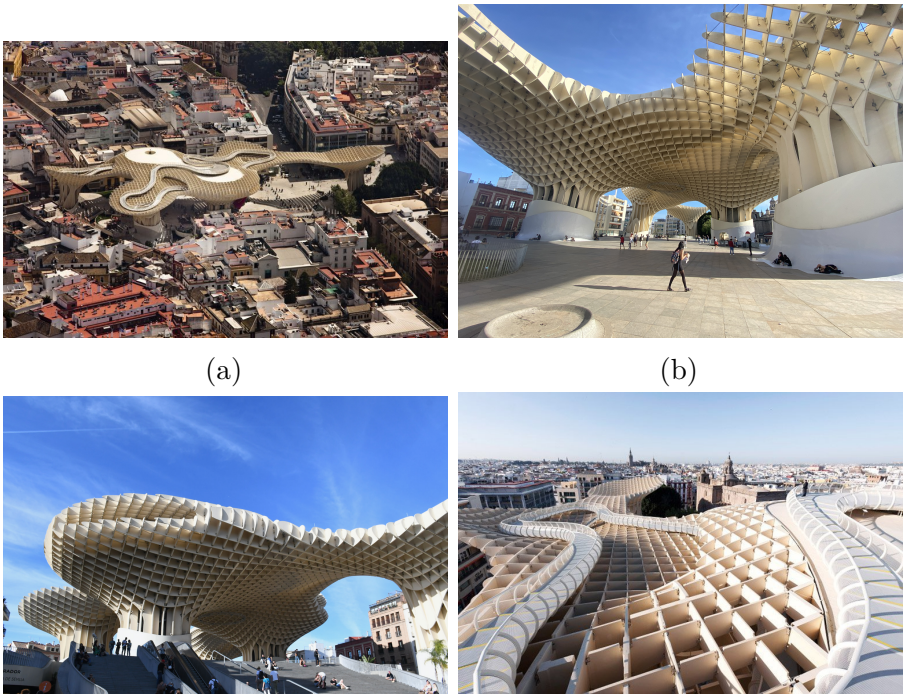
(a) (b)

(c) (d)

Figure 2.7: Market Hall - images by Dienst Toerisme (a)[20], Tim Van de Velde(b,d)[23], and Hufton + Crow (c)[22]

Metropol Parasol - Seville, Spain

The Metropol Parasol[24][25][26](figure 2.8) locally known as "las setas de la Encarnación" was designed in 2004 by the architect Jürgen Mayer H with the help of the engineers from Arup. Its construction finished in April 2011 to fill after 30 years the void left by the destruction of the Mercado de la Encarnación in Seville. The Metropol Parasol is a 30 metres high mushroom/waffle-like structure made out of laminated timber, steel, concrete and glue. It is one of the largest timber structure in the world, and the largest structure held together by glue. The idea of the Parasol was to provide shade and make the square more habitable. The columns supporting the roof could only come from a few places due to Roman ruins underneath the square. From those constraints came the trunk-like uprights that contain lifts, stairs, and the structural system. The Parasol contains a market, multiple shops, a podium for concert and events, the ruins of a Roman district in its basement, and on its roof a restaurant, a viewing gallery and an undulating walkway.



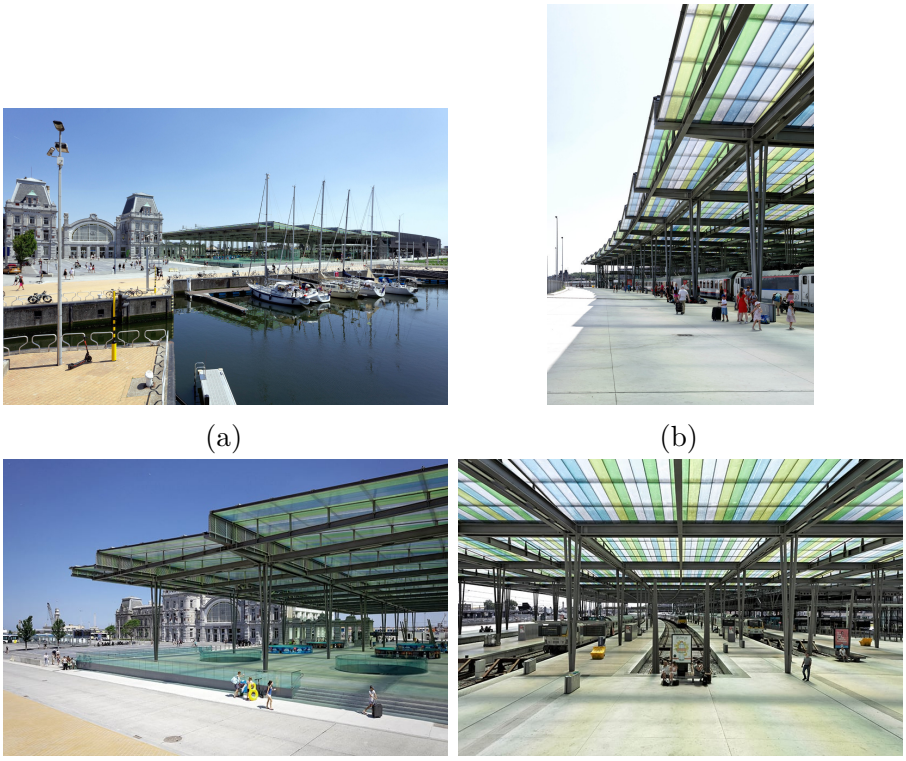
(a) (b)

(c) (d)

Figure 2.8: Metropol Parasol - images by Fernando Alda (a)[26], Léon de Séjournet (b,c), and David Franck (d)[26]

Oostende station - Ostend, Belgium

The roof canopy of Ostend railway station[27][28](figure 2.9) was designed by Diermar Feichtinger Architectes for a competition in 2006 for proposals to overhaul the station. The canopy is a giant roof that is both light and transparent. Its goal is not only to shelter, but also to help the travelers to navigate intuitively through the station. The station is getting more and more passengers over the years with an increased number of buildings and parking, there was a need to unify the site and its train, tram, bus and boat connections. The canopy is a 22,000m^2 roof composed of polycarbonate panels on a supporting steel structure. The panels are colored to give variation of light under the roof depending on the exterior brightness, it also provides sun protection and avoids direct glares. The structure offers an unobstructed view of the adjacent marina with different functions and installations that are integrated under the roof with stairs, elevators, a footbridge, billboards, and electrical installations suspended from it. The renovation of the station took place from 2007 to 2019 for a total cost of €37M.



(a) (b)

(c) (d)

Figure 2.9: Oostende station - images by David Boureau[28]

Perdana Canopy - Kuala Lumpur, Malaysia

The Perdana Canopy[29][30](figure 2.10) was designed by GDP Architects in 2014 and is located in the Perdana Botanical Garden of Kuala Lumpur. It was inspired by the surrounding context of lake and greeneries with its fluidity and organic nature. The canopy is composed of 2,490 panels randomly alternating between perforated aluminium, solid aluminium, clear laminated glass and fritted clear laminated glass giving sufficient light and creating beautiful shadows. The structure has for objective to provide shelter by mimicking lush tall trees while acting has a landmark. The goal was also to adopt camouflage quality by replicating trees so that the canopy do not overshadow the natural reserve around it. The space can be used to host various events and can accommodate large crowds. It is Malaysia's first single layered monocoque system structure.



(a) (b)

(c) (d)

Figure 2.10: Perdana Canopy- images by (a)[29] and Ryan Chin (b,c,d)[31]

Solar Trees Marketplace - Shanghai, China

The Solar Trees Marketplace[32](figure 2.11) designed by Koichi Takada and completed in 2022 was inspired by the rich landscape and forests of Shanghai. The development was completed in 2022 and is situated in the Minhang district, 20kms south-west of Shanghai on the One Tian An Place Residential Masterplan. It is composed of thirty-two architectural trees that rise from the ground to create a canopy of timber and branches sheltering a 3,450 m^2 modular marketplace. The forest concept makes a reference to China's commitment to be Carbon Neutral by 2060. The Solar Trees therefore considered environmental and sustainable design initiatives. Solar panels placed on translucent canopies will generate power and the timber branches and leaves of the man made trees will provide shade and shelter on the footpath, while allowing light and fresh air on the marketplace. The marketplace will become an extension of the natural landscape. Koichi Takada said: "We want to humanise buildings in the district, to be more engaging to the public and contribute to the regeneration of communities and their neighbourhoods. We want architecture to celebrate cultural identity, along with encouraging pedestrian

activities and a more walkable and livable city"[32].



(a) (b)

(c) (d)

Figure 2.11: Solar Trees Marketplace - images by ZY Photography[32]

Theaterplein - Antwerp, Belgium

The Theater Square[33][34](figure 2.12) in Antwerp was designed in 2004 Bernardo Secchi and Paola Vigano and separated into four major spaces: the garden in the south, a covered square in the north, the mall in the west along the Oudewaart square, and an equipped space in the east along the Meis street. The covered part has for role to create a relation and shared proportions between the public space and the theatre. A permeable roof is supported by slim steel columns and allows

the light of day and rain to go through it. Stairs surround the canopy allowing access to the different levels of the of the theater. This covered space is used weekly for a market.



(a) (b)

(c) (d)

Figure 2.12: Theaterplein - images by Teresa Cos[34]

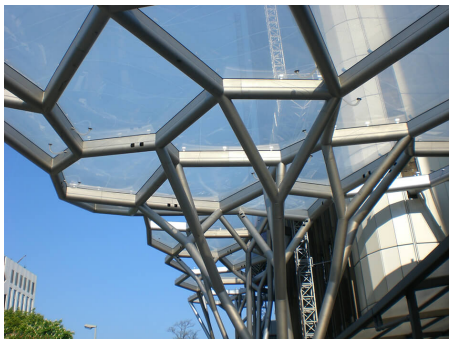
Tree-Structure Canopy - Frankfurt, Germany

The Tree-Structure Canopy[35][36][37](figure 2.13) has been designed by Just Burgeff architeckten and a3lab to protect the entrance and departure area of the WestendGate, one of the most iconic towers of Frankfurt. In addition of providing performance needs such as weather protection, it was required for the canopy to contribute significantly to the building's visual impact at the human scale. The structure covers an area of 1,200 m^2 and has an height between 8 and 14 meters. Due to different design parameters, such as the fact that the Tree-Structure's columns had to be positioned above the columns of the underground parking, or that the office facilities in the tower had to continue during the construction phase. It was therefore decided to use a prefabricated structure which would allow fast and welding-free assembly on site. Before arriving to the final design, several sets of different, planar mesh structures and structural principles were examined based on their performance, cost and design quality. The supporting structure consists

of steel pipes of same diameters, but with three different wall thicknesses. The pipes were welded together in several assembly units and then bolted on site. The hive-like roof surfaces were then fitted with transparent pneumatic ETFE plastic cushions of different shapes. The project was completed in early 2011.



(a)



(b)



(c)

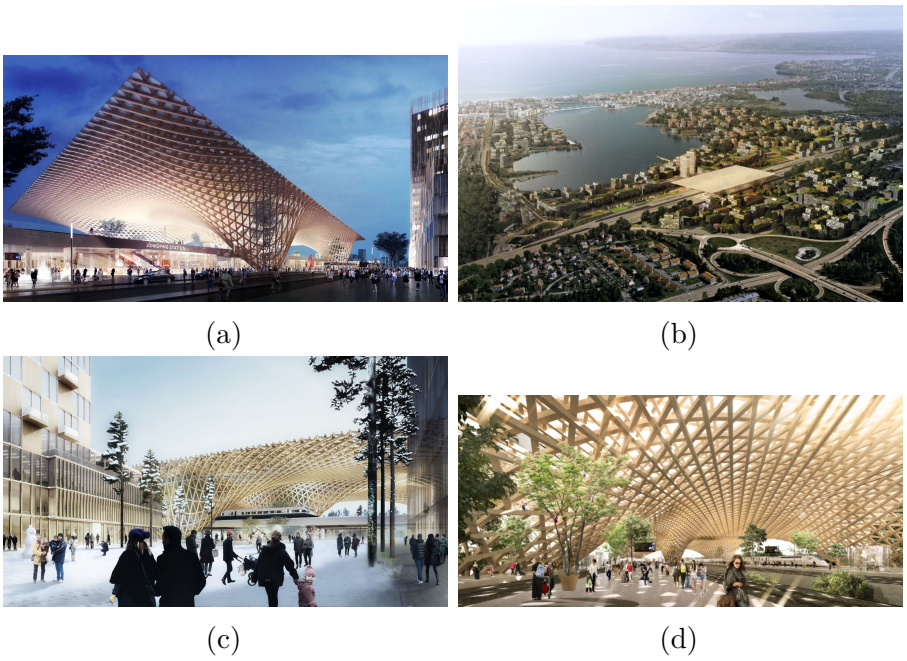


(d)

Figure 2.13: Tree-Structure Canopy - images by Eibe Sönnecken (a,c)[36] and (b,d)[37]

Wooden Canopy - Jönköping, Sweden

The Wooden Canopy[38][39](figure 2.14) designed in 2016 by Erik Giudice Architecture for the station of Jönköping has the philosophy to connect the city with its surrounding nature. The matchstick like structure was done to pay homage to the city's past as the matchstick capital of Sweden. With the use of wood and polycarbonate panels, the structure provides shade, sunlight, natural ventilation, and protection against the elements on a surface of 10,000 m^2. The polycarbonate covering can be integrated with solar panels for the station to generate its own energy and the rainwater can be harvested and reused for the planted area. As a part of the station, the canopy would also shelter shops, cafes, and restaurants.



(a) (b)

(c) (d)

Figure 2.14: Wooden Canopy - image by Erik Giudice Architecture[39]

Urban canopies aims to:

- provide shelter against the elements (rain, hail storms,...)
- combat the heat island effect by providing shade
- improve the quality of life of the users
- bringing people together

- create landmarks
- unify public areas
- develop urban infrastructures and their aesthetics

However, they also have constraints that are to:

- optimize the financial budget and the cost-benefit ratio for the initial investment, manage the maintenance along the time,
- ensure the structural stability
- optimize the limitations on available space,
- ensure the safety of the structure
- comply with the regulatory requirements

Certain canopies can have multiple or all of these goals and constraints combined. In order to solve all of these objectives at once, multi-objective optimization should be used.

Chapter 3

Multi-objective optimization

3.1 Optimization

Optimization[40][41] is the art of modeling in order to obtain the best results under specific circumstances. It is a procedure that finds and compares feasible solutions until no better solution can be found. Solutions are termed good or bad in terms of an objective, which can be the cost of fabrication, the efficiency of a process, the reliability or other factors. A part of the research and applications consider a single objective of optimization, however, most of real-world problems involve more than one objective. When an optimization problem modeling a physical system uses only one objective function, the task of finding the optimal solution is called single-objective optimization. When it involves more than one objective function, the task of finding the optimal solution is called multi-objective optimization. Different methods can be used for optimization[40]:

- Optimization algorithms: they terminate after a finite number of steps.
- Iterative methods: they are used to solve nonlinear programming problems and differ depending on whether they are evaluating gradients, Hessians, or function values. They converge towards a solution.
- Heuristics and metaheuristics: heuristic states to find or discover by trial and errors. It does not guarantee to find optimal solutions but it permits to find good solutions in a realistic period of time for a challenging optimization problem

For this thesis, we will use the metaheuristics which can find successful solutions with less computational effort than the other optimization methods.[40]

Classification of single objective metaheuristic algorithms

Metaheuristic processes are categorized based on their way of functioning. These algorithms are based on inspirational behaviours which means that they take inspiration from behaviours happening in nature. The classification is the following:[40]

- Local and Global Search: this first approach characterizes the search strategy type. An improved simple local search algorithm is one type of search strategy. A well known local search algorithm is the method of ascending the hill, which is used to find optimal locations. The global metaheuristic searches not based on local searches are typically population-based metaheuristic.
- Single Solution Approach and Population-Based Algorithm: the single solution approach concentrates on improving and optimizing individual candidate results. It involves iterated local search, simulated annealing, directed local search, and variable neighborhood search. However, single solution-based algorithms fail to get global optimum solutions. Therefore, the population-based algorithms have earned a large interest in the field of optimization. Population based algorithm can be categorized into the following classes:
  - Swarm based optimization: imitate the intelligent behaviours of several species like ant colonies, bird flocking or fish schooling.
  - Evolutionary algorithms: based on the biological development of species in the form of reproduction, genetic mutation, and natural selection. These algorithms are mainly used for numerical optimization methods. This algorithm type will be described more in depth further in this chapter.
  - Physics-based optimization: based on laws and theories of physics.
  - Ecology based optimization: based on the interactions among different species of the natural ecosystem. They can be both inter-species and intra-species interactions. These algorithms are mainly used to solve modern engineering and computer science problems.
- Hybridization of Algorithms and Memetic Algorithms: the hybrid approach blends a metaheuristic method with additional forms of optimization.
- Parallel Metaheuristic Approaches: these approaches are unique. They use identical programming procedures to perform multiple similar metaheuristic searches. These searches range from unique scattered schemes to simultaneous exploration search that interacts to boost global results.

3.2 Multi-Objective Optimization

In multi-objective optimization[42][43][40], we usually have objectives conflicting with each other, which prevent simultaneous optimization of these objectives. There are two general approaches to multi-objective optimization using four methods. These methods are the Priori method, the No Preference method, the A Posteriori method, and the Interactive method. They are described in the next subsection. The first approach also called scalarizing approach, is to combine the different objective functions into a single composite function or set all but one objective function as constraints. The determination of a single objective can be done by methods such as utility theory, weighted sum method, etc... However it is complicated to select the proper weights or utility functions to characterize the decision maker's preferences. Small perturbations in the selection of the weight can lead to very different results. If we want to set the objective functions as constraint, a constraining value must be established for each of the former objectives. In both cases, the optimization method will give one single solution rather than a multitude of solutions that can be examined. For this reason, decision makers often prefer to have a set of good solutions with multiple objectives.

The second approach is to determine a set of Pareto optimal solutions also called Pareto front. A Pareto front is a set of solutions that are non-dominated over one another. In the different solutions, there is always one objective that is better off for the worsening of an other. Pareto optimal solution sets are often preferred over single solutions so that the choice for the final solution go to the decision maker.

3.2.1 Classification of multi-objective optimization algorithms

There are often multiple Pareto solutions for Multi-objective Optimization Problems (MOPs), the traditional single-objective problem is therefore not suited for these situations. That's the reason we use the following methods:[40]

- Priori Method: requires that sufficient knowledge about the expectation is stated before the solution process
- Scalarizing: is a MOP with priori process expressed as a single-objective optimization problem, where ideal solutions for the single-objective problem are Pareto solutions for the MOP.
- No Preference Method: are methods where there are no preferential knowledge over the decisions.

- A Posteriori Method: aims to generate all Pareto optimal solutions or a representative subset. Most posteriori methods are based on the two following classes: posteriori-based mathematical programming methods and evolutionary algorithms.
- Interactive Method: is an iterative process where the decision maker continually communicates with the system while looking for the desired solutions.

For this thesis we will use the evolutionary algorithms of the a posteriori method because we want to find a multitude of Pareto solutions for our model. Moreover, our optimization is of a numerical state and evolutionary algorithm are mainly used for numerical optimization[40].

3.2.2 Evolutionary algorithms

Evolutionary algorithms(EAs)[44][45][46] are algorithms based on biological mechanism such as mutations and crossovers. Mutation is a genetic operator to maintain genetic diversity in a population. A crossover is the genetic operator used to combine genetic information of two parents to produce an offspring. They have become popular for these three main reasons: EAs do not require derivative information, EAs are relatively simple to implement and EAs are flexible and have a wide spread applicability. EAs mimic nature's evolutionary principle to find an optimal solution and use a population of solutions for each iteration. The outcome is therefore also a population of solutions. If the EA has only one optimum solution, the outcome of the population members will converge toward that optimum solution. However, if the optimization problem has multiple optimal solutions, an EA will be able to have multiple optimal solutions in its final population. Moreover, this ability of an EA to find multiple Pareto solutions in one run makes it ideal for MOPs. In the EAs domain, we can find genetic algorithms (GAs), genetic programming (GP), differential evolutions (DEs), evolution strategies (ESs), and evolutionary programming (EP). They all have many different varieties and are used in many different applications.[47] A general loop for EAs can be seen on figure 3.1[48]

Genetic algorithm

GA[41][40] was developed by Holland in the 1970s and its optimization process is inspired by natural selection and genetics. It is relatively easy to understand and uses operators like mutation and crossover. We will continue describing GAs in a further section.

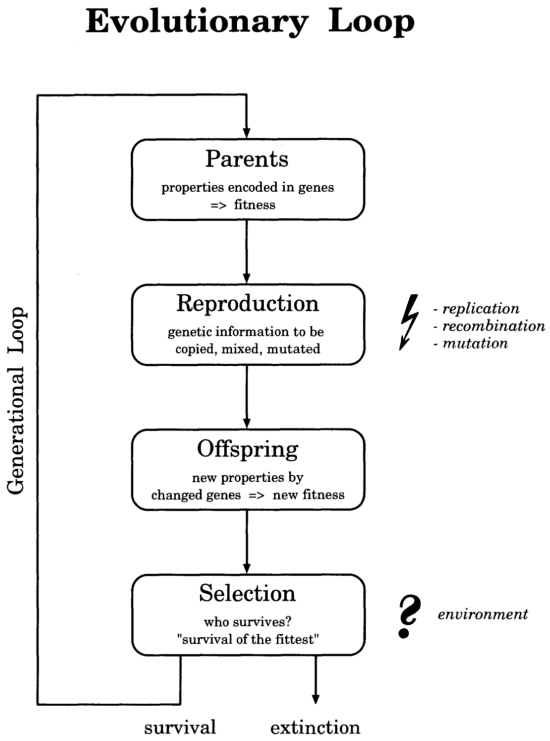


Figure 3.1: The general evolutionary algorithm[48]

Genetic programming

GP[49][40] was developed by Koza in 1988 and is a systematic method to get computers to automatically solve a problem based on a statement of what needs to be done. It is a domain-independent method that genetically breeds a population of computer programs to solve a problem. The process is illustrated in figure 3.2[49]. It uses genetic operation such as crossover and mutation. GP is an extension of GA in which structures in the population are not fixed length character strings that encode candidate solutions to a problem, but programs that, when executed are the candidate solution to the problem. These programs are expressed as syntax trees. However, it does not give direct solutions to an optimization problem.

Differential evolution algorithm

DE[50][51][40] was developed by Storn and Price in 1995 and is used for minimizing continuous space functions. It uses similar computational step as other standard EAs. However, unlike them DE perturb the current-generation population members with the scaled differences of randomly selected and distinct population members. By doing so, no separate probability distribution are needed to generate

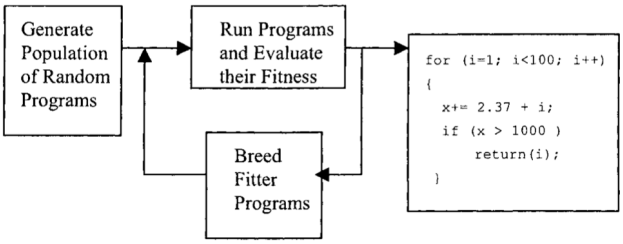


Figure 3.2: Genetic programming process[49]

the offspring population. DE has now many variants with improved performances. However, DE does not guarantee an optimal solution.

Evolution strategies

ES[48] was developed by Rechenberg in 1973. ESs differentiate them self from GAs mainly by the method of selection and and whether the sensible strategy parameters are adjusted (during the evolution) or not.

Evolutionary programming

EP[41][40] as been developed by David Fogel in 1988 following the work of his father Larry Fogel in 1962 and is a mutation-based evolutionary algorithm applied to discrete search spaces. However its methodology has no fixed structure and is therefore difficult to study.

For our optimization model, we will be using genetic algorithms.

3.2.3 Genetic algorithms

The genetic algorithm (GA)[41][42][52], created by Holland in the 1970s, is an optimization algorithm that draws inspiration from Darwin's theory of natural selection and Mendel's theory of genetics. It is a highly parallel, random and adaptive optimization algorithm which is based on "natural selection and survival of the fittest". GAs have unique solutions called chromosomes. Chromosomes are made of discrete units called genes. These genes are binary digits in earlier implementation. In later implementations more varied gene types have been introduced. Each genes control one or more features of the chromosome. In the first implementations, genes used to be binary, but there are now more varied gene types.

The GA begins by selecting a population of random chromosomes and then evolves new chromosomes by using the objective evaluation, selection, crossover, and mutation operators. For the crossover operators, we have two chromosomes called parents that are combined to form a new chromosome called offspring. By iteratively applying the crossover the genes of good chromosomes are expected to appear more frequently in the population and lead to a convergence. For the mutation operators, it introduces random changes into characteristics of chromosomes, it is generally applied at the genes level.

Crossover will make the population converge and thus making the chromosomes alike while mutation reintroduces genetic diversity into the population and help to evade local optima. The reproduction is all about selecting the right chromosomes for the next generation. The fitness of an individual will determine the probability of its survival for the next generation. The selection can be done via proportional selection, ranking or tournaments.

The procedure of a generic genetic algorithm is the following[42]:

- Step 1: Create a random parent population P_0 of size N and set $t = 0$. Evaluate the fitness of the solutions P_0
- Step 2: Crossover: Generate an offspring generation Q_t as follows:
  - Step 2.1: Choose two solutions x and y from P_t based on their fitness value
  - Step 2.2: Using the crossover operator, generate offspring and add them to Q_t
- Step 3: Mutation: Mutate each solution $x \in Q_t$ with a predefined mutation rate
- Step 4: Fitness assignment: Evaluate and assign fitness value to each solution $x \in Q_t$ based on its objective function value and infeasibility
- Step 5: Selection: Select N solutions from Q_t based on their fitness and add them to P_t
- Step 6: If the stopping criterion is satisfied, terminate the search and return the current population, else, set $t = t + 1$ and go to step 2

Multi-Objective Genetic Algorithms

A specific type of genetic algorithms are the multi-objective genetic algorithms MOGA. GAs are well suited for multi-objective optimization thanks to their population-based approach. The basic GA can be modified to find a set of non-dominated solutions. Because most MOGA do not require to prioritize, scale or weight objectives, GA is the most popular heuristic approach for multi-objective optimization problems.

The first MOGA, called vector evaluated GA (or VEGA), was proposed in 1985 by Schaffer. It was the first GA to approximate the Pareto optimal set by a set of non-dominated solutions. Afterwards, several multi-objective evolutionary algorithms were developed including:[42][52]

- Niched Pareto Genetic Algorithm (NPGA)
- Weight-based Genetic Algorithm (WBGA)
- Random Weighted Genetic Algorithm (RWGA)
- Non-dominated Sorting Genetic Algorithm (NSGA)
- Strength Pareto Evolutionary Algorithm (SPEA)
- Improved SPEA (SPEA2)
- Pareto-Archived Evolution Strategy (PAES)
- Pareto Envelope-based Selection Algorithm (PESA)
- Region-based Selection in Evolutionary Multi-objective Optimization (PESA-II)
- Non-dominated Sorting Genetic Algorithm II (NSGA-II)
- Multi-objective Evolutionary Algorithm (MEA)
- Micro-GA
- Rank-Density Based Genetic Algorithm (RDGA)
- Dynamic Multi-objective Evolutionary Algorithm (DMOEA)

For Grasshopper, see section 4.2, the modeling tool that will be used in this thesis, four plugins permits to solve multi-objective optimization problems using different algorithms. Wallacei, Octopus, Opossum and Tunna. We will only consider Wallacei and Octopus because they are the most used and best rated on food4rhino[53], a website where the different plugins for Grasshopper and Rhino3D are available. Wallacie uses NSGA-II and Octopus uses SPEA2.

The Non-dominated Sorting Genetic Algorithm II (NSGA-II) is an improved version of the Non-dominated Sorting Genetic Algorithm (NSGA). The NSGA[54] was developed by Srinivas and Deb in 1994. It differs from simple genetic algorithm just by the way the selection works. The crossover and mutation operators remain the same. The population is first ranked based on an individual's non-domination. The non-dominated individuals present in the population are first identified from the current population. It follows the flow chart that can be seen in figure 3.3. The main criticism of NSGA were that there is a high computational complexity

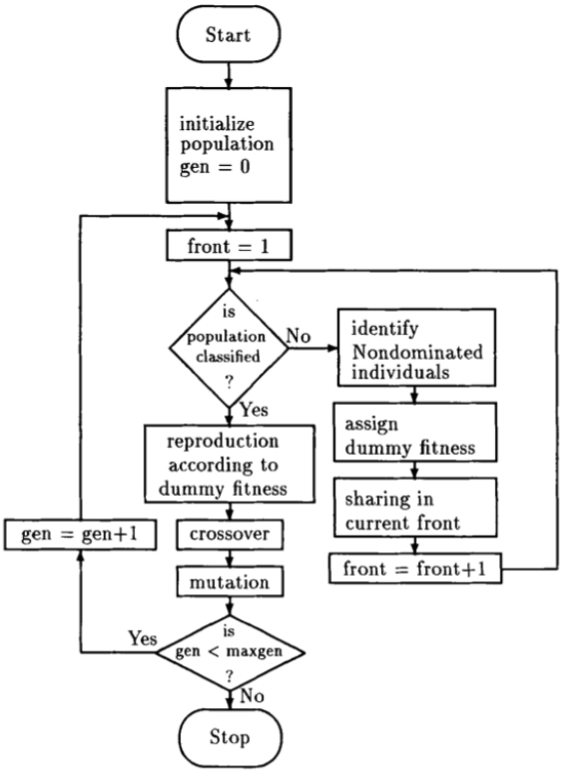


Figure 3.3: Flow chart of NSGA

of non-dominated sorting, a lack of elitism and a need to specify the sharing

parameter.

To address these issues, the NSGA-II[44] was developed in 2000 by Deb, Agrawal, Pratap, and Meyarivan. NSGA-II is one of the most popular evolutionary multi-objective algorithm and attempts to find multiple Pareto-optimal solutions in a multi-objective optimization problem. It has as the following three main features:

- The use of an elitist principle
- The use of an explicit diversity preserving mechanism
- The emphasis on non-dominated solutions

Its procedure is the following and is schematized in figure 3.4[45].

- Step 1: Create an initial random parent population P_0 of size N and set $t = 0$
- Step 2: Apply crossover and mutation operators to P_0 to create an offspring population Q_0 of size N
- Step 3: If the stopping criterion is satisfied, return Q_t
- Step 4: Combine the two populations for a new population R_t of size 2N
- Step 5: The different non-dominated front F_1, F_2, ..., F_k of R_t are identified
- Step 6: Not all fronts can be accommodated in the N slots available for the new population, we therefore do the following steps with $i = 1, ..., k$
  - Step 6.1: Calculate the crowding distance of the solutions in F_i
  - Step 6.2: Create P_{t+1} as follows
    - Case 1: If $|P_{t+1}| + |F_i| \leq N$, then set $P_{t+1} = P_{t+1} \cup F_i$
    - Case 2: If $|P_{t+1}| + |F_i| > N$, then add the least crowded $N - |P_{t+1}|$ solutions of F_i to P_{t+1}
- Step 7: Use binary tournament selection based on the crowding distance to select the parents from P_{t+1}. Apply crossover and mutation operators to P_{t+1} to create an offspring population Q_{t+1} of size N
- Step 8: Set $t = t + 1$ and go to step 3

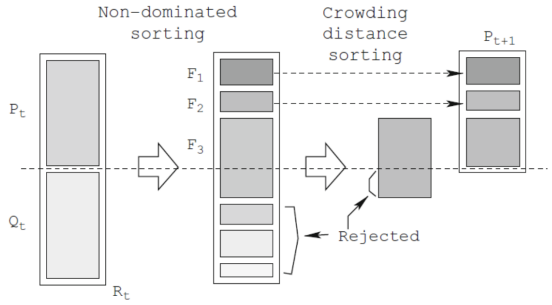


Figure 3.4: Schematic procedure for NSGA-II[45]

We know that the algorithm worked if the solutions converge toward the Pareto-optimal front. To calculate the crowding distance d_i of point i, we must measure the objective space around i which is not occupied by any other solution in the population. We can calculate d_i by estimating the perimeter of the cuboid, see figure 3.5[45], formed by using the nearest neighbors in the objective space as the vertices.

[44][45]

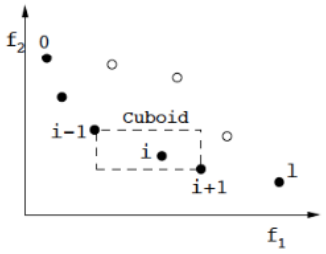


Figure 3.5: Crowding distance calculation

The Strength Pareto Evolutionary Algorithm 2 (SPEA2) is an improved version of Strength Pareto Evolutionary Algorithm (SPEA). The SPEA[55] was developed by Zitzler and Thiele in 1999. It starts with a regular initial population and an empty archive. The next steps are then performed trough iterations. All non-dominated population members are copied to the archive, all the dominated individuals or duplicates are removed. If the size of the updated archive reached its predefined limit, archive members are deleted by a clustering technique that keeps the characteristics of the non-dominated front. Fitness values are then assigned to both archives and population members. The next step is the mating selection phase. Individuals from the union of population and archive are selected by means of binary tournaments. Finally, after recombination and mutation, the old population

is replaced by the offspring population. SPEA performed well in different studies, but other studies showed its weaknesses.

Therefore SPEA2[55] was developed in 2001 by Zitzler, Laumanns and Thiele, and these were the main changes that were made:

- An improved fitness assignment scheme.
- A nearest neighbor density estimation technique is incorporated. It permits a more precise guidance of the search process.
- A new archive truncation method guarantees the preservation of boundary solutions.

The SPEA2 algorithm go as follow:[55]:

- Step 1: Initialization: Generation of an initial random population P_0 of size N and creation of the empty archive $\overline{P_0} = \emptyset$ of size $\overline{N}$. Set t=0 with a maximal number of generations T
- Step 2: Fitness assignment: Calculate the fitness values of individuals in P_t and $\overline{P}_t$
- Step 3: Environmental selection: Copy all non-dominated individuals in P_t and $\overline{P}_t$ to $\overline{P}_{t+1}$.
  - Case 1: If $|\overline{P}_{t+1}| > \overline{N}$ then reduce $\overline{P}_{t+1}$ by means of the truncation operator
  - Case 2: If $|\overline{P}_{t+1}| < \overline{N}$ then fill $\overline{P}_{t+1}$ with dominated individuals in P_t and $\overline{P}_t$
- Step 4: Termination: If $t \geq T$ or another stopping criterion is satisfied then return $\overline{P}_{t+1}$, the non-dominated individual and stop
- Step 5: Mating selection: Perform binary tournament selection with replacement on $\overline{P}_{t+1}$ in order to fill the mating pool

According to a study[55] by Zitzler, Laumanns and Thiele, it would seem that SPEA2 and NSGA-II achieve similar results for different problems and performed better than the other algorithms that where tested for the study(PESA and SPEA). In some case, NSGA-II reaches a broader spread and hence a better value of the performance measure, while SPEA2 provides a better distribution of points, especially when the number of objectives increases. However the number of objectives used for this thesis is limited. We will therefore use NSGA-II. Moreover, Wallacei is the best rated of multi-objective optimization plugins available on Grasshopper as we can see on the food4rhino website[53]

3.2.4 Applications of multi-objective optimization in engineering

Multi-objective evolutionary algorithms applications are almost unlimited. They are mainly suited for optimization, scheduling, planning, design, and management problems. These kind of problems are everywhere, engineering, finance, economics, chemistry, transportation and so forth.[56] In this section, we will show examples of engineering problems solved by evolutionary algorithms.

Yi et al. made a paper about the multi-objective optimization of a skylight roof system. As a test case, a truss system was selected for maximizing the daylight into the indoor space, maximizing the structure strength, and minimizing the system's weight, and the overall material cost. Grasshopper was used for the geometries, Ladybug was used for the daylight simulation, Karamba3d was used for structural analysis and MATLAB was used for multi-objective optimization. NSGA-II was the algorithm being used for the study. It all permitted to find several solutions that could satisfy the goals and their ranking order.[57]

Yu et al. proposed a multi-objective optimization model that could assist designers in green building design. This model uses the NSGA-II algorithm to simulate and optimize an improved back-propagation network. This permits to characterize residential buildings behaviors and predicting their energy consumption and the indoor thermal comfort. They then present a case study using the multi-objective approach for typical Chinese building design that gives a wide range of solutions for thermal comfort and energy consumption.[52]

Quagkia et al. worked on a multi-objective shape optimization methodology for the design of an origami-inspired shelter to be used as relief housing in case of disasters. The geometric parameters were used as variables to optimize the structural performances and energy efficiency. By using a Simulated Annealing algorithms for the optimization, a solution has been found and compared with existing military solutions.[58]

Van Ameijde et al. report the multi-objective optimization of the form-finding and structural optimization of a site specific shaded public seating design. It is taking in consideration the relationship between local public places to their surroundings and by achieving a low-cost and light-weight structure. Their method is applied on a small urban canopy prototype in a public housing facility in Hong Kong. The method was done using the evolutionary solvers available on the Grasshopper platform, Galapagos for the process design phase and Wallacei for

the design research and development phase. This was all part of a larger project exploring form-finding and environmental psychology.[59]

Sgambi et al. used genetic algorithms combined with a finite elements method to assess the serviceability of a long-span suspension bridge. The GA is used to find the most severe load scenarios from which the analysis focus on the maximum vertical displacement of the bridge, its maximum longitudinal and transversal slope and the maximum tension in the main cable and in the tower legs. The use of a GA permitted to support the decision process for the design of complex structure. The GA approach is suitable to make trustworthy evaluations of design parameters.[60][61][62]

Sgambi et al. used genetic algorithm and the finite element method for the optimization of precast hollow core slabs. Precast hollow core slabs are now widely used due to their versatility, their multipurpose potential and their low cost. The study focus on the structural design and optimization of their mechanical and geometric characteristics. GA is used to optimize the cross section of the slab by using five geometric features and the strand prestressing as genes and is optimized considering the total slab weight while verifying the local and global stresses.[63]

Chapter 4

What are the different tools used

We are now more familiar with multi-objective optimization and the concept of urban canopies. However, we still have to get familiar with the right tools in order to make the multi-objective optimization of an urban canopy possible. The different tools that were used for this project are Rhino3D, Grasshopper, Karamba3D, Ladybug and Wallacei. Having never used any of these programs before, the first step was to get familiar with them.

4.1 Rhinoceros3D

Rhinoceros3D[64] or Rhino3D is a 3D modeling program. It is best known to give the opportunity to model with NURBS (non-uniform rational basis spline). The complexity of a model is only limited by hardware. For my part, I used both the McOS and windows version. As for the use of Rhino in itself, I mostly used it as an interface for Grasshopper and for visual renderings.

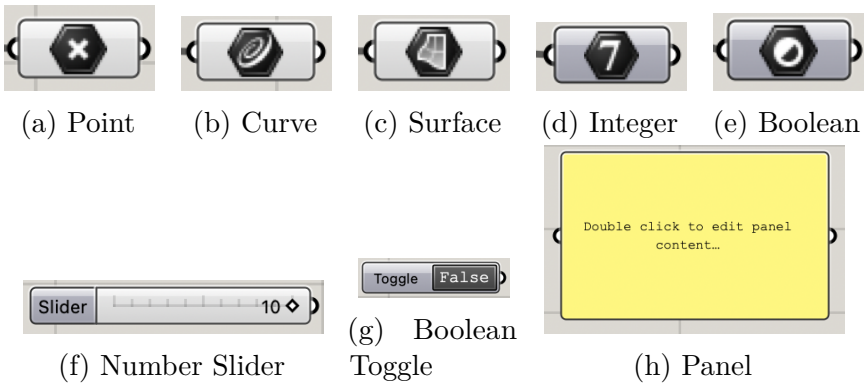
4.2 Grasshopper3D

Grasshopper3D[65] is graphical algorithm that runs as a plug-in of Rhino3D. It is greatly used for parametric modeling.
Its utilisation is quite intuitive. It rely on boxes. These boxes called components can have several inputs and outputs which are linked by different function for each of the different boxes. The output of the components are then linked trough wires to the input of the next component. Some of those boxes are parameters, see figure 4.1 and can be geometries like points, curves or surfaces, others can be integers, booleans or number sliders, boolean toggle and panels. Components like the number slider are very useful to help with parametrization. With it, we can

easily change the length of a beam, the number of beams in a structure or the intensity of a load.

For any of the inputs or outputs, we will have the possibility to add an action. These actions are the followings:

- Principal: will change the input into a principal parameter
- Reverse: will reverse the order of a list
- Flatten: will flatten all data into a single list
- Graft: will graft all data
- Simplify: will simplify the data by removing all redundant path elements
- Expression: will permit to add an expression trough an expression editor



(a) Point (b) Curve (c) Surface (d) Integer (e) Boolean

(f) Number Slider (g) Boolean Toggle (h) Panel

Figure 4.1: Parameter Components

4.3 Karamba3D

Karamba3D[66][67] is embedded into Grasshopper. It is a parametric structural engineering tool using finite elements. It is used to make static and dynamic analysis of geometries designed using Grasshopper and Rhino. It enables us to work with beam(1D) and shells (2D).

4.3.1 Getting familiar

To get familiar with Grasshopper and Karamba3D, and make sure that it gives us the right results, we must start with basic structure that we can easily calculate by hand. We will therefore start by modeling a set of simple beams.

Beam

To model a beam with Grasshopper and Karamba3D, we need to define the spatial elements and the structural elements such as the forces and the supports. For the spatial elements we must start by constructing two points using the *Construct Point* component of Grasshopper see figure 4.2.

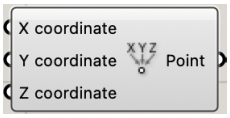


Figure 4.2: Construct Point Component

This component requires 3 inputs 1)X 2)Y 3)Z. One of the *Construct Point* component can stay on the default setup (0,0,0). We give the other *Construct Point* component a variable X value with a number slider as the X input. We then use the two points as input of the *Line* component see figure 4.3. This gives us a line with a parametric length.



Figure 4.3: Line Component

For the rest of the model, to input the structural elements, we have to use Karamba3D. For a functioning model, we need to input 1) the elements 2) the support, 3) the loads 4) the cross-section. in the *Assemble Model* component see figure 4.4.

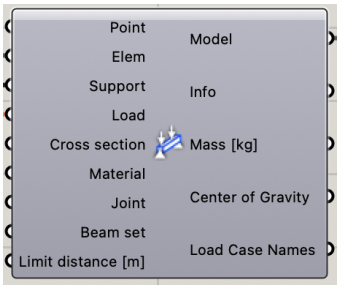


Figure 4.4: Assemble Model Component

We use the *Line to Beam* component see figure 4.5 and input the line to get an element as output. The cross-section. can also be inputted in the *Line to Beam* component. It is especially useful when we have different types of beams in a model.

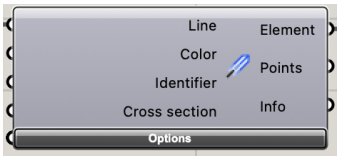
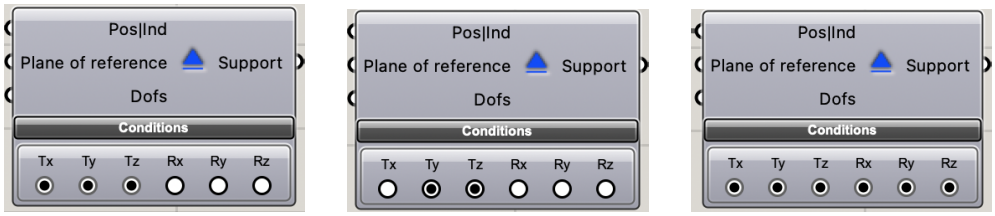


Figure 4.5: Line to Beam Component

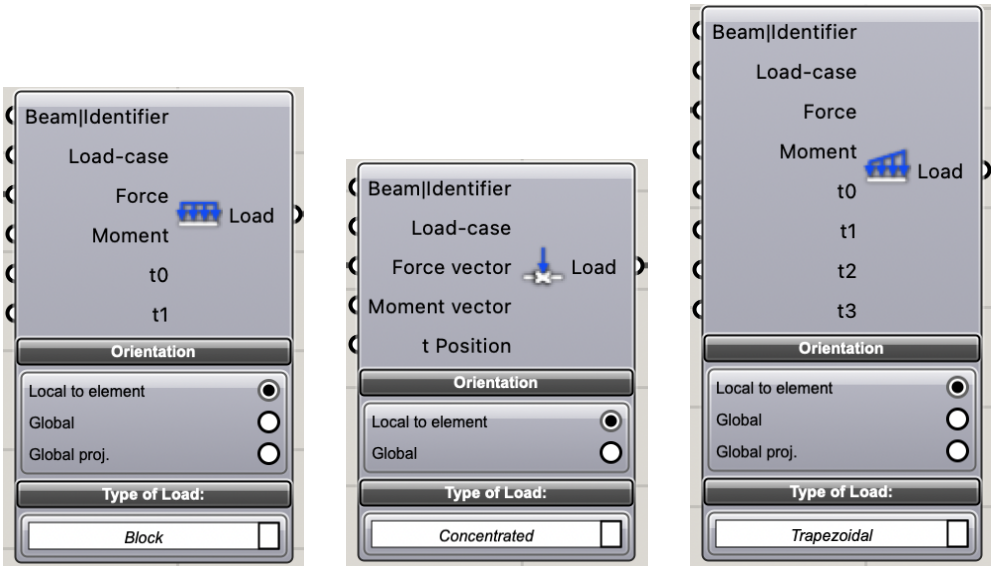
For the supports, we use the *Support* component see figure 4.6. In order to have a beam with a roller support and a pin support, we use the *Support* component twice. We use the two initial points as input, to create a support at both end of the beam. We can for the supports decide to lock or not the 6 degrees of freedom just by a simple click.



(a) Pinned Support (b) Roller Support (c) Fixed Support

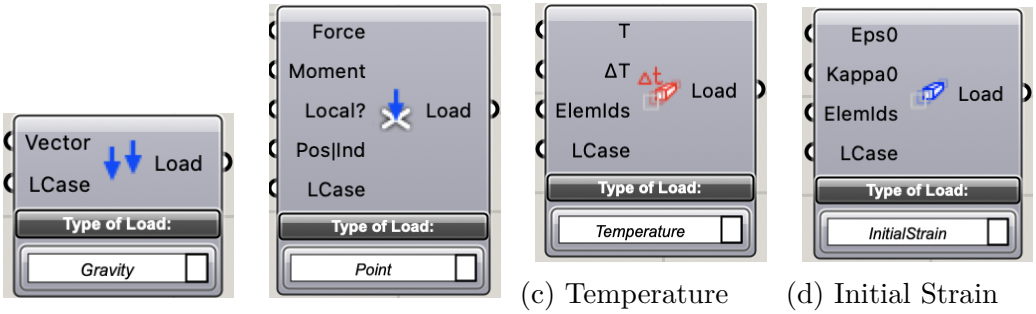
Figure 4.6: Support components

To apply the loads we use the *Beam Loads* component see figure 4.7. With it, it is easy to create punctual loads, uniform loads or even trapezoidal loads and others. There is also a *Loads* component see figure 4.8 but when using beams, it is easier to use the one dedicated to it. We will use the *Loads* component when working on surfaces or when the loads are due to gravity, temperature or an initial strain. The required inputs to apply a load on a beam are vector for the force, and the position of the load. For an uniform load, see figure 4.7a, on the default setup, the load is applied on the entire beam with $t_0 = 0$ and $t_1 = 1$. For a punctual load, see figure 4.7b, on the default setup, the load is applied on the middle of the beam. For the vector used for the force, we will use a *Unit X*, *Unit Y* or *Unit Z* component, see figure 4.9, linked with a negative or positive number slider, depending on the direction of the force, to have a parametric force. We will usually use the *Unit Z* component.



(a) Uniform Load (b) Punctual Load (c) Trapezoidal Load

Figure 4.7: Beam Loads components



(a) Gravity Loads (b) Punctual Loads (c) Temperature Loads (d) Initial Strain Loads

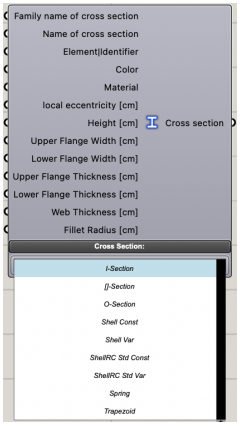
Figure 4.8: Loads components



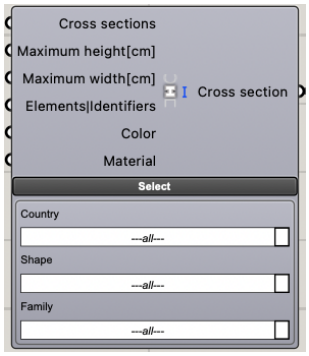
(a) Unit X Vector (b) Unit Y Vector (c) Unit Z Vectors

Figure 4.9: Unit Vectors components

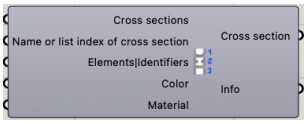
We have different ways to input a cross section. The first one is to use the *Cross Section* component, see figure 4.10a and chose the cross-section. type (eg. I section, O section, etc) and input all its characteristics. The second way is to use the *Cross Section Range Selector* and the *Cross Section Selector* components, see figures 4.10b and 4.10c.



(a) Cross Section



(b) Cross Section Range Selector



(c) Cross Section Selector

Figure 4.10: Cross Section components

We first select a country, a shape and a family of cross-sections. with the *Cross Section Range Selector*. We then, using a panel as output, determine the cross-section we would like to use. Using the *Cross Section Selector*, we input the cross-sections given by the *Cross Section Range Selector* and input the index of the cross-section we want to use.

Once we have the elements, the supports, and the loads, and cross-sections, we can input them into the *Assemble Model* component see figure 4.4. We get as output: the model, its mass, the center of gravity and the load case's names.

We then use the model as input in the *Analyse*, see figure 4.11. It gives us the calculated model, the maximum displacement, the resulting force of gravity and the elastic energy change.

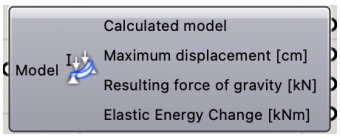
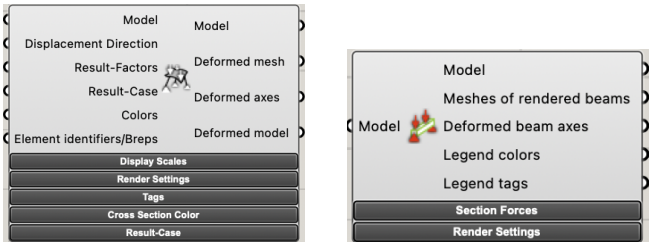


Figure 4.11: Analyse component

To be able to visualise the model and its results, we use the *Model View* and *Beam View* components.

The *Model View*, see figure 4.12a, will enable us to see the deformation, the supports reactions, the loads, the local axis, the joints and their values. It also gives us tags to have the name of the different elements.

The *Beam View*, see figure 4.12b, gives us the forces and moments acting in the sections with graphs to visualise them, the displacement of the beam, the axial stresses, its utilisation and its cross section.



(a) Model View (b) Beam View

Figure 4.12: View components

Analysis of different load cases

In this section, the static behaviour of different load cases of beams will be analysed. We will verify the internal loads and maximal deflection given by Karamba3D with hand calculations. The internal loads are the normal force, the shear force, and the bending moment. A visual representation of internal loads can be seen on figure 4.13. This will enable us to determine whether Karamba3D is appropriate for us to use.

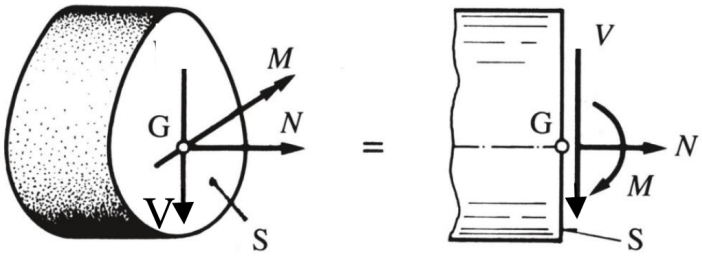


Figure 4.13: Internal loads[68]

Normal Force The normal forces N also called axial forces are the internal forces in the direction of the axis of the element. It is positive when the element is in traction and negative in compression. Karamba3D expresses it in kN. It will be negligible in these load cases as no load will be applied in the axis' direction.

Shear Force The shear force V are the internal forces transverse to the element. They are caused by external forces with a component perpendicular to the main axis. Karamba3D expresses it in kN. The shear force follows the following formula:

$$V(x) = \pm \frac{dM(x)}{dx} \tag{4.1}$$

Bending Moment The bending moment M is the reaction induced by an external force or moment that causes the element to bend. Karamba3D expresses it in kNm. At equilibrium, if we take a section of a beam, the bending moment is equal to the sum of the moments induced by all external forces on one side of this section. This must apply to both side of the section and the resulting bending moments must be equal for both sides.

Maximal deflection The deflection v for a beam in flexion can be given by the Euler-Bernoulli beam theory that gives the following equation:

$$\frac{d^2v(x)}{dx^2} = \frac{M(x)}{EI} \tag{4.2}$$

Where E is the young modulus and I is the inertia. This theory is only valid for small displacement. However, Karamba3D uses the Timoshenko beam theory which is similar to Euler-Bernoulli, but it takes into account into account shear deformation and rotational bending effects. Its equation for the deflection goes as follows:

$$\frac{d^2v(x)}{dx^2} = \frac{M(x)}{EI} + \frac{d}{dx}(\frac{V(x)}{\kappa GA}) \tag{4.3}$$

With G the shear modulus, κ the shear correction factor and A is the area of the section.

For this analysis, we will use the Euler-Bernoulli equation and neglect the shear effect on the displacement, the results should however be pretty similar.

- For the first load case in table, we will take a 10 meter long beam with a uniform vertical load of $-1kN/m$ with a pinned support and a roller support and an IPE300 cross section. See table 4.1 and figure 4.14.

- For the second load case, we will take a 3 meter long beam with a punctual vertical load of $-2kN$ applied at the middle of the beam with a pinned support and a roller support and an RB100 cross section. See table 4.2 and figure 4.15.
- For the third load case, we will take a 20 meter long beam with two punctual vertical loads of $7kN$ applied at 1/3 and 2/3 of the beam with a pinned support and a roller support and an HEAA200 cross section. See table 4.3 and figure 4.16.
- For the fourth load case, we will take a 5 meter long cantilevered beam fixed on the extremity A and with a $2kN$ vertical load on point B and with a HEA200 cross section. See table 4.4 and figure 4.17.
- For the fifth load case, we will take a 8 meter long cantilevered beam fixed on the extremity A and with a $-5kN/m$ uniform vertical load with a HEB100 cross section. See table 4.5 and figure 4.18.

Load Case 1			
Data			
Length	$L = 10[m]$		
Load	$q = -1[kN/m]$		
Support	one pinned and one roller		
Cross section	IPE300		
Inertia	$I = 83,6 * 10^6[mm^4]$		
Young Modulus	$E = 210000[N/mm^2]$		
Results			
	Formula	Karamba3D	Hand calculation
$V_{z,max}$	$V_{max} = V_A = V_B = \frac{qL}{2}$	5[kN]	5[kN]
$M_{y,max}$	$M_{max} = M(\frac{L}{2}) = \frac{qL^2}{8}$	12,5[kNm]	12,5[kNm]
Max displacement	$v_{max} = v(\frac{L}{2}) = \frac{5qL^4}{384EI}$	7,496[mm]	7,417 [mm]

Table 4.1: Load Case 1

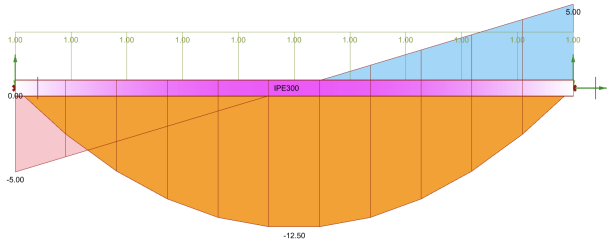


Figure 4.14: Load Case 1

Load Case 2			
Data			
Length	$L = 4[m]$		
Load	$Q = 2[kN]$ at 0,5L		
Support	one pinned and one roller		
Cross section	HEM100		
Inertia	$I = 11,4 * 10^6[mm^4]$		
Young Modulus	$E = 210000[N/mm^2]$		
Results			
	Formula	Karamba3D	Hand calculation
$V_{z,max}$	$V_{max} = V_A = V_B = \frac{Q}{2}$	1[kN]	1[kN]
$M_{y,max}$	$M_{max} = M(\frac{L}{2}) = \frac{QL}{4}$	2[kNm]	2[kNm]
Max displacement	$v_{max} = v(\frac{L}{2}) = \frac{QL^3}{48EI}$	1,132[mm]	1,114 [mm]

Table 4.2: Load Case 2

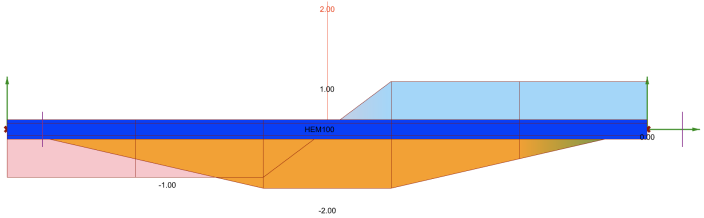


Figure 4.15: Load Case 2

Load Case 3			
Data			
Length	$L = 20[m]$		
Load	$Q = 7[kN]$ at L/3 and 2L/3		
Support	one pinned and one roller		
Cross section	HEAA400		
Inertia	$I = 312 * 10^6[mm^4]$		
Young Modulus	$E = 210000[N/mm^2]$		
Results			
	Formula	Karamba3D	Hand calculation
$V_{z,max}$	$V_{max} = V_A = V_B = \frac{Q}{3} + \frac{2Q}{3} = Q$	7[kN]	7[kN]
$M_{y,max}$	$M_{max} = M(\frac{L}{3}) = \frac{2QL}{3}$	46,67[kNm]	46,667[kNm]
Max displacement	$v_{max} = v(\frac{L}{2}) = \frac{23L^3}{648EI}$	30,455[mm]	30,337[mm]

Table 4.3: Load Case 3

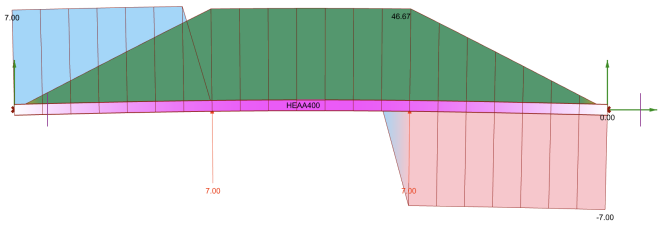


Figure 4.16: Load Case 3

Load Case 4			
Data			
Length	$L = 5[m]$		
Load	$Q = 2[kN]$ at B		
Support	Fixed in A		
Cross section	HEA200		
Inertia	$I = 36,9 * 10^6[mm^4]$		
Young Modulus	$E = 210000[N/mm^2]$		
Results			
	Formula	Karamba3D	Hand calculation
$V_{z,max}$	$V_{max} = V_A = Q$	2[kN]	2[kN]
$M_{y,max}$	$M_{max} = M_A = QL$	-10[kNm]	-10[kNm]
Max displacement	$v_{max} = v(L) = \frac{QL^3}{3EI}$	10,854[mm]	10,754[mm]

Table 4.4: Load Case 4

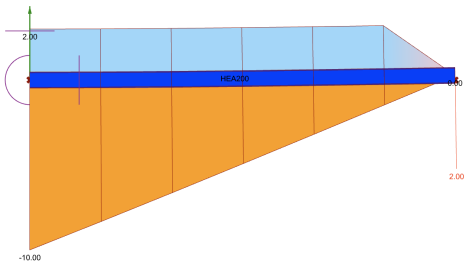


Figure 4.17: Load Case 4

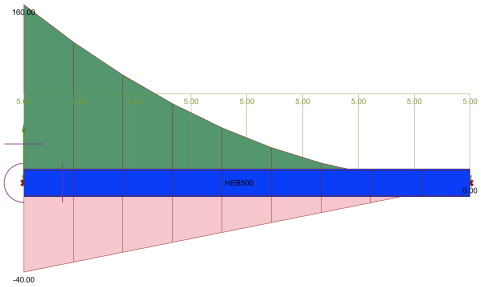


Figure 4.18: Load Case 5

Load Case 5			
Data			
Length	$L = 8[m]$		
Load	$q = -5[kN/m]$		
Support	Fixed in A		
Cross section	HEB500		
Inertia	$I = 1070 * 10^6[mm^4]$		
Young Modulus	$E = 210000[N/mm^2]$		
Results			
	Formula	Karamba3D	Hand calculation
$V_{z,max}$	$V_{max} = V_A = qL$	-40[kN]	-40[kN]
$M_{y,max}$	$M_{max} = M_A = \frac{qL^2}{2}$	160[kNm]	-160[kNm]
Max displacement	$v_{max} = v(L) = \frac{qL^4}{8EI}$	11,661[mm]	11,393[mm]

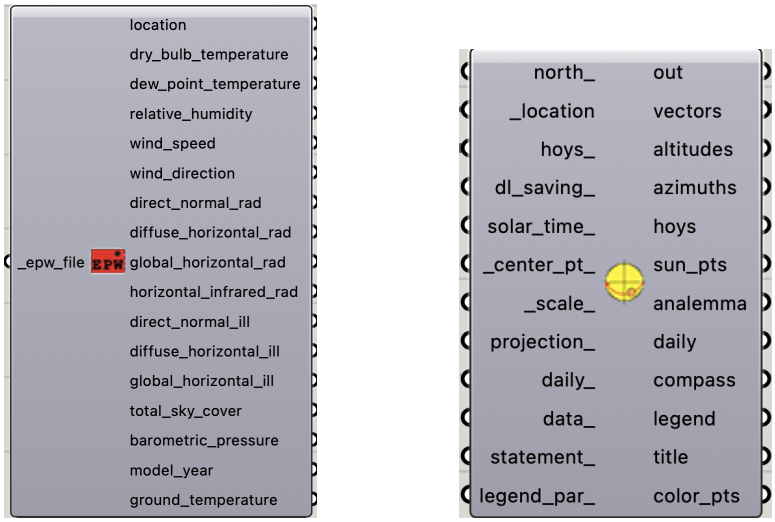
Table 4.5: Load Case 5

As we can see from these analysis, the results for the maximal shear forces and bending moments are the same in both the hand calculations and the Karamba3D results. However, the max displacement varies by a small percentage due to the use of Euler-Bernoulli's equation instead of Timoschenko's equation for the hand calculations, this can be neglected. We can therefore conclude that it seems reasonable to continue to use Karamba3D for more complex scenarios.

4.4 Ladybug Tools

Ladybug[69] is also embedded into Grasshopper. It performs detailed analysis of climate data to produce customized, interactive visualizations for environmentally-informed design. It imports standard EnergyPlus Weather files into Grasshopper. EnergyPlus Weather[70] (EPW) is a standard weather data format that contains hourly information like temperature, humidity, wind, solar radiation, and precipitation at different locations around the globe. We can simulate the sun path of almost any location in the world by importing a epw file of the chosen city from the ladybug website using the *LB Import EPW* component, see figure 4.19a. It gives as output various information about the meteorological data of the location.

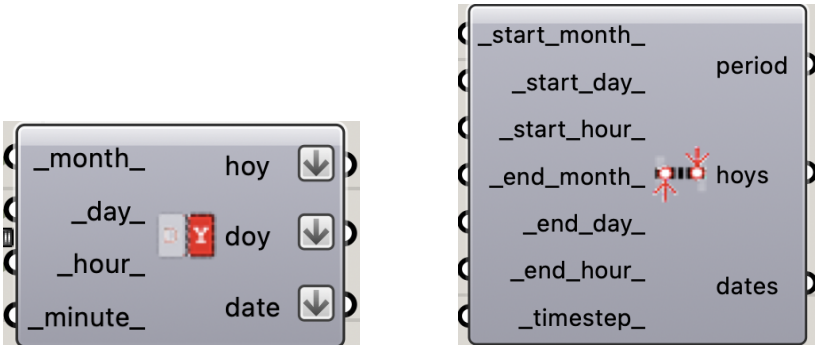
The *LB Sun Path* component, see figure 4.19b, will then allow us to simulate the sun at any hour of any day of any month by inputting the *location* from the *LB Import EPW* component and hoys (Hours Of Year) from the *LB Calculate Hoy* component, see figure 4.20a, or from the *LB Analysis Period* component, see figure,



(a) LB Import EPW (b) LB Sun Path

Figure 4.19: LB components

4.20b depending on if we want to analyse a specific time or a period of time. The default North will be the positive Y direction, but can be modified by inputting a value between -360 and 360 in the *north_* input.



(a) LB Calculate Hoy (b) LB Analysis Period

Figure 4.20: Hoy components

From the *LB Sun Path* component outputs, we will use the *vectors* which are parallel to each other and perpendicular to a fictive plane representing the sun. We can then use the *Mesh Shadow* component of Grasshopper, see figure 4.21, to see the outline of the shadow of a given geometry using the *vectors* from the sun path as input. We then use the *Area* component, see figure 4.22, to get its area.

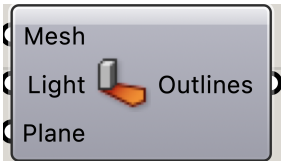


Figure 4.21: Mesh Shadow



Figure 4.22: Area

To make sure that we can use the results given by ladybug, we will in tables 4.6 and 4.7 verify by hand the results of a few vertical rectangular surfaces at different moments of the year using the altitudes and azimuths of the sun given by the *Sun Path* component.

Ladybug will allow us to analyse the shaded area produced by our structure and therefore its efficiency.

Shadow Case 1	
Length	$L = 8[m]$
Height	$H = 3[m]$
Direction of the surface	parallel to the North to South direction
Location	Brussels
Date and time	16^{th} of December at 2PM
Altitude	Alt=13,642528[°]
Azimuth	Az=199,405552[°]
Grasshopper Area	$A = 32,854096[m^2]$
Hand calculated Area	$A = \frac{H}{tan(Alt)} * L * sin(360 - Az) = 32,854098[m^2]$

Table 4.6: Shadow Case 1

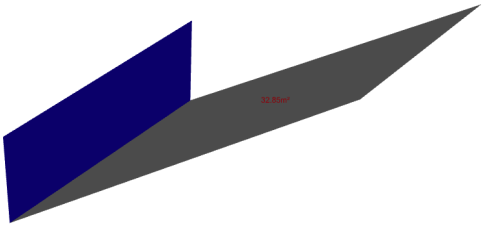


Figure 4.23: Shadow Case 1

Shadow Case 2	
Length	$L = 16[m]$
Height	$H = 7[m]$
Direction of the surface	parallel to the East to West direction
Location	Brussels
Date and time	21^{th} of June at 5AM
Altitude	$Alt = 3,41678[°]$
Azimuth	$Az = 55,746381[°]$
Grasshopper Area	$A = 1055,86[m^2]$
Hand calculated Area	$A = \frac{H}{tan(Alt)} * L * sin(Az + 90) = 1055,86[m^2]$

Table 4.7: Shadow Case 2



Figure 4.24: Shadow Case 2

4.5 Wallacei

Wallacei[71][72] is an evolutionary multi-objective optimization engine that allows to run evolutionary simulations in Grasshopper, by using its main component, the *Wallacei X* component, see figure 4.25. Wallacei X employs the NSGA-2 algorithm as the evolutionary algorithm.

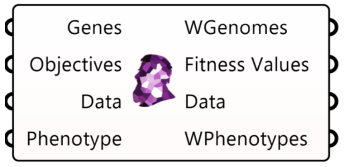


Figure 4.25: Wallacei X Component

In order to understand better how to use Wallacei, we will make several multi-objective optimizations.

We will start by optimizing an IPE beam, we will then optimize a rectangular beam with parametric height and width and finally, we will optimize urban canopies. All of these models will first be optimized in a structural way. We will therefore minimize the weight of the structure while limiting the maximum displacement to $L/200$. We will then add another fitness objective to maximize the shaded area for a shade analysis.

For all of these different cases, most of the steps to follow are the same, and similar to what we could do in the previous sections. Mainly the geometry, the cross-section, and the optimization will differ between the models.

We will start by defining the geometries of the problem. Once the structural lines and support points are defined, we will input them into the *Line to Beam* component and the *Support* component. We then apply the load caused by the weight of the structure and the required external loads.

We can now defined the cross-sections: these will be parametric and dependent on the requirements of the problem.

We then use the *Assemble Model* component and input all the parameters. The component will give us the model, but also its mass that we will make sure to keep into a *Number* component that we call *Mass*.

We then input the model into the *Analyse* parameter for which we can have the calculated model, and the maximum displacement that we also keep in a *Number* component that we call *Max displacement*.

We then input the model into the *Model View* and the *Beam View component* to visualise the model but most importantly, we input the mesh of rendered beam from the *Beam View*'s outputs to a *Mesh* parameter that we will call *Beam Mesh*.

If we want to use the shaded area for the optimization, we will use a similar method as used in the Ladybug section.

We will start by importing the EPW file of the location of our choice, in our case Brussels, using the *LB Import EPW* component. We then use its *location* output for the *LB Sunpath* and input hoys from either from a *LB Calculate HOY* component or from *LB Analysis Period* if we want the shadow from a punctual time of the day or from a period of time. For the following models, we used the sun path in Brussels at 10AM on the 21st of July with the north as the positive Y direction.

We can now input the *vectors* from the sun path and the *Beam Mesh* that has been defined earlier into the *Mesh Shadow* component. We can also input a plane parallel to the XY plane with a parametric height to simulate the ground level and be able to easily modify the height of the structure.

We now use the *Boundary Surfaces* component to make sure all the outlines are reconnected into one surface, otherwise, in the case of structures with multiple beams, when we want to calculate the shaded area, it will tend to calculate the area of the surfaces created between the shadows and not of the shadows. We will export the surface into a *Mesh* component that we call *Shadow Mesh* and in the *Area* component.

If we have used a period of time instead of a punctual time, we can use the *Mass Addition* component by first flattening the input, to have the cumulative area of all the shaded surfaces. We then keep the area or the sum of the areas into a *Number* component that we will call *Shaded Area*.

For the optimization, we have to input the genes and fitness objectives into the *Wallacei X* component. The genes will be sliders, in our case, they will be sliders to select or modify the cross-section or modify beam structure. The fitness objectives will be the results that we want to minimize.

If we want to maximize one of the objectives, it should be converted to a minimization by making it negative. If we want to make constraints, we still must have a fitness objective, but we can use the *Expression* component to adjust it. To limit the maximum displacement, we can therefore use the following script: $if(x \leq \frac{z}{200}, 1, 10)$ with x the maximum displacement and y the length of the beam. This will encourage Wallacei to select solutions that respect the limit of maximum displacement.

We can name the sliders and fitness objectives with names starting with "wlc_"

followed by a number to automatically select them by using the "Select all Sliders" and " Select all Objectives" function when we right click on the *Wallacei X* component. This will automatically rank them in order depending on the chosen number. It is also better to use the Flatten function to make sure that the objectives stay in the right order.

In the following cases, will select the fitness objectives among the followings:

- Minimize mass: we input the *Mass* into a flattened *Number* component that we call *wlc_1Minimize mass*
- Maximize shaded area: we input the shaded area into the *Negative* component and input the result into a flattened *Number* component that we call *wlc_2Maximize shaded area*
- Limited displacement: we input the output of the script described above into a flattened *Number* component that we call *wlc_3Limited displacement*

Once we have inputted the genes and objectives into the *Wallacei X* component, we can double click on the icon of the *Wallacei X* component to open a window with the Wallacei X interface. We have now access to five tabs: Wallacei Settings see figure 4.26, Wallacei Analytics see figure 4.27, Wallacei Selection see figure 4.28, Wallacei Forum and the Wallacei Primer.[72]

The Wallacei Settings tab, is used for setting up the simulation before running it. We have access to a control panel and different graphs and the primary buttons. The primary buttons are the followings:

- Snap: takes a screenshot of the tab.
- Start: clears any existing data in the solver and start a new simulation.
- Stop: Stops the simulation.
- Reset: Clears any data stored in the solver and resets simulation settings to the default values.

In the control panel, we have:

- Population: we can modify the population by changing the generation size (how many individuals per generation) and generation count (how many generation for the simulation).
- Algorithm Parameters: for these parameters, we kept all the default values.

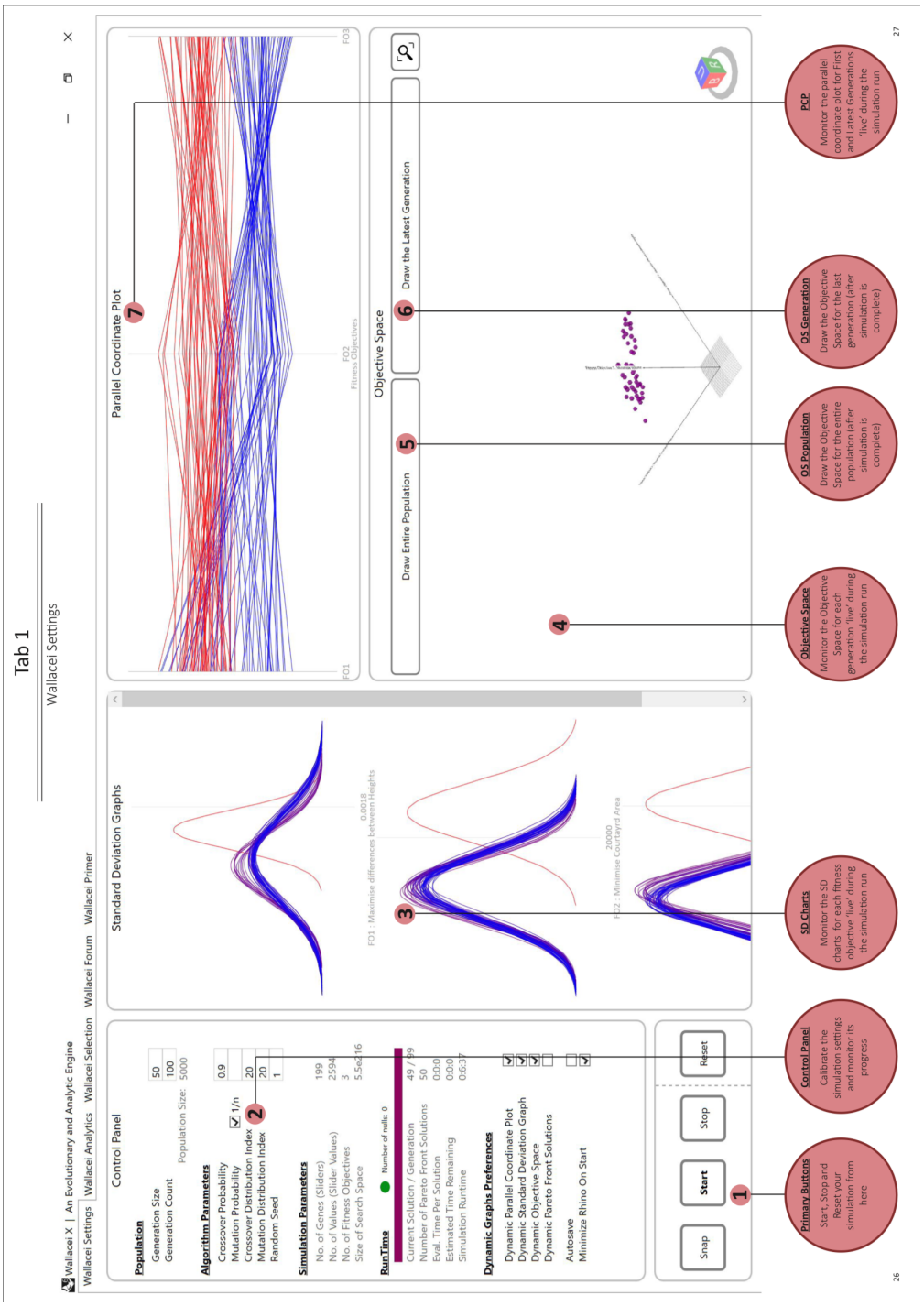


Figure 4.26: Wallacei Settings[72]

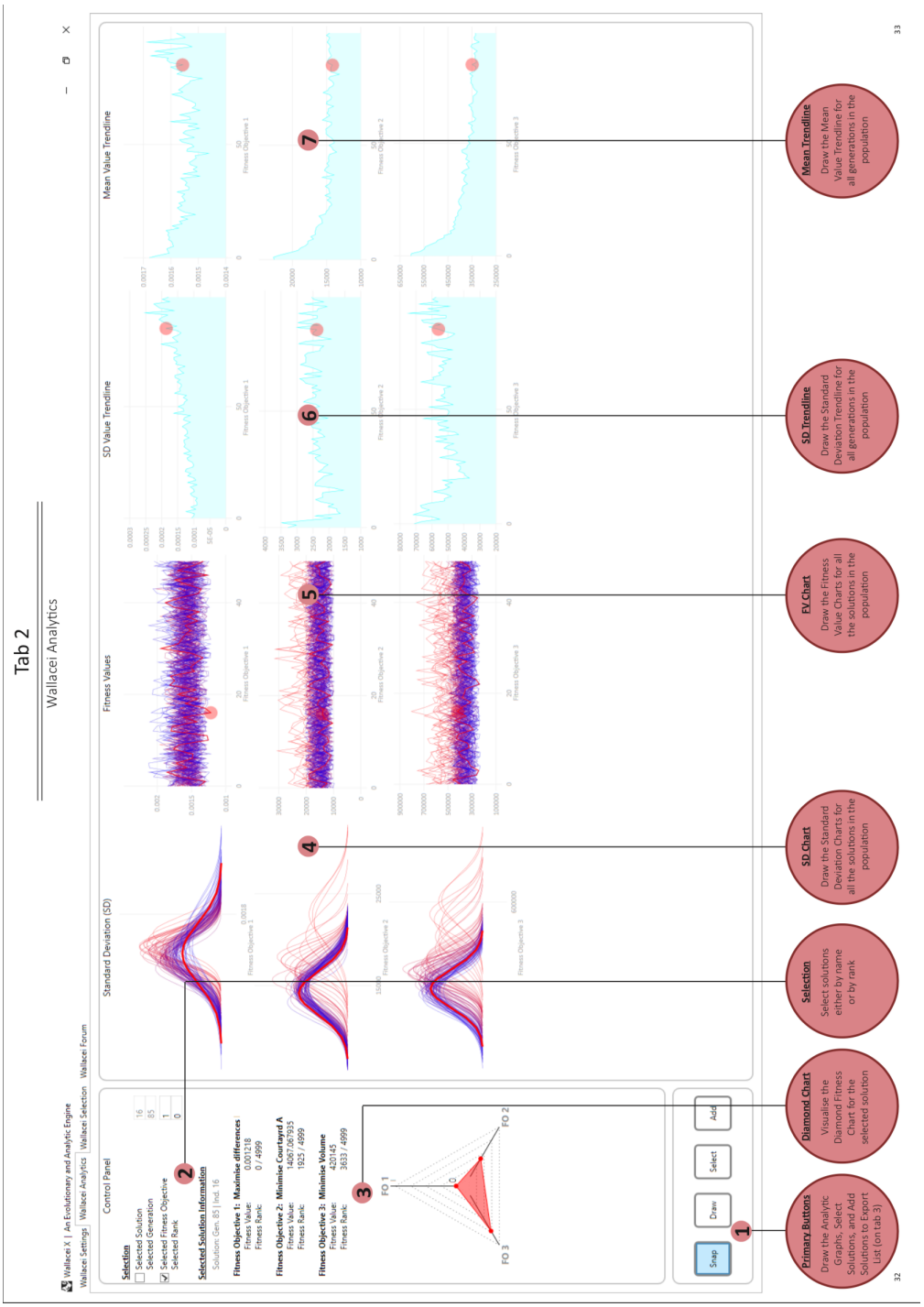


Figure 4.27: Wallacei Analytics[72]

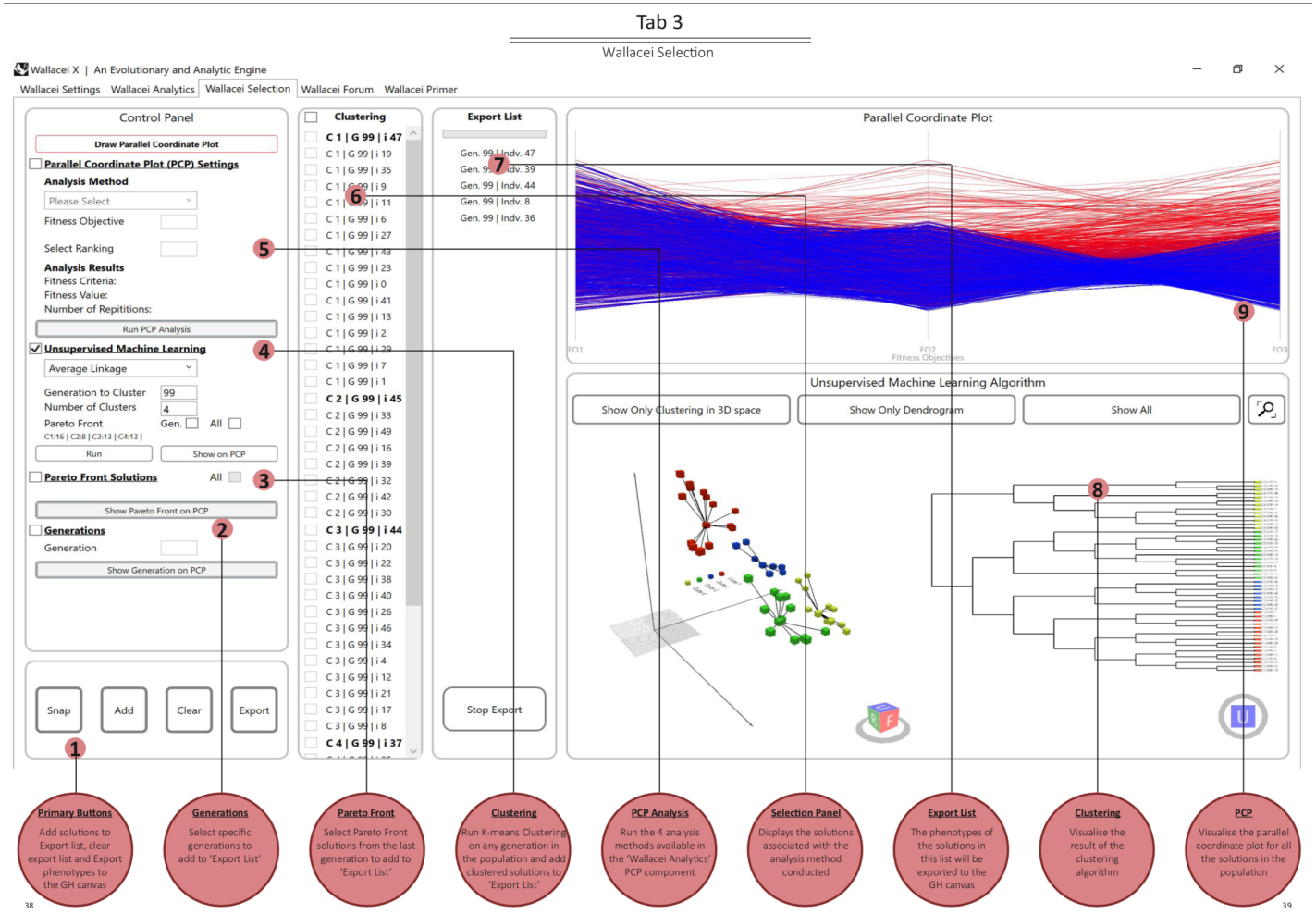


Figure 4.28: Wallacei Selection[72]

  - Crossover Probability: the percentage of the population that will reproduce for the next generation. Between 0.0 and 1.0. Default: 0.9.
  - Mutation probability: the percentage mutations taking place in the generation. Between 0.0 and 1.0. Default: 1/n with n the number of genes (sliders).
  - Crossover and Mutation Distribution Index: a large distribution index gives a higher probability for creating offspring near parent solutions, a small distribution index allows distant solutions to be selected as offspring solutions. Between 0 and 100. Default: 20 for both indexes.
  - Random Seed: If 1, it allows to recreate the exact same results every times for the same optimization problem. If 0, we allow the randomness and the results won't be the same between simulations.

- Simulation Parameters: gives the number of genes (sliders), values (slider values), fitness objectives, and the size of the search space.

- Run Time: gives the current solution and generation of the simulation, the number of Pareto front solutions that as been found, the time taken per solution, the estimated remaining time and the simulation run time. The run time will depend on the population size, the complexity of the model, and the computational power of the computer.

- Dynamic Graphs Preferences: toggle to allow different graphs to be drawn while the simulation is running. Those graphs give an indication of the simulation's performance.

The different graphs are the followings:

- Standard Deviation Graphs: dynamically draws the standard deviation chart for each fitness objectives independently. It shows the first generation and the latest 50 and goes from red (first generation) to blue (last generation).

- Parallel Coordinate Plot: dynamically draws the parallel coordinate plot for the simulation. It compares the fitness values of each solution across all fitness objectives and shows the first and latest generation of the simulation from red to blue. Each solution is displayed as a line going trough the vertical lines corresponding to the different objectives. The lower the solution line connects with the objective line, the fitter the solution is for the corresponding objective.

- Objective Space: dynamically draws the objectives space for each generation in the simulation. It can display up to 6 dimensions, X, Y, Z, Colour, Size,

and Transparency. Pareto solutions are represented as Yellow cubes. Once the simulation is completed, we can choose to draw the objective space of the entire population or of the latest generation.

The Wallacei Analytics tab is used for analysing the simulation's results and cross referencing the different simulation results to one another. On the tab we can find the following:

- Primary buttons:
  - Snap: takes a screenshot of the tab.
  - Draw: draws the graphs for all solutions. It must be clicked to start analysing.
  - Select: highlight the selected solution in the graphs.
  - Add: add the selected solution to the export list of tab 3
- Selection: we can select a solution either by inputting the generation and solution number or by inputting the fitness objective and the solution's fitness rank. Then click select.
- Selected Solution Information: gives the fitness value and fitness rank of the selected solution for all fitness objectives.
- Diamond Fitness Chart: draws the diamond fitness chart for the selected solution. Each axis represent a fitness objective. The closer the point is from the center, the fitter the solution.
- Standard Deviation Chart: draws the standard deviation chart for all generations in the population and for each fitness objectives independently. The standard deviation represents the distribution of a set of values around the mean. A low standard deviation factor indicates that most values are clustered around the mean, while a high standard deviation factor indicates that the values are spread out farther from the mean. It aims to represent and analyse the levels of variation/convergence for each generation of the population.

  We can also check whether the generations are getting fitter throughout the simulation. A flat curve represents an increased variation while a narrow curve represents an increased convergence. A shift to the left indicates a better mean performance. It plots three standard deviation values on either side of the mean for each generation.

- Fitness Value Chart: draws the fitness value chart for all solutions in the population and for each fitness objective independently. The solutions are displayed per generation from left to right. Each generation is connected with polyline and are colored from first (red) to last (blue). It aims to visualise how solutions are performing in relation to one another, both within each generation and across the population.
- Standard Deviation Trendline Chart: plots the standard deviation values for each generation as a line chart (first generation on the left) for each fitness objective independently. Its aims to highlight specific trends in the variation and/or convergence of each generation across the population
- Mean Value Trendline Chart: plots the mean fitness value for each generation as a line chart (first generation on the left) for each fitness objective independently. It aims to highlight specific trends in the mean fitness value for each generation across the population.

The Wallacei Selection tab is used for analysing the results of the simulation to select and export them. We can see the following on the tab:

- Primary Buttons:
  - Snap: takes a screenshot.
  - Add: adds the selected solution to the export list.
  - Clear: clears the solutions from the export list.
  - Export: Exports the phenotypes of the solutions added to the export list.
- The Parallel Coordinate Plot Analysis: it analyses all the solutions in the population by comparing the fitness values for each solutions across all fitness objectives. It gives us four methods to do so:
  - The *most repeated fitness values* method gives us the most repeated fitness values in the population and output the corresponding data.
  - The *solutions with most repeated fitness values* method gives us the solutions associated with the most repeated fitness values calculated in the first method. It permits to highlight the frequency of repeated fitness values across the simulation
  - The *relative difference between ranks* method orders the solutions according to the relative difference between the fitness ranks of the different objectives. The 'fittest' solution is the one that has the same rank for all fitness objectives.

  - The *average fitness rank* method orders the solutions according to their mean fitness by calculating the mean fitness rank of each solution's fitness objectives. The 'fittest' solution is the one with the lowest mean rank.

- The Unsupervised Machine Learning: it clusters solutions generated by the simulation. It uses two primary clustering algorithms, Kmean Clustering and Agglomerative Hierarchical Clustering that permits to cluster solutions from any given generation, the Pareto front of any given generation, or the Pareto front of the entire population. The clustered solutions can be displayed on the Parallel Coordinate Plot and on the objective space.

- The Pareto Front Solutions: it displays the Pareto front solutions of either the final generation or of the entire population. These solutions can be displayed in the Parallel Coordinate Plot to compare them with the other solutions.

- The Generations: it enables to export complete generations.

The Wallacei Forum tab, gives access to the Wallacei forum which can also be accessed online

The Wallacei Primer tab, gives access to the Wallacei Primer.[72]

Once we have selected our solutions, we can export them and input in the *Wallacei X* component the phenotypes which in our case are *Beam Mesh* and *Shadow Mesh*. In order to visualise the different results, we use the *Distribute to Grid* component, see figure 4.29. We input into it the Fitness values and the phenotypes from the *Wallacei X* component and it gives us in the rhino interface the meshes of all the different solutions that have been exported. The structure meshes will here be displayed in black, and the shadow meshes in grey. We can also display the objectives value and the genes value in order to help us choose the final values.

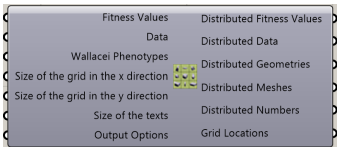


Figure 4.29: Distribute to Grid

In the following sections, so that we don't explain the whole model over and over again, we will just explain the geometry, the cross-section, the genes, the fitness objectives, and the analysis.

4.5.1 IPE Beam

For this first model, we will determine the fittest cross-section of a beam through multi-objective optimization. For the structural optimization, we want to find the lightest beam from a certain cross-section family to respect the condition for the maximum displacement of $v_{max} \leq L/200$ with L the length of the beam. The beam will be a horizontal 5 m IPE beam with a $5[kN/m]$ uniform load and supported by a pinned and a roller support. For the shade optimization, we will add the objective to maximize the shaded area created by the beam.

The changes applied to the method described in section 4.5 are the following:

- Geometry: modeling of a line of the required length by using two *Construct Point* component and a *Line* Component. The two points will be used for the corresponding *Support* component.
- Cross-section: a *Cross Section Range Selector* component will be used to select the IPE cross-section family and output a cross-section list. We then use a *Cross Section Selector* with a number slider to select cross-section of the list. We will call this slider *wlc_ Cross section selector*.
- Genes: the *wlc_ Cross section selector* slider will be the only slider used.
- Fitness objectives: the *wlc_1Minimize mass* and the *wlc_3Limited displacement* fitness objectives for the structural optimization. We add the *wlc_2Maximize shaded area* fitness objective for the shade optimization.

Structural optimization analysis

Before we launch the simulation, we can already observe in the simulation parameters of the Wallacei Settings tab that we have 1 gene, 18 values, 2 fitness objectives and 18 possible solutions in the search space. In this case, the gene is the cross-section type, the values are the 18 different cross-sections available, and the search space are these same 18 available cross-sections because there is only one gene. Because of the small search space, we can have a small population we therefore choose a generation size of 10 and a generation count of 20 for a total population of 200 solutions. The simulation lasted for only 1 second the model being simple and the population small.

We can quickly observe on the first tab see figure 4.30, that the simulation settled towards two Pareto solutions. We can see this on the Parallel Coordinate Plot which only has two blue lines indicating that only two solutions have been kept for the latest generations. We can also see on the Objective Space that only two solutions are in a yellow cubes, the yellow cubes indicating the Pareto solutions. We can also observe on those two graphs that one of the solution is selected because it is the lightest but has maximum displacement $f_{max} \geq L/200$ and that the other solution is the lightest that respect the displacement constraint. We can therefore conclude that we will keep the second solution. We will still however analyze the results on the other tabs.

On tab 2, see figure 4.31, we can observe on the first Standard Deviation graphs that the curve of the first generation is flat. This is due to its variation of solutions. This phenomenon is confirmed on the fitness value chart with very different fitness values for each solutions. We can also see on the four charts that the fitness value for the minimization of the mass quickly decreases. We can also see that the fitness values for the minimization of the mass are constrained after the 3rd generation between the two Pareto solutions. And after the 4th generation, all the solutions are Pareto solutions. There are less things to note from the charts of the limited displacement due to the fact that the solutions varies between two values. We can however still see a shift of the standard deviation chart to the right and an increase for the trendline charts due to the fact that there are more possible solutions that respect the constraint than those who don't. We therefore have more 1 than 10 at the beginning, however there is later only two possible solutions and we can see that they are roughly equally represented from the 6th generation onward.

On tab 3, see figure 4.32, we can confirm that there are only two Pareto solutions for the whole population. We can use the *average fitness rank* method to add our solution to the export list and export it. Our solution is a IPE160 beam of 78.9 kg, it can be seen on figure 4.33. We then verify by hand calculation if the chosen beam is the right one in tab 4.8. We can conclude that IPE160 is indeed the lightest beam to respect the deflection constraint.

Beam Optimization verification			
Data			
Length	$L = 5[m]$		
Load	$q = -5[kN/m]$		
Support	one pinned and one roller		
Max displacement	$f_{max} = \frac{L}{200} = 25[mm]$		
Young Modulus	$E = 210000[N/mm^2]$		
Cross section	IPE160	IPE140	
Weigth per meter	$p = 0,155kN/m$	$p = 0,127kN/m$	
Inertia	$I = 8,69 * 10^6[mm^4]$	$I = 5,41 * 10^6[mm^4]$	
Results			
	Formula	IPE160	IPE140
$V_{z,max}$	$V_{max} = V_A = V_B = \frac{qL}{2}$	12.89[kN]	12,82[kN]
$M_{y,max}$	$M_{max} = M(\frac{L}{2}) = \frac{qL^2}{8}$	16,11[kNm]	16,02[kNm]
Max displacement	$v_{max} = v(\frac{L}{2}) = \frac{5qL^4}{384EI}$	22,98[mm]	36,72[mm]

Table 4.8: Verification of beam optimization

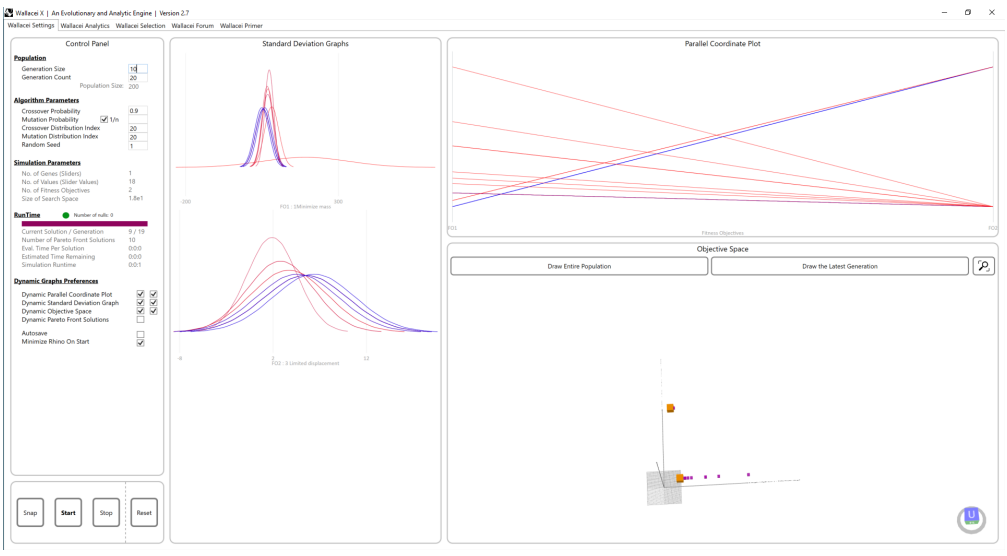


Figure 4.30: Wallacei Settings for the structural optimization of an IPE beam

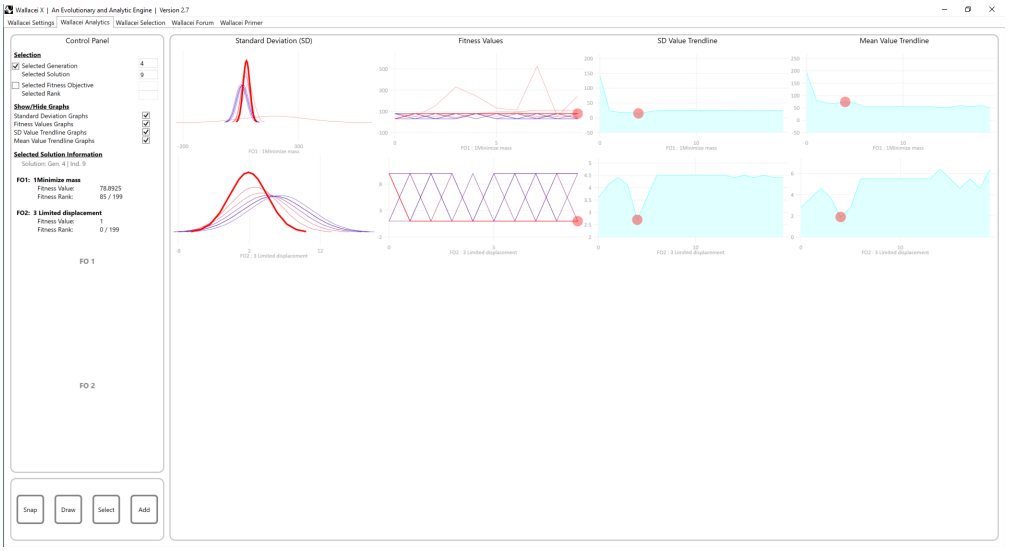


Figure 4.31: Wallacei Analytics for the structural optimization of an IPE beam

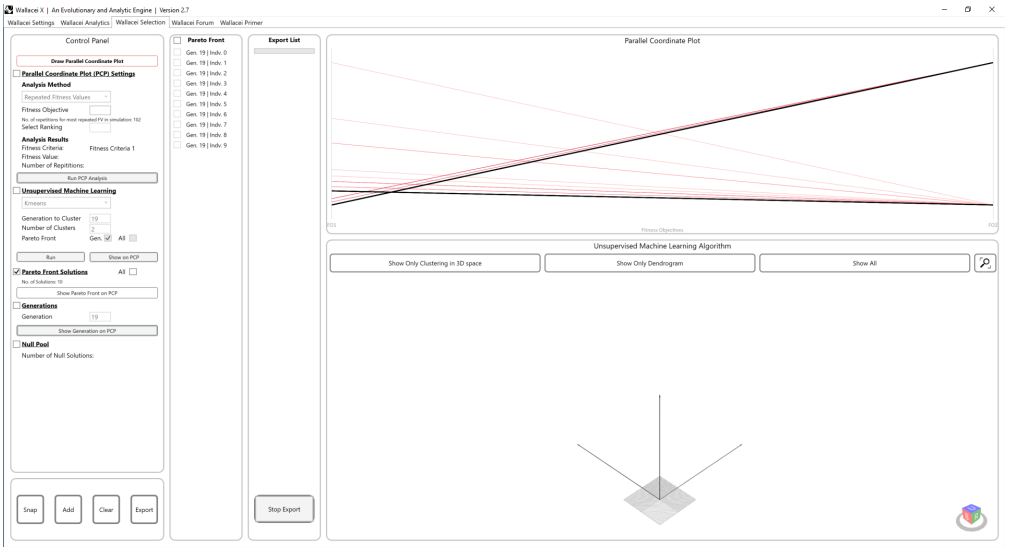


Figure 4.32: Wallacei Selection for the structural optimization of an IPE beam

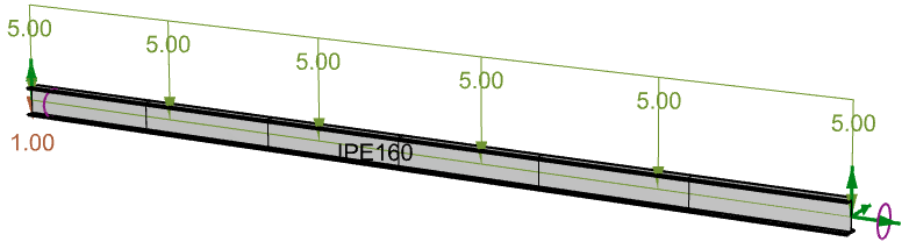


Figure 4.33: Result of the structural optimization of an IPE beam

Shade optimization analysis

Before we launch the simulation, we can already observe in the simulation parameters of the Wallacei Settings tab, see figure 4.35, that we still have 1 gene, 18 values, and 18 values in the search space but we now have 3 fitness objectives. We use the same population parameters with a generation size of 10 solutions and a generation count of 20 generations for a total population of 200 solutions. The simulation lasted for 2 seconds. We can directly observe on the Objective Space diagram when we draw the entire population that all the solutions are part of the Pareto front.

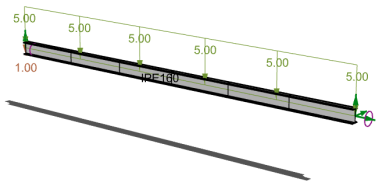
We can see on tab 2, see figure 4.36, on the fitness value chart that all the solutions keep getting selected for the new generations. This is because they are all Pareto solutions. It's also the cause of the non convergence of the Mean Value Trendline plot. We can see on the Standard Deviation charts a flattening of the curve showing an increase of variation after the first generations.

In order to find the right solution, we will have to take some decisions. Do we prefer to maximize the shade, minimize the weight while respecting the deflection constraint or choose a solution in between. We use the Kmeans of tab 3, see figure 4.37, to find the lightest solution and the solution with largest shaded area. For this we use the Kmeans to cluster the Pareto solutions of the last generation that respects the deflection constraint. From these results we select the lightest one and the one with the largest shaded area. If we want to find a good in-between solutions, we can use the *average fitness rank* method, the solution with the lowest

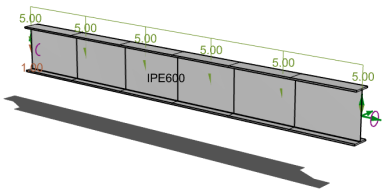
mean rank which is an IPE300 cross-section. We can see these three solutions on table 4.9 and on figure 4.34.

	Solution	Mass $[kg]$	Shaded Area $[m^2]$
Lightest beam	IPE160	78.9	0.8
Largest shaded area	IPE600	612.3	2.5
Average of fitness ranks	IPE300	211.2	1.4

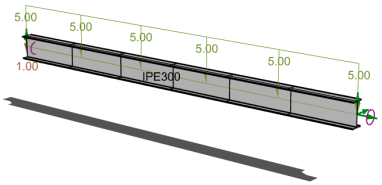
Table 4.9: Properties of the selected solutions for the shade optimization of an IPE beam



(a) Lightest IPE beam



(b) Largest shaded area for an IPE beam



(c) Best average fitness rank for an IPE beam

Figure 4.34: Perspective view of the selected solutions for the shade optimization of an IPE beam

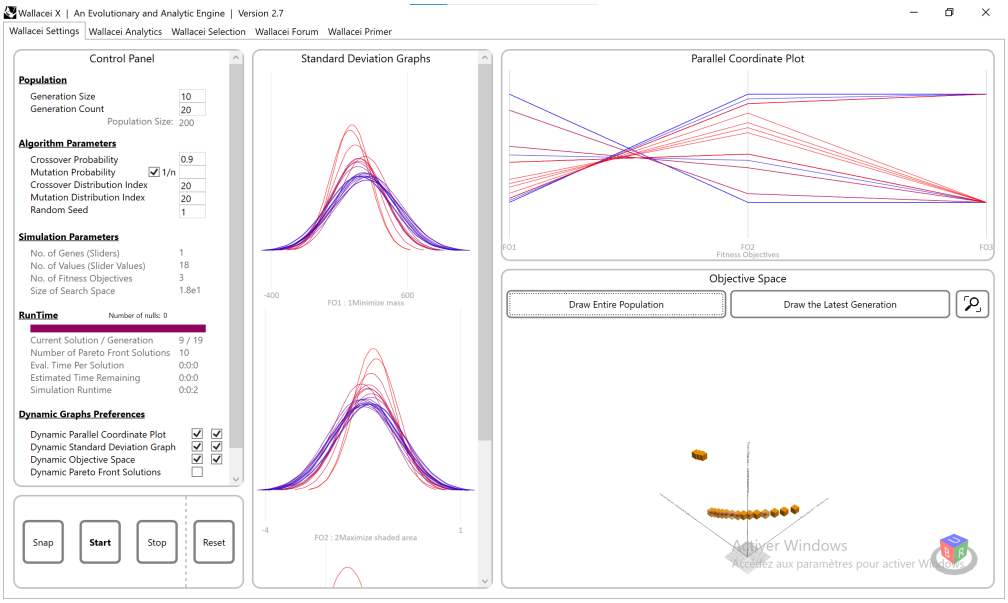


Figure 4.35: Wallacei Settings for the shade optimization of an IPE beam

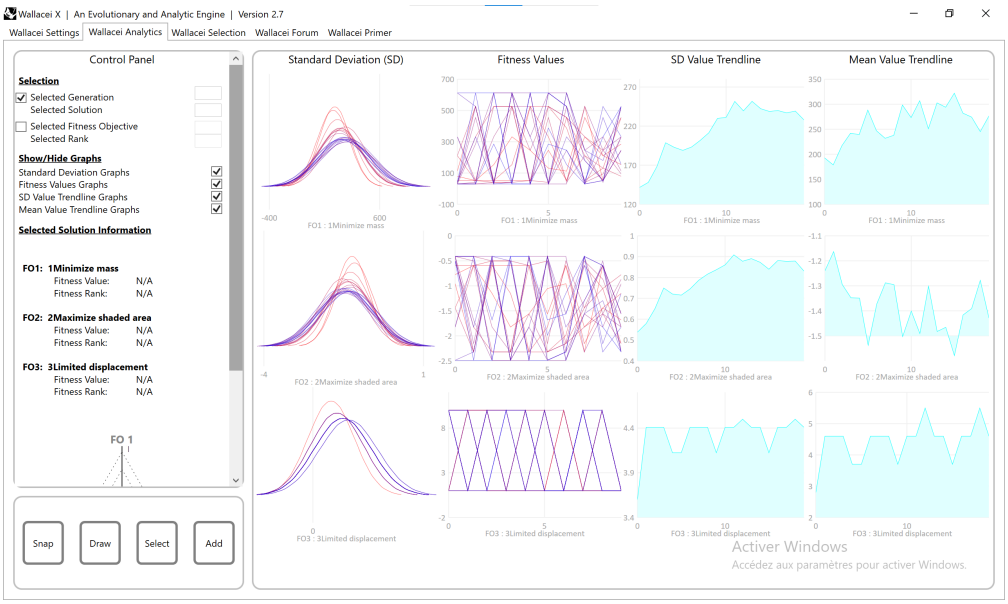


Figure 4.36: Wallacei Analytics for the shade optimization of an IPE beam

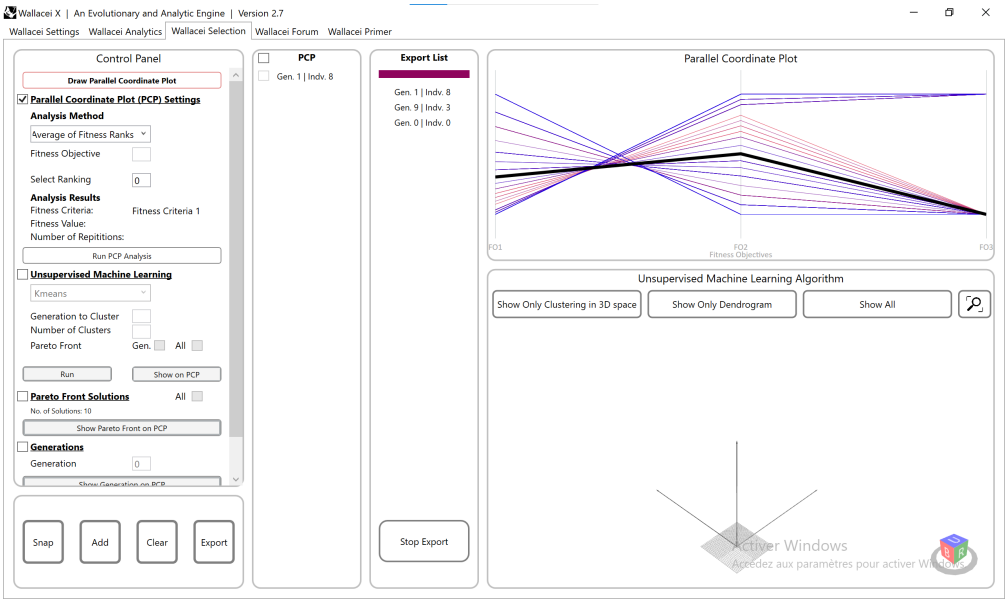


Figure 4.37: Wallacei Selection for the shade optimization of an IPE beam

4.5.2 Rectangular beam

For this second model, we will determine the fittest rectangular cross-section for a beam through multi-objective optimization. For the structural optimization, we want to find the ideal width and height to have lightest beam that respects the deflection constraints of $f_{max} \leq L/200$ with L the length of the beam. We will apply this to a horizontal 5m rectangular beam with a $5[kN/m]$ uniform load and supported by a pinned and a roller support. For the shade optimization, we will add the objective to maximize the shaded area created by the beam.

The changes applied to the method described in section 4.5 are the following:

- Geometry: modeling of a line of the required length by using two *Construct Point* components and a *Line* Component. The two points will be used for corresponding *Support* component.
- Cross-section: we use the *Cross Section* component and select a trapezoid cross-section. We then create two sliders going from 1 to 50 and call them *wlc_Cross Section Height* and *wlc_Cross Section Width*. We then connect the first to the Height and the second to the Upper and Lower Width input of the *Cross Section* component.
- Genes: the *wlc_Cross Section Height* and the *wlc_Cross Section Width* sliders will be the genes.

- Fitness objectives: the *wlc_1Minimize mass* and the *wlc_3Limited displacement* fitness objectives for the structural optimization. We add the *wlc_2Maximize shaded area* fitness objective for the shade optimization.

Structural optimization analysis

Before we launch the simulation, we can already observe in the simulation parameters of the Wallacei Settings tab see figure 4.39 that we have 2 genes, 100 values, 2 fitness objectives and 2500 possible solutions in the search space. The two genes now represent the width and height of the rectangular beam, with a total of 100 values, 50 possible width and height for each gene. The search space represents every possible combination of widths and heights.

Due to the bigger search space, we will have to increase the population size in comparison to the first case. We choose a generation size of 20 individuals and a generation count of 30 generations. The simulation lasted for 5 seconds. We notice straight away on the objective space graph that there are only two Pareto solutions (in yellow cubes) for the model. We can also see them on the Parallel Coordinate Plot. We deduce that the two Pareto solutions are the lightest possible beam and the lightest beam that respect the deflection constraint.

We can see on the second tab, see figure 4.40 that the trendline values for the first objective (mass minimization) quickly converge towards zero. We can also observe this on the fitness value chart. On the Standard deviation chart, that the blue curves(latest generations) are narrow and shifting towards the left showing a convergence and a decrease in the solution values due to the fact that there are only two solutions close to one another compared to the rest of the solutions. The red curves (first generations) are however flatter due to a larger range of solutions. For the second objective (limited displacement), we notice a shift to the right in the standard deviation chart and an increase in the trendline charts because there are more solutions that respect the deflection constraint and were therefore chosen more often but the lightest solution that doesn't respect the constraint is chosen more often afterwards.

On the third tab, see figure 4.41, we will use the unsupervised machine learning tool using the Kmeans on the last generation and separate the solutions into two clusters. This will separate the two solutions and permit us to select the right one easily. The first Pareto solution that we have to reject has a height and width of 1 cm. The second Pareto solution, the solution that we keep, has a height of 22 cm and a width of 1 cm. The solution can be seen on figure 4.38.

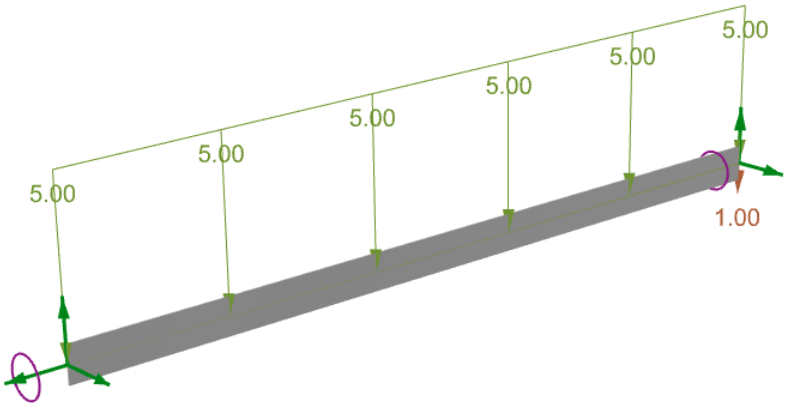


Figure 4.38: Perspective view of the selected solution for the structural optimization of an rectangular beam

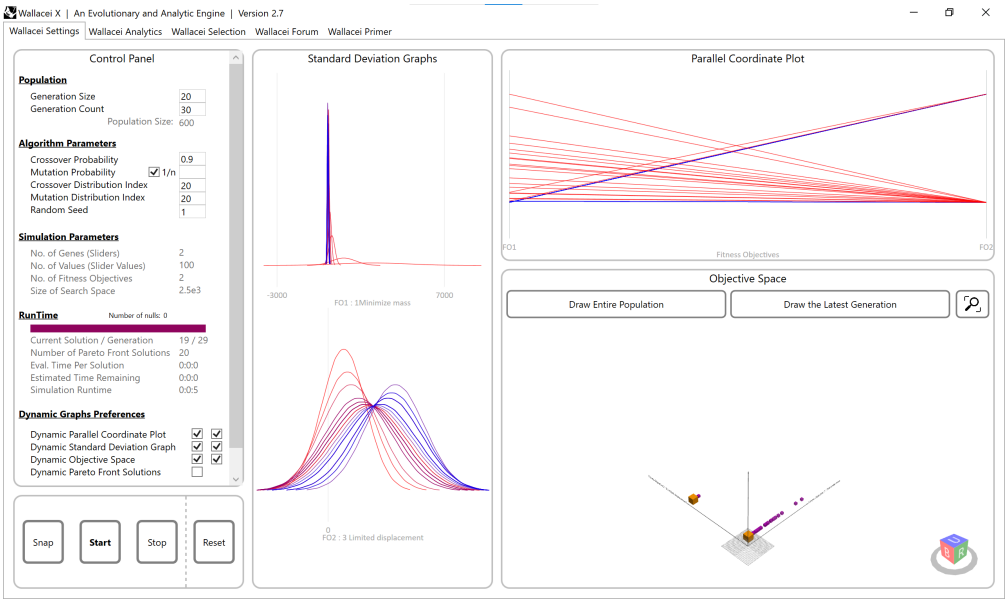


Figure 4.39: Wallacei Settings for the structural optimization of a rectangular beam

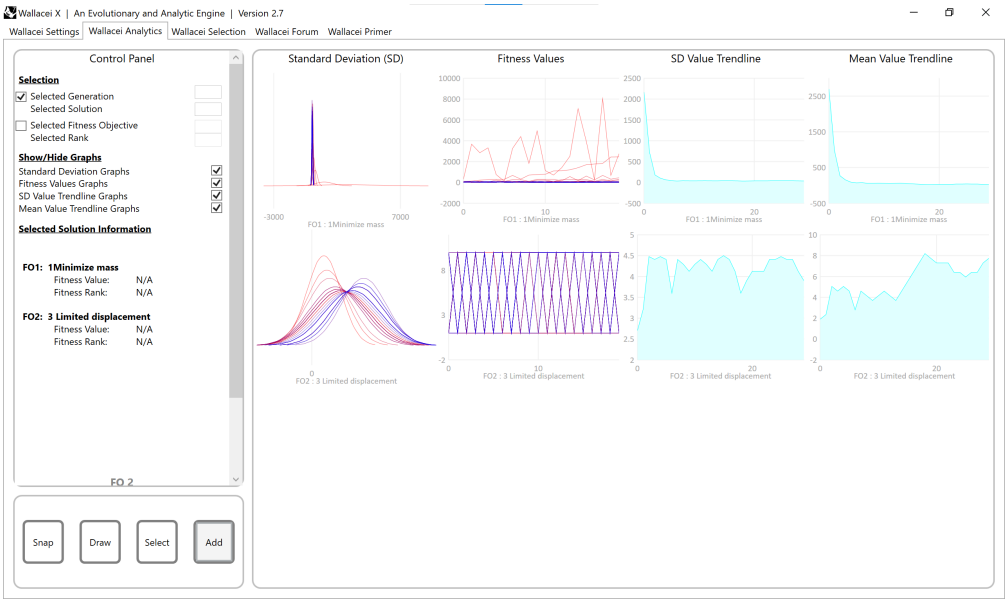


Figure 4.40: Wallacei Analytics for the structural optimization of a rectangular beam

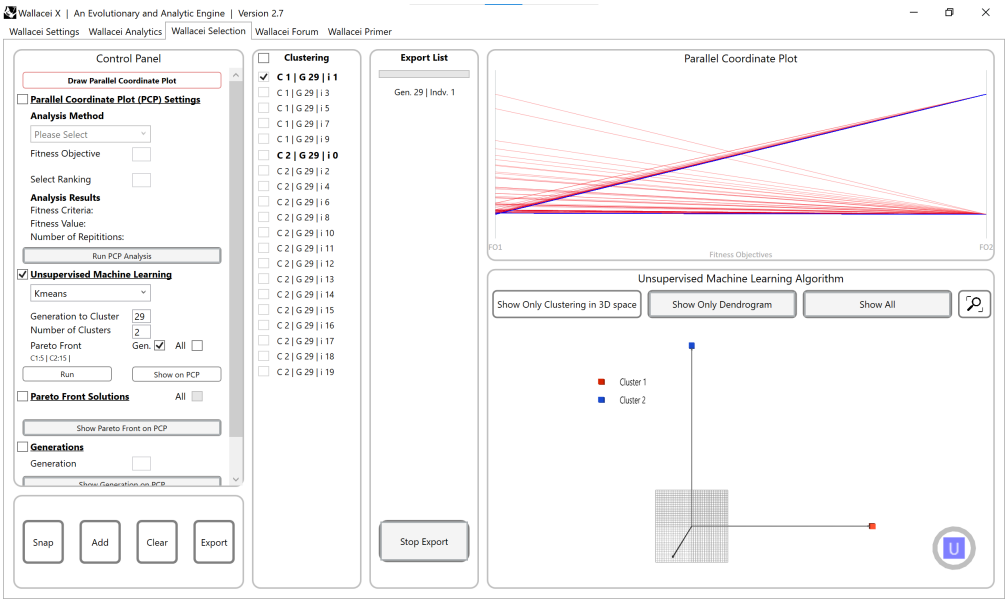


Figure 4.41: Wallacei Selection for the structural optimization of a rectangular beam

Shade optimization analysis

Because we add an objective, the Pareto front gets much larger than for the structural optimization, we will use a population with a generation size of 50 individuals and 100 generations. The simulation lasted for 3 minutes and 44 seconds. Unlike the first shade optimization with the IPE beam, not all solutions are part of the Pareto front.

We can see on tab 2, see figure 4.45, a shift to the right for the standard deviation chart of the first objective (mass minimization) and a shift to the left for the second (shadow maximization). This is normal because the two objectives are opposites to one another.

We also notice a slight flattening of the curve in both cases. Meaning an increase in variation in the solutions, this is due to the fact that the Pareto front is wide and therefore the solution range in each generation is wide too. We can see for the same reason that the fitness values are chaotic. The mean mass stabilizes around 3,500 kg and its standard deviation between 3,000 and 3,500 kg. The mean shaded area stabilizes between -2.4 and -2.2 m^2 and its standard deviation between 1.1 and 1.2 m^2.

The trenlines for the third objective (deflection), show no sign of convergence its fitness values however are well structured due to the fact that there are only two possible values. By using the Kmeans and the *average of fitness ranks* method from tab 3, see figure 4.46, we export the Pareto solutions from the last generation that respect the deflection constraint by creating two clusters, and the solution with the best average fitness rank from the entire population.

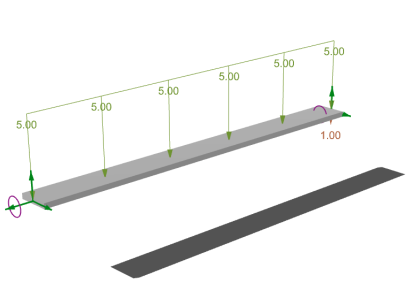
From the exported solutions of figure 4.42, we are selecting three solutions: the lightest, the largest shaded area and the best average fitness rank. The properties of these solutions can be seen on table 4.10, and a perspective view can be seen on figure 4.43.



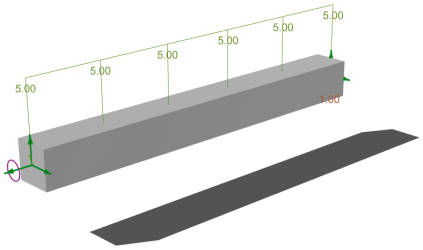
Figure 4.42: Top view of the result of the shade optimization of a rectangular beam

	Solution	Height $[cm]$	Width $[cm]$	Mass $[kg]$	Shaded Area $[m^2]$
Lightest beam	{99;14}	7	43	1,181	2.33
Largest shaded area	{99;1}	50	50	9,813	3.85
Average of fitness ranks	{7;41}	7	50	1,374	2.69

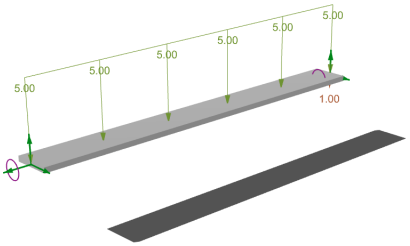
Table 4.10: Properties of the selected solutions for the shade optimization of an rectangular beam



(a) Lightest rectangular beam



(b) Largest shaded area for a rectangular beam



(c) Best average fitness rank for a rectangular beam

Figure 4.43: Perspective view of the selected solutions for the shade optimization of an rectangular beam

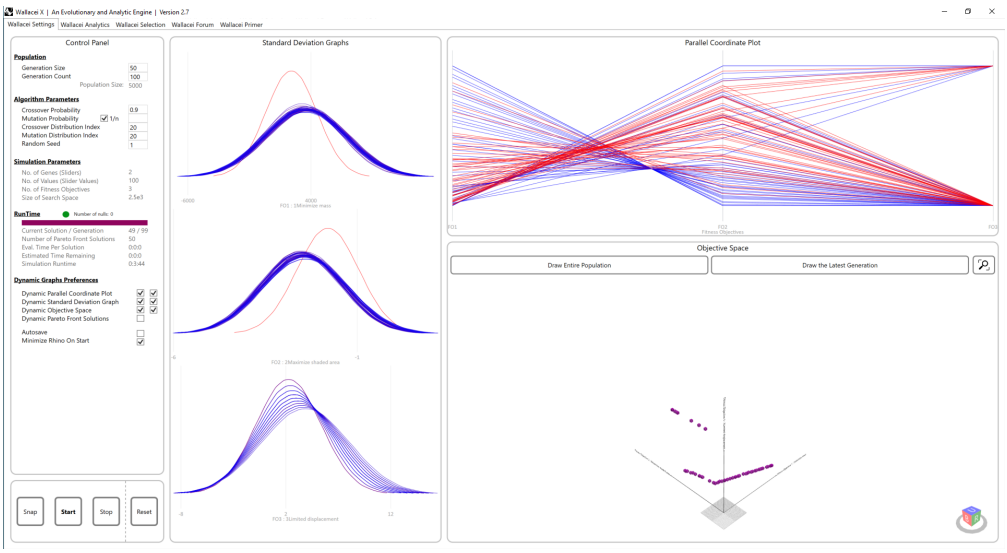


Figure 4.44: Wallacei Settings for the shade optimization of a rectangular beam

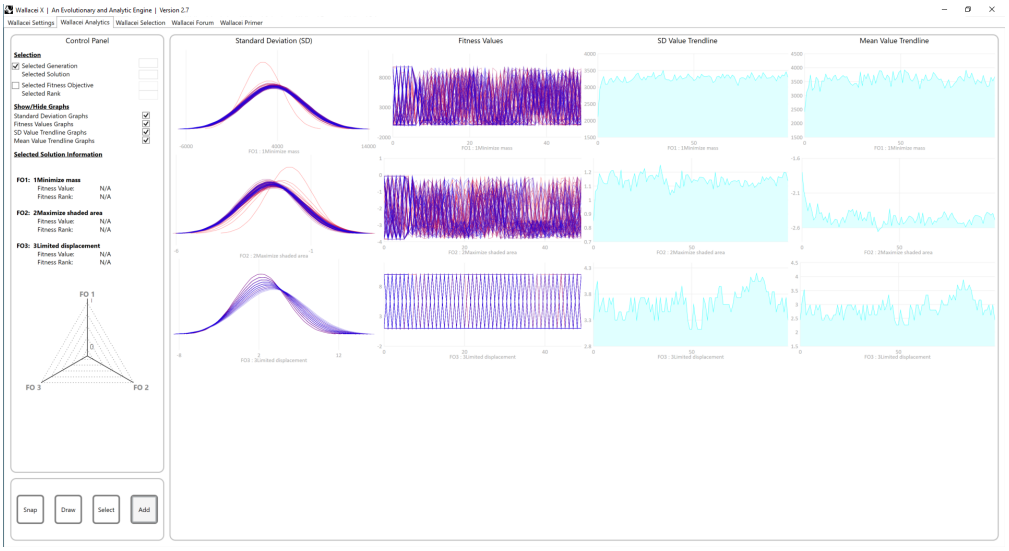


Figure 4.45: Wallacei Analytics for the shade optimization of a rectangular beam

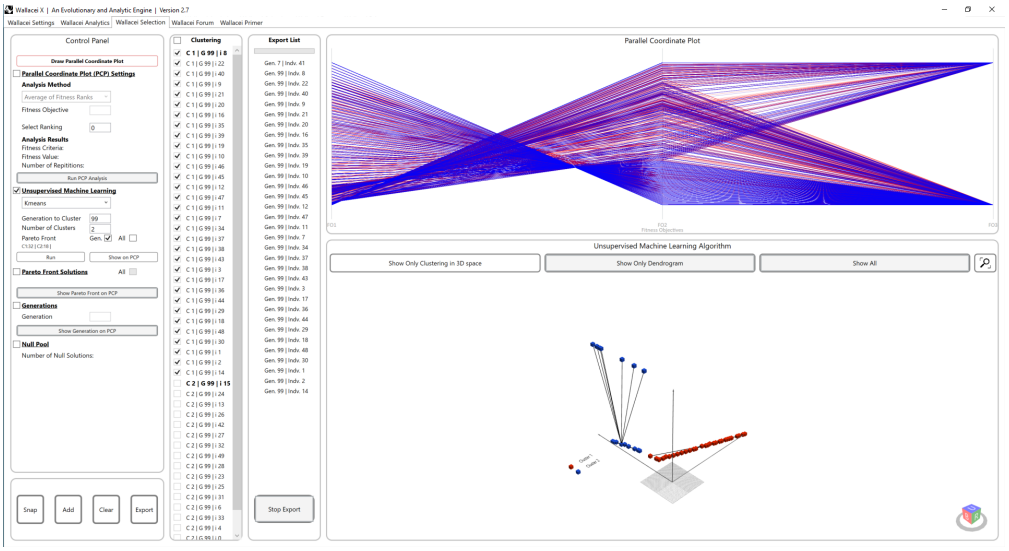


Figure 4.46: Wallacei Selection for the shade optimization of a rectangular beam

Chapter 5

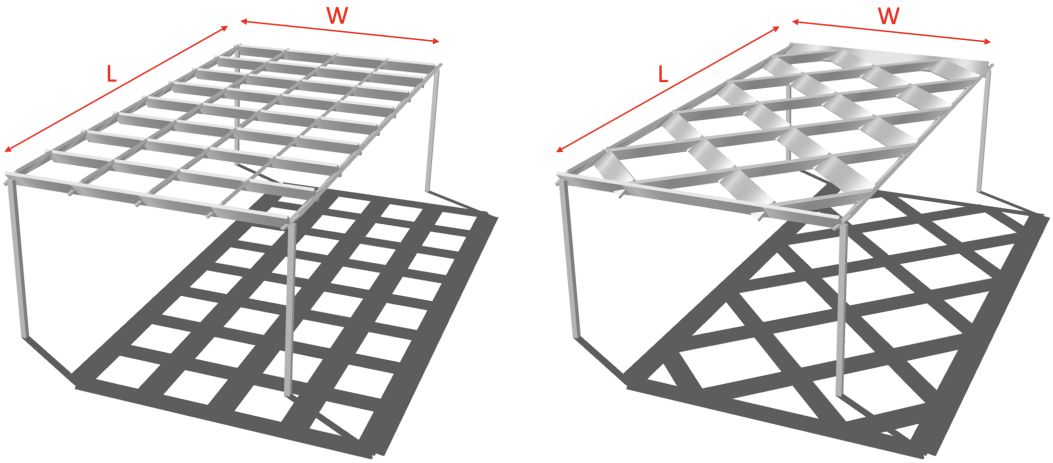
Optimization of an urban canopy

Following the analysis done in section 4.5 and using the same modeling method, we will in this chapter model and optimize urban canopies. We will be optimizing canopies of various sizes first with a structural optimization then with a shaded area optimization. For the structural optimization we will minimize the mass of the canopy while respecting a deflection constraint of $L/200$. $L/200$ is the maximum deflection authorized for a secondary beam[68]. As our structure is not made to be walked upon, we consider our beams as being secondary beams. For the shaded area optimization, we will maximize the shaded area produced by the canopy while minimizing its mass and respecting the deflection constraint. We will call the shaded area to mass ratio, the efficiency of the canopy. The larger the efficiency, the better.

5.1 Modelization of an urban canopy

For our urban canopy model, that can be seen on figure 5.1, we have a rectangular structure of length L and width W with a pinned support placed on each of the four corners. The number of support is fixed and we won't be dimensioning them in this thesis. We then add M beams in the vertical direction and N beams horizontal direction following either a diamond pattern or a rectangular pattern. These beams have an height h and the width w and are tilted of an angle α. All of the elements will be made out of steel S235. The goal of the optimization will be to modify specific parameters in order to optimize the canopy structurally or to maximize its shaded area. These are the parameters that will be modified during the optimization process:

- Pattern: the canopy has two possible patterns for the disposition of the beams. The beams can either be disposed in a rectangular grid or in a diamond grid see figure 5.1.



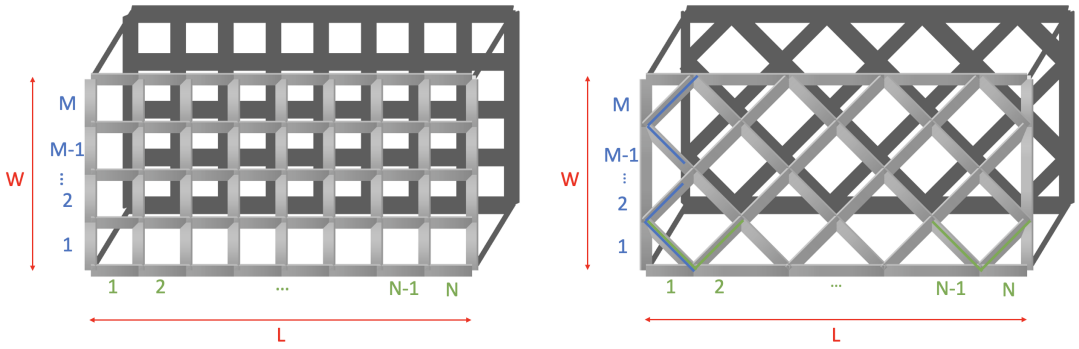
(a) Rectangular grid (b) Diamond grid

Figure 5.1: Perspective view of our canopy model

- Beam spacing: if we have a rectangular grid we can modify the number M and N of beam spacing in the vertical and horizontal directions, see figure 5.2a. If we have a diamond grid, we can modify the number of beam M and N in the vertical and horizontal directions.
- Cross-section: the beam's height h and width w can be modified and selected from the ArcelorMittal cross cross-section catalogue[73] in the flat bars section see figure 5.6. We made the simplification to allow all combination of width and thicknesses. See figure 5.3
- Beam angle: the beam can all be inclined by an angle α from 0 to 45°. See figure 5.3

This results in 6 genes allowing changes in the characteristics of the canopy.

The changes applied to the method described in section 4.5 are explained in the followings sub-sections.



(a) Rectangular grid (b) Diamond grid

Figure 5.2: Top view of our canopy model

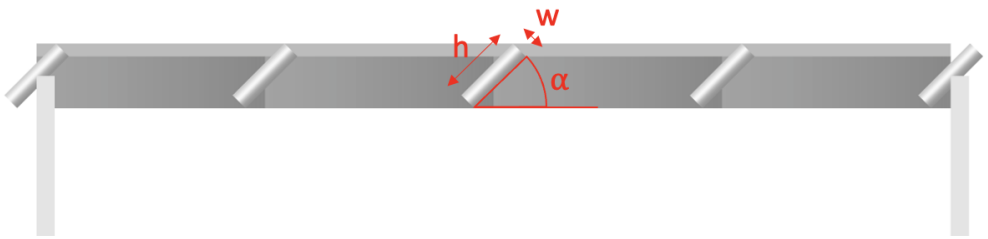


Figure 5.3: Sectional view of our canopy model

5.1.1 Geometry

For the geometry of the canopy, we use the *Rectangle* component to make a rectangle of length L and width W and input this rectangle into a *Surface* parameter. We want two different patterns for the structure were each direction of beam are separated into different sets of beams, we will therefore have two different path:

- For the rectangular grid pattern, see figure 5.2a, we will input the previously defined surface into a *Mesh Surface* component. We will also input two sliders that we will call *wlc3_U Div* and *wlc4_V Div* that will determine the number of spacing N and M in the horizontal and vertical directions. With $1 \leq N \leq 3L$ and $1 \leq M \leq 3W$ where L and W are the length and width

of the rectangle respectively. Meaning that there will be a maximum of one beam every 33 *cm*. These sliders will also be used for the second pattern.

We will then use the *Mesh Edges* component and input the *naked edges* and *interior edges* into a flattened *Curve* parameter that we will call *Rectangular Structural Lines*.

For the support points, we use the *Explode* component on the rectangular surface which gives us the four segments of the rectangle and input those segments into the *End Points* component. We then input the starting points into a *Point* component that we call *Rectangle Support Points*. We also retrieve the mesh from the *Mesh surface* that we keep in a *Mesh* component that we call *Mesh rectangle*.

- For the diamond grid pattern, see figure 5.2b, we will use the *Diamond Panels* component, see figure 5.4, from a Grasshopper plugin called LunchBox.



Figure 5.4: Diamond Panels component

We input into it the rectangular surface and *wlc3_U Div* and *wlc4_V Div*. It will fill the area with a diamond shape pattern with N and M diagonals separating the horizontal and vertical directions where N and M are the values given from *wlc3_U Div* and *wlc4_V Div*. We input both outputs of the *Diamond Panels* component into the *Brep Edges* component and then all the naked edges into the *Explode* component to explode the different diamond multi-curves. We use the *removeDuplicateLines* from Karamba3D. We input and flatten into it the segments to have only unique lines. We input the resulting lines into a *Curve* component that we call *Diamond Structural Lines*.

For the supports, we can use the support point used in for the rectangular grid. We retrieve the mesh from the *Diamond Panels* that we keep in a *Mesh* component that we call *Mesh diamond*.

We now have to define a method to select one of the two pattern types. We therefore use *Entwine* components that will flatten and combine a collection of data

streams. We make sure to input into the branch {0,0} data from the rectangular grid and in the branch {0,1} data from the diamond grid. We will use two *Entwine* component, the first one for the *Rectangular Structural Lines* and the *Diamond Structural Lines*, and the second one for the *Mesh rectangle* and *Mesh diamond*. The supports don't need to be entwined because they are the same in both cases.

By using the *Tree Statistics* component, on one of the *Entwine* outputs, we get the different paths {0,0} and {0,1}. By using the *List Item* component, we are able to select one of the path using a number slider that we call *wlc_6Pattern type index* is composed of integer that goes between 0 and 1 because of the two different patterns. We use 2 *Tree Branch* component, and using the selected path, we are able to retrieve the corresponding structural lines and mesh. We input the structural lines in the *Line to Beam* component, the support points in a *Pinned Support* component.

For the mesh, we input it into the *Loads* component using the *MeshLoad Const* type of load to have a punctual loads uniformly distributed on the entire structure as can be seen on figure 5.5. We use a load of 1 kN/m^2 to take into account eventual loads that could be applied to the structure.

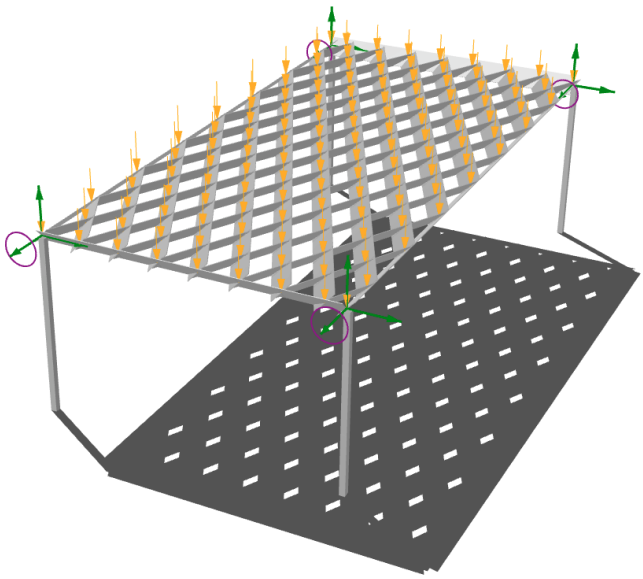
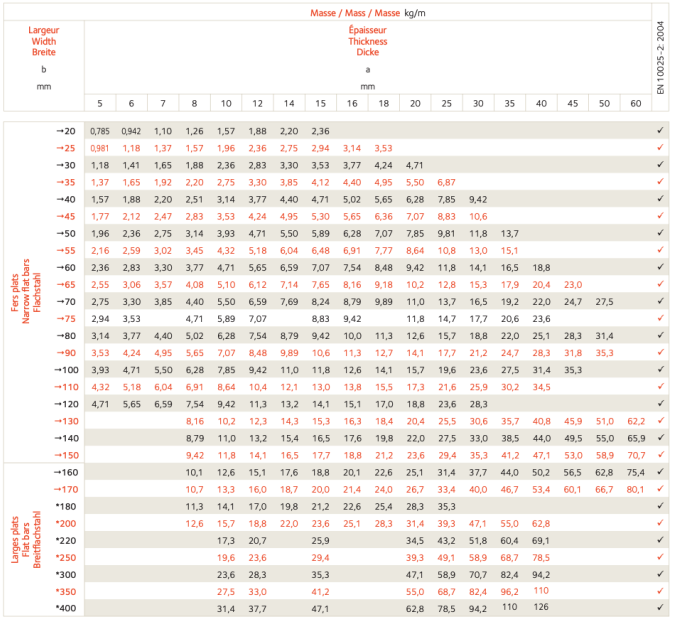


Figure 5.5: Load distribution on a canopy

5.1.2 Cross-section

For the cross-section, see figure 5.3, we create a list with all the widths and a list with all thicknesses available on the flat bars section ArcelorMittal cross-section catalogue[73] see figure 5.6. We then use two sliders going from zero to N-1 where N



Masse / Mass / Masse kg/m

Largeur Width Breite b mm	Épaisseur Thickness Dicke a mm																		EN 10025-2: 2004
	5	6	7	8	10	12	14	15	16	18	20	25	30	35	40	45	50	60	
Fers plats Narrow flat bars Flachstahl																			
→20	0,785	0,942	1,10	1,26	1,57	1,88	2,20	2,36											✓
→25	0,981	1,18	1,37	1,57	1,96	2,36	2,75	2,94	3,14	3,53									✓
→30	1,18	1,41	1,65	1,88	2,36	2,83	3,30	3,53	3,77	4,24	4,71								✓
→35	1,37	1,65	1,92	2,20	2,75	3,30	3,85	4,12	4,40	4,95	5,50	6,87							✓
→40	1,57	1,88	2,20	2,51	3,14	3,77	4,40	4,71	5,02	5,65	6,28	7,85	9,42						✓
→45	1,77	2,12	2,47	2,83	3,53	4,24	4,95	5,30	5,65	6,36	7,07	8,83	10,6						✓
→50	1,96	2,36	2,75	3,14	3,93	4,71	5,50	5,89	6,28	7,07	7,85	9,81	11,8	13,7					✓
→55	2,16	2,59	3,02	3,45	4,32	5,18	6,04	6,48	6,91	7,77	8,64	10,8	13,0	15,1					✓
→60	2,36	2,83	3,30	3,77	4,71	5,65	6,59	7,07	7,54	8,48	9,42	11,8	14,1	16,5	18,8				✓
→65	2,55	3,06	3,57	4,08	5,10	6,12	7,14	7,65	8,16	9,18	10,2	12,8	15,3	17,9	20,4	23,0			✓
→70	2,75	3,30	3,85	4,40	5,50	6,59	7,69	8,24	8,79	9,89	11,0	13,7	16,5	19,2	22,0	24,7	27,5		✓
→75	2,94	3,53		4,71	5,89	7,07		8,83	9,42		11,8	14,7	17,7	20,6	23,6				✓
→80	3,14	3,77	4,40	5,02	6,28	7,54	8,79	9,42	10,0	11,3	12,6	15,7	18,8	22,0	25,1	28,3	31,4		✓
→90	3,53	4,24	4,95	5,65	7,07	8,48	9,89	10,6	11,3	12,7	14,1	17,7	21,2	24,7	28,3	31,8	35,3		✓
→100	3,93	4,71	5,50	6,28	7,85	9,42	11,0	11,8	12,6	14,1	15,7	19,6	23,6	27,5	31,4	35,3			✓
→110	4,32	5,18	6,04	6,91	8,64	10,4	12,1	13,0	13,8	15,5	17,3	21,6	25,9	30,2	34,5				✓
→120	4,71	5,65	6,59	7,54	9,42	11,3	13,2	14,1	15,1	17,0	18,8	23,6	28,3						✓
→130				8,16	10,2	12,3	14,3	15,3	16,3	18,4	20,4	25,5	30,6	35,7	40,8	45,9	51,0	62,2	✓
→140				8,79	11,0	13,2	15,4	16,5	17,6	19,8	22,0	27,5	33,0	38,5	44,0	49,5	55,0	65,9	✓
→150				9,42	11,8	14,1	16,5	17,7	18,8	21,2	23,6	29,4	35,3	41,2	47,1	53,0	58,9	70,7	✓
Larges plats Flat bars Breitflachstahl																			
→160				10,1	12,6	15,1	17,6	18,8	20,1	22,6	25,1	31,4	37,7	44,0	50,2	56,5	62,8	75,4	✓
→170				10,7	13,3	16,0	18,7	20,0	21,4	24,0	26,7	33,4	40,0	46,7	53,4	60,1	66,7	80,1	✓
*180				11,3	14,1	17,0	19,8	21,2	22,6	25,4	28,3	35,3							✓
*200				12,6	15,7	18,8	22,0	23,6	25,1	28,3	31,4	39,3	47,1	55,0	62,8				✓
*220					17,3	20,7		25,9			34,5	43,2	51,8	60,4	69,1				✓
*250					19,6	23,6		29,4			39,3	49,1	58,9	68,7	78,5				✓
*300					23,6	28,3		35,3			47,1	58,9	70,7	82,4	94,2				✓
*350					27,5	33,0		41,2			55,0	68,7	82,4	96,2	110				✓
*400					31,4	37,7		47,1			62,8	78,5	94,2	110	126				✓

Figure 5.6: ArcelorMittal flat bars catalog

is the size of each list. We call these slider *wlc_1Width Index* and *wlc_2Thickness Index*. By using the sliders and *List Item* components, we will be able to select one width and one thickness from the lists. We will use the *Cross Section* component using a trapezoid type and use the selected width as the height h of the cross-section, and the selected thickness for the upper and lower width w.

To rotate the cross-sections of an angle α around their x axis, we use the *Series* component to create a list with every multiple of five from 0 to 45°. We then create a slider that we call *wlc_5Beam angle index* to select one of the angle using the *List Item* component. To apply the angle to the beams, we use the *Orientate Elem* component, see figure 5.7, after the *Line to Beam* component.

We will first input in the *X-Orientation* the position {-1,0,0} that has been found manually to ensure that the beam of same orientation also have the same direction and that when applying the angle, the shaded area will be maximized. Otherwise, some beams would be rotating in opposite directions. We now input the angle in the *Alpha* input of the *Orientate Elem* component.

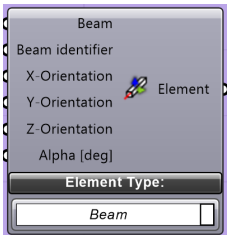


Figure 5.7: Orientate Elem component

5.1.3 Shaded area

In order to calculate the shaded area, the *LB Analysis Period* is now being used instead of the *LB Calculate HOY* to maximize the shaded area over a period of time of the day instead of at a specific time. This will give us more accurate results. The shadow will be measured on every hours from 12h to 16h on the 21st of July, the day of the summer's solstice. The sum of the shadows will be maximized. However only the 14h shadow will be displayed on the rhino interface.

We will also use the expression $round(x/5)$ in order to have the average shaded area. Rounding the area, will permit us to decrease significantly the number of Pareto solutions and limit the mass of the canopy, otherwise, the simulations would propose canopies with ever increasing mass in order to gain a few cm^2 of shaded area. Choosing the average shaded area instead of the total shaded area, permits us to decrease the size of the Pareto front even further.

5.1.4 Stress

In this section, we will have to verify that the structures do not cross the stress limits of steel S235. To do so, we will calculate the maximal shear stress and normal stress. The normal stress for a beam subject to bending and compression as seen on figure 5.8 is calculated by the following formula:

$$\sigma_{tot}(y,z) = \pm\frac{N}{A} \pm \frac{M_z}{I_z}y \pm \frac{M_y}{I_y}z \tag{5.1}$$

With N the normal force, A the area of the cross-section, M the bending moment around the Y and Z axis, I the moment of inertia of the cross section around the Y and Z axis and y and z are the distance from the neutral axis in the horizontal and vertical directions at which the normal stress is calculated. We therefore have the maximal normal stress for:

$$\sigma_{max} = \sigma(y = b/2, z = h/2) = \pm\frac{N}{A} \pm \frac{M_z}{I_z}\frac{b}{2} \pm \frac{M_y}{I_y}\frac{h}{2} \tag{5.2}$$

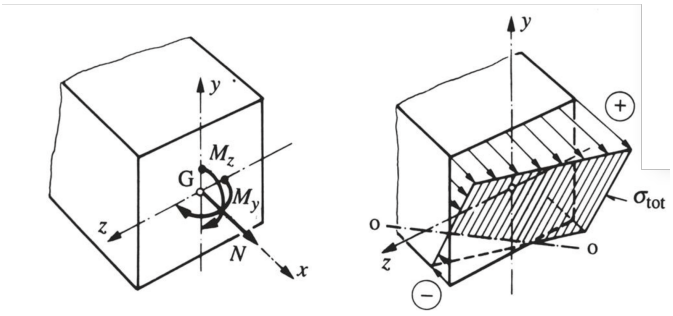


Figure 5.8: Normal stress of a beam subject to bending and compression[68]

For our rectangular cross-sections, we have has inertia $I_y = \frac{bh^3}{12}$ and $I_z = \frac{hb^3}{12}$ with h the height and b the width of the cross-section.

For the shear stress, we have shear stress due to shear force and shear stress due to torsion. Shear stress due to shear force for a rectangular section is calculated with the following formulas:

$$\tau(z) = \frac{V_z}{2I_y}(\frac{h^2}{4} - z^2) \tag{5.3}$$

$$\tau(y) = \frac{V_y}{2I_z}(\frac{b^2}{4} - y^2) \tag{5.4}$$

Where V_z and V_y is the shear force in the Z and Y directions. We find that $\tau_{z,max} = \tau(z=0) = \frac{V_z}{2I_y}\frac{h^2}{4} = \frac{3V_z}{2bh}$ and $\tau_{y,max} = \tau(y=0) = \frac{V_y}{2I_z}frac b^2 4 = \frac{3V_y}{2bh}$.

The maximal shear stresses due to torsion on each faces of a rectangular section is calculated with the following formula:

$$\tau_{z,max} = \tau(z=0; y=\pm\frac{b}{2}) = \frac{3T}{b^2h} \tag{5.5}$$

$$\tau_{y,max} = \tau(z=\pm\frac{h}{2}; y=0) = \frac{3T}{h^2b} \tag{5.6}$$

Where T is the torsion. It is maximal at the center of the largest face of the rectangular section. The normal stress is as we can see minimal when the shear stress due to shear force is maximal and vice versa, see figure 5.9.

In order to verify if the stress induced in the beam structure is higher than the stress limit of steel S235 we will use the Tresca criteria which goes as follows:

$$\sqrt{\sigma^2 + 4\tau^2} \leq \frac{f_e}{1.15} \tag{5.7}$$

Where f_e is the rupture limit and is 235 N/mm^2 for steel S235 and 1.15 is the security factor used for steel. In our structure however, the bending moment is

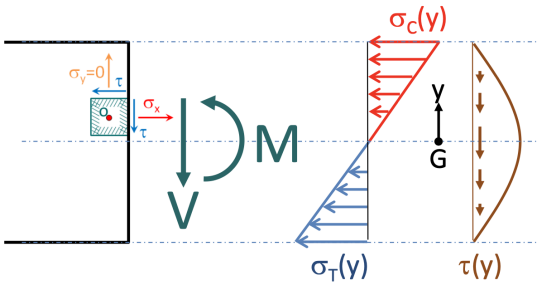


Figure 5.9: Normal stress and shear stress when bending is applied to a beam[68]

maximal near the corners of the rectangular section, where the shear force and torsion are minimal. In addition the normal stress σ_{max} is significantly larger than the combination of the shear stresses τ_max.

Therefore Tresca criteria is maximal a $y = \frac{h}{2}$ and therefore the maximal stress of our structure will have to fulfill the following constraint $\sigma_{max} \leq \frac{f_e}{1,15} = 205N/mm^2$.

To apply this to our structure, we use the *Beam Force* component from which we get normal forces and the bending moments and apply them to the normal stress formula we found earlier using *Expression* components, we make sure that we have all possible combination of + and - signs. We then retrieve the largest absolute stress value in order to verify if there are risks of rupture in the proposed solutions.

In order to verify if the shear stresses could indeed be neglected, we made an optimization of our model with the following objectives: limiting the deflection to $L/200$, limiting the maximal Normal Stress to 205 N/mm^2 while maximizing the shear stress. The two constraints were added because if these constraint are not respected, the maximal shear stress that we would find would have to be rejected any way. The solution we found can be seen on figure 5.10. The maximal shear stress for this canopy is caused by torsion but is significantly smaller than the normal stress: $\tau = 22 \ll \sigma = 186[N/mm^2]$. Moreover and as explained earlier, these stresses are not maximal in the same place. This confirm that we can neglect the shear stresses.

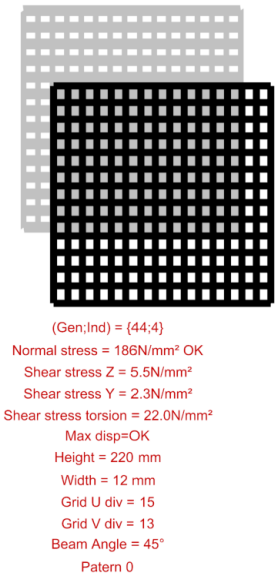


Figure 5.10: Top view of the canopy with the maximal shear stress

5.1.5 Genes

The genes for the optimization will be the following sliders:

- *wlc_1Width index*
- *wlc_2Thickness index*
- *wlc3_U Div*
- *wlc4_V Div*
- *wlc_5Beam angle index*
- *wlc_6Pattern type index*

For the structural analysis, we will ignore the *wlc_5Beam angle index* genes because a 0° angle will be most favorable in a structural point of view.

5.1.6 Fitness objectives

The fitness objectives for the optimization will be the following:

- *wlc_1Minimize mass*
- *wlc_2Maximize shaded area*

- *wlc_3Limited displacement*

The second objective is only used for the shade optimizations. For the limited displacement we had to replace the previously defined *Expression* component by two *Expression* components.

The first one has for expression: $if(x \leq y/200, -y/5, x)$ with x the maximum displacement and y the structure's maximal length.

The second one as for expression: $if(x \leq y/20, x, y/20)$ where x is the output of the first expression and y is the structure's maximal length.

These two expressions permit to separate more easily the solutions respecting the constraint from those who do not. It also helps the simulation to find solutions that respect the constraint when there are only a few of them relatively to the size of the search space.

5.2 Optimization of an urban canopy

We will start with a structural optimization with canopies of various sizes which will then be followed by two shade optimizations. For the shade optimizations, we will first do an optimization with a 5x5m canopy and analyse the evolution of the simulation depending on the population parameters by varying the generation size and count. We will then analyse the impact of the dimensions of the canopy on its different genes.

5.2.1 Structural analysis

In this section, we will do the structural optimization of canopies of 10x5m, 5x5m, 20x2m and 15x10m. We will each time retrieve and present the lightest solution respecting the deflection constraint.

10x5m

For his simulation we have 5 genes, 94 values, 2 fitness objectives, and a search space with around 470k possible solutions. For a generation size of 20 individuals and 50 generations, the simulation lasted for 29 seconds. We can observe on tab 2, see figure A.2, a convergence of the mass trendlines around the 15th generation and around the 20th generation for the deflection trendlines.

From tab 3, see figure A.3, we retrieve 1 Pareto solution appearing 4 times that respects the deflection constraint. The solution is composed of four beams that have 5 mm of width and 110 mm of height. This results to a weight of 129,5 kg.

With the normal stress $\sigma = 8.9\ N/mm^2$, we are well under the rupture limit of steel S235. The canopy can be seen on figure 5.11

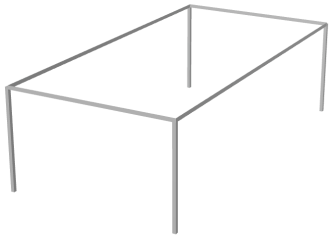


Figure 5.11: Perspective view of the structural optimization of a 10x5m urban canopy

5x5m

For this simulation, we have 5 genes, 79 values, 2 fitness objectives resulting in a search space of around 230k solutions. The run time was of 26 seconds. We can observe on tab 2, see figure A.5, a convergence of the mass trendlines around the 5th generation around the 25th generation for the deflection trendlines.

From tab 3, see figure A.6, we retrieve 1 Pareto solution appearing 5 times that respects the deflection constraint. This solution is composed of 4 rectangular beams with a width of 5 mm and a height of 40 mm resulting in a structure of 31,4 kg. As can be expected, smaller dimensions results in smaller elements. With the normal stress $\sigma = 19.2\ N/mm^2$, we are well under the rupture limit of steel S235. The solution can be seen on figure 5.12.



Figure 5.12: Perspective view of the structural optimization of a 5x5m urban canopy

20x2m

For this simulation we have 5 genes, 115 values, 2 fitness objectives resulting in a search space of around 380k solutions. The run time was of 34 seconds. We can observe on tab 2, see figure A.5, a convergence of the mass trendlines around the 10th generation and around the 25th generation for the deflection trendlines.

From tab 3, see figure A.6, we retrieve 1 Pareto solution appearing 4 times that respects the deflection constraint. The solution is composed of 4 rectangular beams with a width of 5 mm and a height of 350 mm resulting in a structure of 604,5 kg. With the normal stress $\sigma = 0.4\ N/mm^2$, we are well under the rupture limit of steel S235.

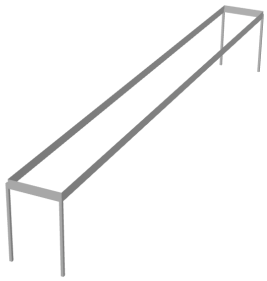


Figure 5.13: Result of the structural optimization of a 20x2m beam structure with 50 generations and 20 individuals per generations

15x10m

For this simulation we have 5 genes, 124 values, 2 fitness objectives resulting in a search space of around 1.4M solutions. The run time was of 55 seconds. We can observe on tab 2, see figure A.5, a convergence of the mass trendlines around the 10th generation and around the 25th generation for the deflection trendlines.

From tab 3, see figure A.6, we retrieve 1 Pareto solution appearing 4 times that respects the deflection constraint. This solution is composed of 5 rectangular beams with a width of 5 mm and a height of 250 mm resulting in a structure of 667,5 kg. The diamond grid is now prioritized to make the lightest structure while respecting the constraint. With the normal stress $\sigma = 19.2\ N/mm^2$, we are well under the rupture limit of steel S235. The solution can be seen on figure 5.14.

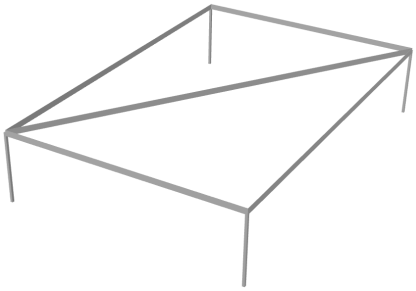


Figure 5.14: Perspective view of the structural optimization of a 15x10m urban canopy

Conclusion

We can see from this analysis, that when we are only optimizing the structure, we will always have the simplest structure possible. The Pareto front is in each cases composed of the lightest canopy and lightest canopy respecting the deflection constraint. The larger the structure is, the larger the elements are. We also notice that the larger the area of the structure is, the more time it takes for the simulation trendline plots to converge.

5.2.2 Shade and population based analysis

For this shade optimization we used a 5x5m canopy to analyse the impact of the population parameters on the results of the simulation. The simulation of a 5x5m canopy has 6 genes, 89 values, 3 fitness objectives resulting in a search space of 2.6M solutions. We will analyse five populations of 10,000 individuals by varying the generation size and the generation count in order to determine which population characteristics are most adapted for our model. These populations will be the following: 10-1000, 50-200, 100-100, 200-50 and 1000-10, where the first number is the generation size and the second number the generation count.

For both of the shade optimizations, we use the Kmeans from the *Wallacei selection* tab to separate the entire population's Pareto front into clusters and retrieve all solutions respecting the deflection constraint. We also use the *average of fitness ranks* method to find the solution with the best average of fitness ranks. We then discard the solutions that have a shaded area $\geq \frac{\text{maximum shaded area}}{2}$ and the duplicate solutions to keep their first occurrence. For a 5x5m canopy, the maximal shaded area is 56 m^2, we will therefore keep all canopies with a shaded area above or equal to 28 m^2.

From these solutions, we then selected 4 canopy types:

- The lightest canopy
- The canopy with the largest shaded area
- The canopy with the best efficiency (the best $\frac{\text{shaded area}}{\text{mass}}$ ratio)
- The canopy with the best average of fitness ranks

We represent graphically and numerically all of these solutions. This is to help the decision maker to choose the right canopy. The decision maker can however choose a canopy out of our selection depending on his own criteria. We have to note that a canopy could fit in multiple canopy type. We also disabled the dynamic graphs of the first tab to reduce significantly the run time.

10-1000

For this first simulation, we will use a generation size of 10 individuals over 1000 generations. The simulation lasted for 2 hours 37 minutes and 50 seconds. We see on tab 2, see figure A.14, that the mean values and standard deviation vary largely from a generation to the next. We can however see that these values area generally limited between boundaries.

From tab 3, see figure A.15, 13 Pareto solutions were found with the cluster 1 (red) that respect the deflection constraint and the minimal shaded area. These solutions can be seen on figure 5.15. All solutions are below the stress rupture limit of steel S235. We will use these 13 solutions in the conclusion.

From these solutions, we will retrieve 4 canopies. Their characteristics can be found in table 5.1, a graphical comparison can be found on figure 5.17 and their visual representations are on figure 5.16.

	Solution	X divisions	Y divisions	Height $[mm]$	Width $[mm]$	Angle $[°]$	Mass $[kg]$	Shaded Area $[m^2]$	Efficiency $[m^2/kg]$	Pattern
Lightest canopy	{47;5}	5	9	300	5	40	842	17	0.020	Diamond
Largest shaded area	{82;1}	12	13	400	7	30	2,967	29	0.010	Rectangular
Best efficiency	{41;7}	6	9	300	5	40	872	18	0.021	Diamond
Average of fitness ranks	{41;5}	11	13	400	5	40	1,651	27	0.016	Diamond

Table 5.1: Properties of the selected solutions for the 10-1000 optimization of a 5x5m canopy

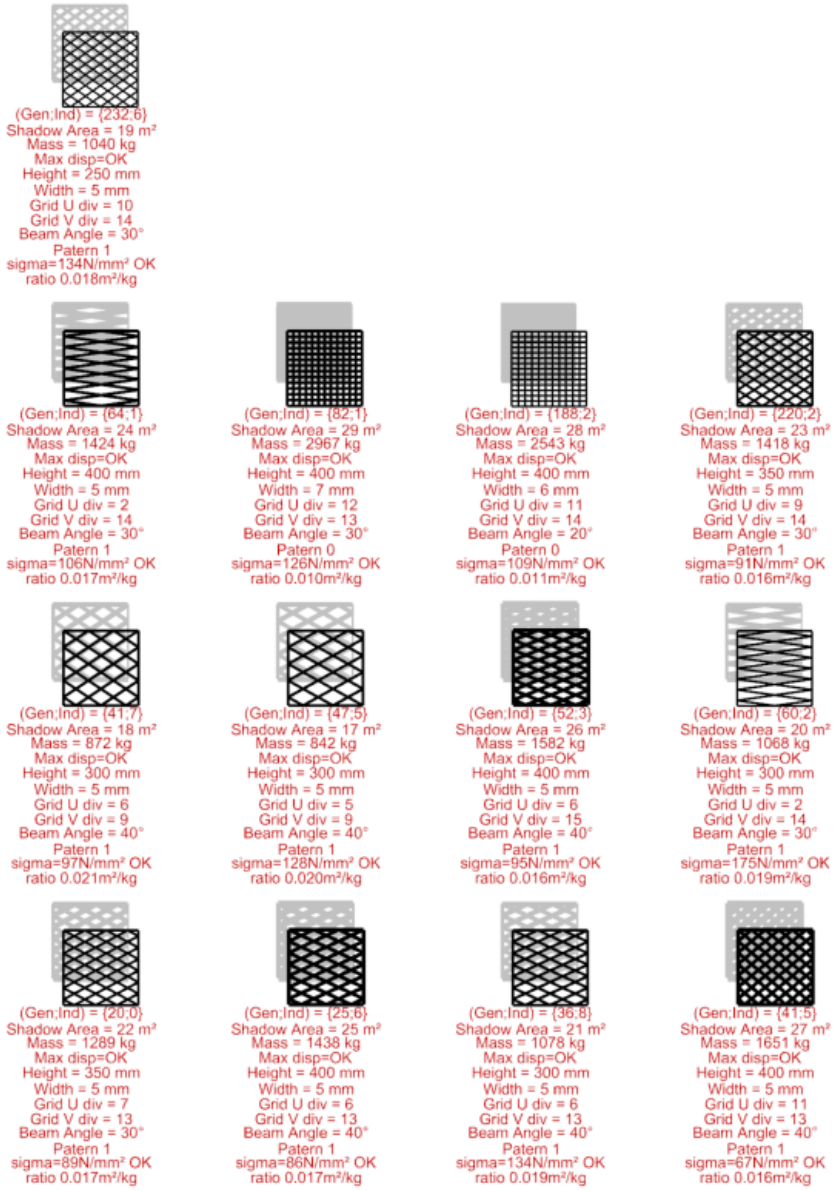
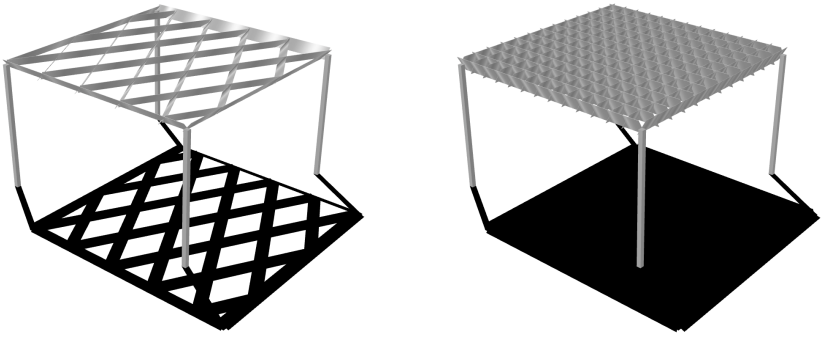
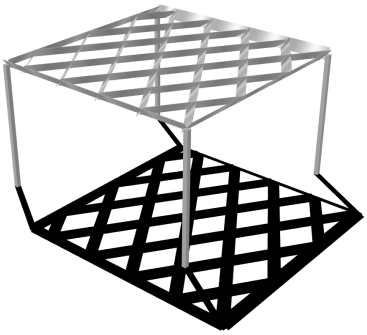


Figure 5.15: Top view of the results of the 10-1000 optimization of a 5x5m canopy



(a) Lightest canopy

(b) Largest shaded area



(c) Best efficiency



(d) Best average of fitness ranks

Figure 5.16: Perspective view of the selected solutions for the 10-1000 optimization of a 5x5m canopy

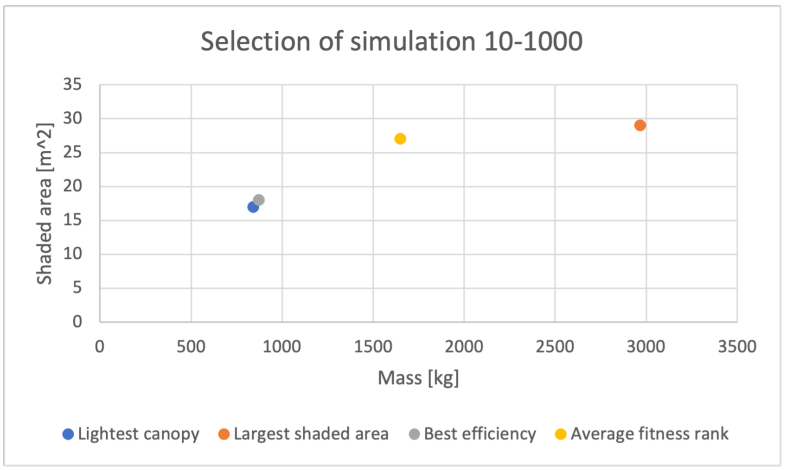


Figure 5.17: Graphical comparison of the selected solutions for the 10-1000 optimization of a 5x5m canopy

50-200

For this simulation, we will use a generation size of 50 individuals over 200 generations. The simulation lasted for 2 hours 38 minutes and 9 seconds. As we can see on tab 2, see figure A.17, a general convergence of the mass and shaded area trendlines. We observe a convergence of the mean mass around 800 kg and its standard deviation around 600 kg, and a convergence of the mean shaded area around -16 m^2 and its standard deviation around 9 m^2. The deflection shows no sign of convergence. We can see from figure 5.18 that no modification were made to the part of the Pareto front that respects the deflection constraint after the 158th generation. We therefore consider the Pareto front to be the true Pareto front or very close to it.

From tab 3, see figure A.18, 15 Pareto solutions were found in cluster 1 (red) that respect the deflection constraint and the minimal shaded area. These solutions can be seen on figure 5.18. All solutions are below the stress rupture limit of steel S235. We will use these 15 solutions in the conclusion.

From these solutions, we will retrieve 4 canopies. Their characteristics can be found in table 5.2, they are compared on the graph of figure 5.20 and their visual representations are on figure 5.19.

	Solution	X divisions	Y divisions	Height $[mm]$	Width $[mm]$	Angle $[°]$	Mass $[kg]$	Shaded Area $[m^2]$	Efficiency $[m^2/kg]$	Pattern
Lightest canopy	{129;45}	5	6	300	5	45	695	15	0.022	Diamond
Largest shaded area	{139;1}	15	15	400	5	45	1,979	29	0.015	Diamond
Best efficiency	{66;11}	6	9	250	5	45	727	16	0.022	Diamond
Average of fitness ranks	{98;3}	5	15	400	5	45	1,555	27	0.017	Diamond

Table 5.2: Properties of the selected solutions for the 50-200 optimization of a 5x5m canopy

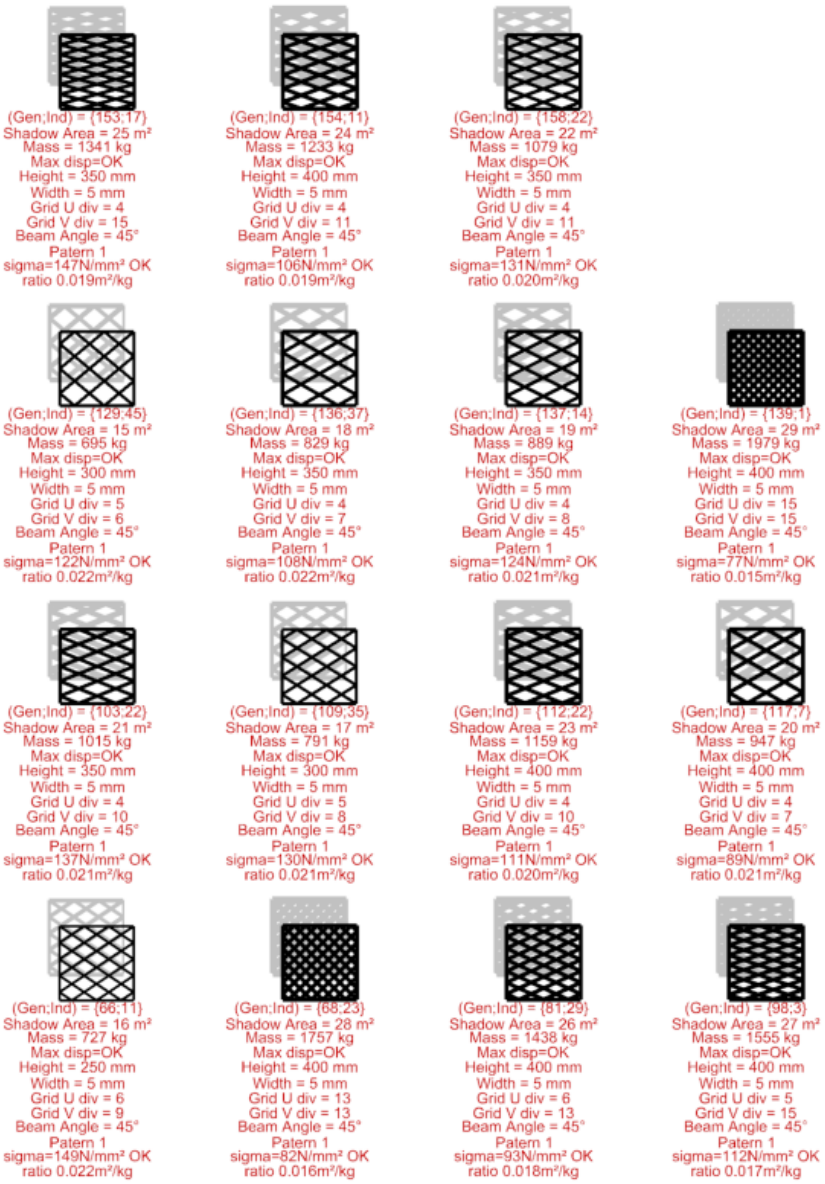
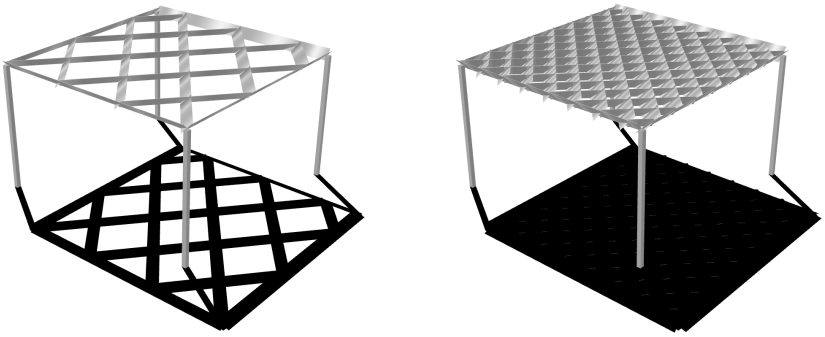
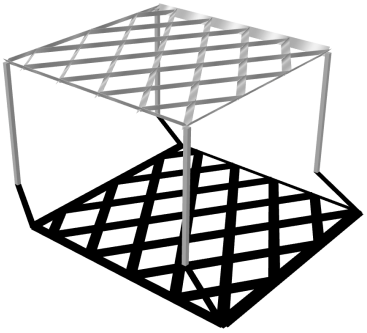


Figure 5.18: Top view of the results of the 50-200 optimization of a 5x5m canopy

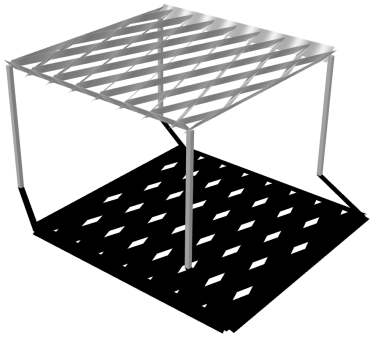


(a) Lightest canopy

(b) Largest shaded area



(c) Best efficiency



(d) Best average of fitness ranks

Figure 5.19: Perspective view of the selected solutions for the 50-200 optimization of a 5x5m canopy

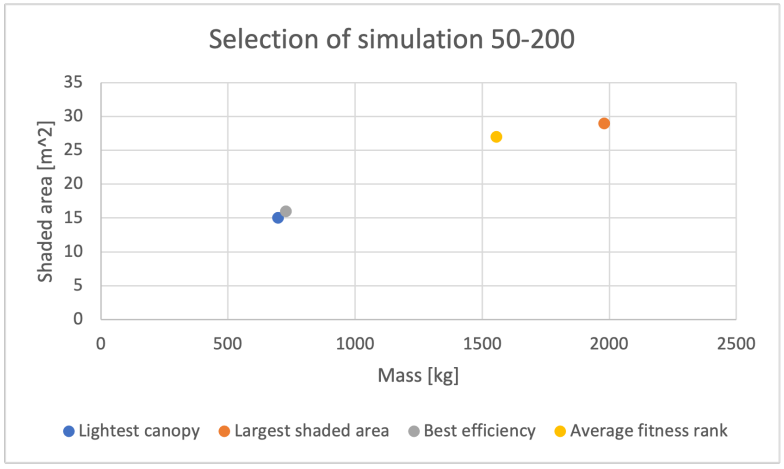


Figure 5.20: Graphical comparison of the selected solutions for the 50-200 optimization of a 5x5m canopy

100-100

For this simulation, we will use a generation size of 100 individuals over 100 generations. The simulation lasted for 2 hours 40 minutes and 35 seconds. We see on tab 2, see figure A.20 a general convergence of the mass and shaded area trendlines. We observe a convergence of the mean mass around 1,200 kg and its standard deviation around 900 kg, and a convergence of the mean shaded area around -18 m^2 and its standard deviation around 9 m^2. The deflection shows no sign of convergence.

From tab 3, see figure A.21, 15 Pareto solutions were found with the cluster 1 (red) that respect the deflection constraint and the minimal shaded area. These solutions can be seen on figure 5.21. All solutions are below the stress rupture limit of steel S235. We will use these 15 solutions in the conclusion.

From these solutions, we will retrieve 4 canopies. Their characteristics can be found in table 5.3, they are compared on the graph of figure 5.23 and their visual representations are on figure 5.22.

	Solution	X divisions	Y divisions	Height $[mm]$	Width $[mm]$	Angle $[°]$	Mass $[kg]$	Shaded Area $[m^2]$	Efficiency $[m^2/kg]$	Pattern
Lightest canopy	{80;6}	5	4	350	5	45	715	15	0.021	Diamond
Largest shaded area	{14;2}	15	14	400	6	30	2,920	29	0.010	Rectangular
Best efficiency	{5;55}	7	11	250	5	45	836	18	0.022	Diamond
Average of fitness ranks	{72;0}	11	13	400	5	45	1,703	28	0.016	Diamond

Table 5.3: Properties of the selected solutions for the 100-100 optimization of a 5x5m canopy

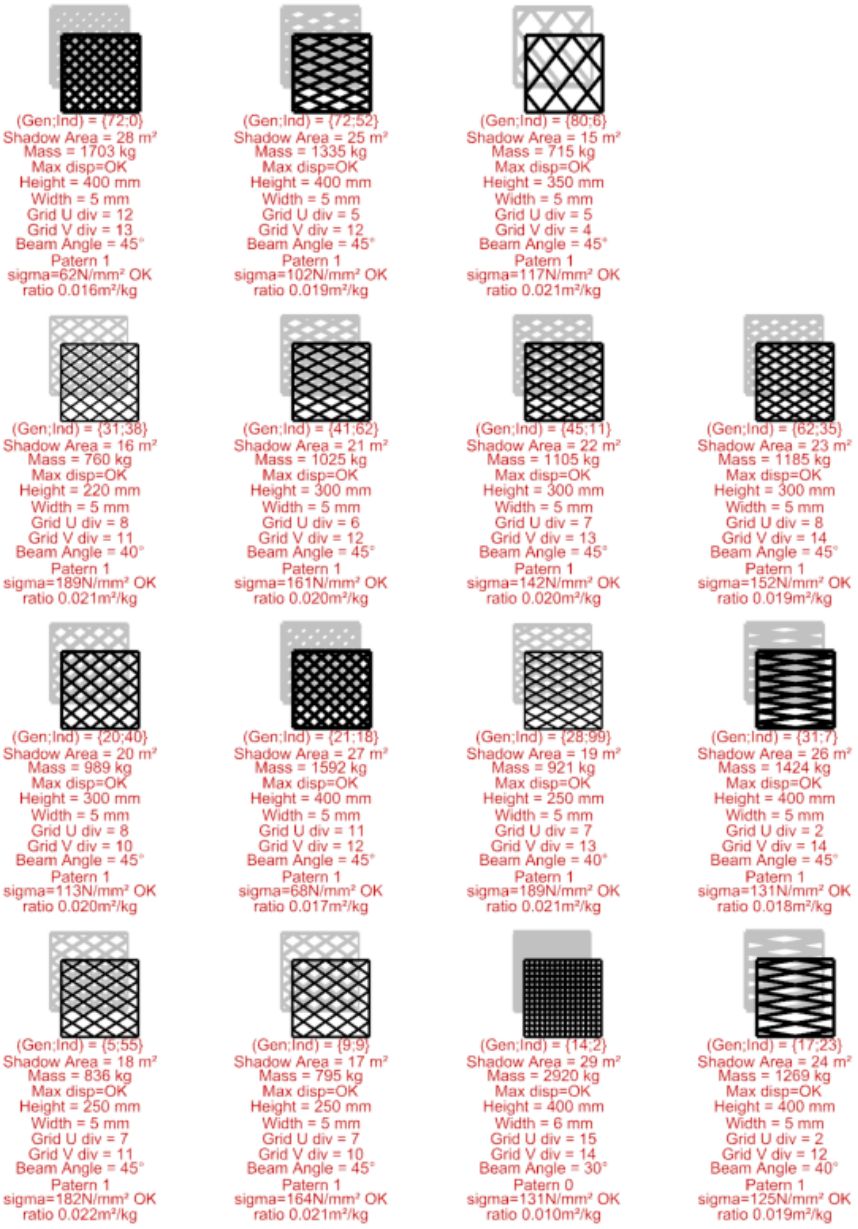
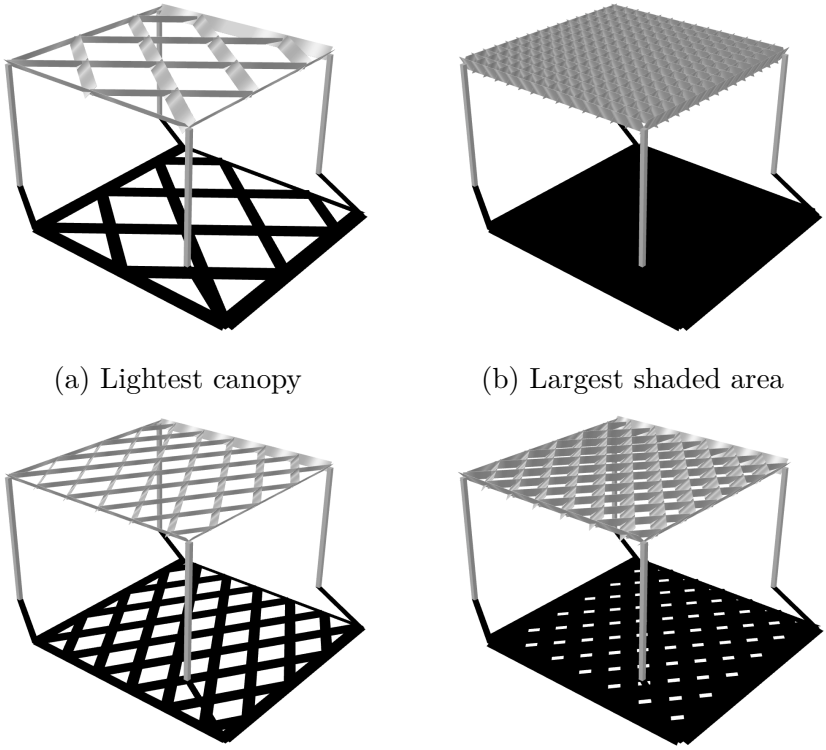


Figure 5.21: Top view of the results of the 100-100 optimization of a 5x5m canopy



(a) Lightest canopy

(b) Largest shaded area

(c) Best efficiency

(d) Best average of fitness ranks

Figure 5.22: Perspective view of the selected solutions for the 100-100 optimization of a 5x5m canopy

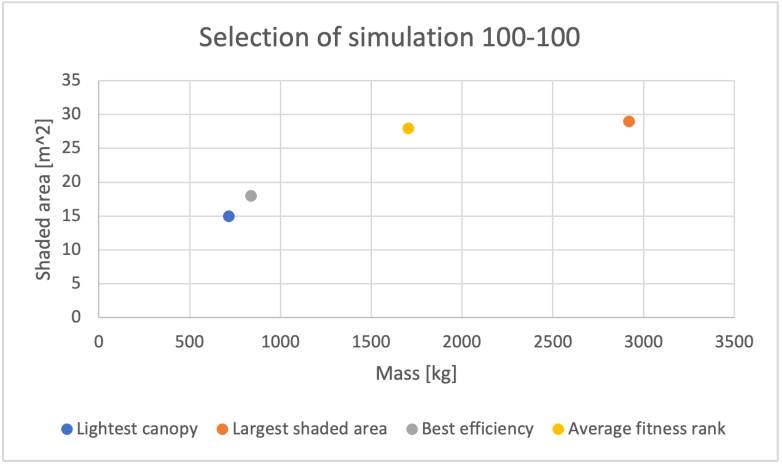


Figure 5.23: Graphical comparison of the selected solutions for the 100-100 optimization of a 5x5m canopy

200-50

For this simulation, we will use a generation size of 200 individuals over 50 generations. The simulation lasted for 2 hours 2 minutes and 5 seconds. We see on tab 2, see figure A.23 a general convergence of the mass and shaded area trendlines. We observe a convergence of the mean mass around 900 kg and its standard deviation around 700 kg, and a convergence of the mean shaded area around -18 m^2 and its standard deviation around 9 m^2. The deflection shows no sign of convergence.

From tab 3, see figure A.24, 15 Pareto solutions were found with cluster 2 (blue) that respect the deflection constraint and the minimal shaded area. These solutions can be seen on figure 5.24. All solutions are below the stress rupture limit of steel S235. We will use these 15 solutions in the conclusion.

From these solutions, we will retrieve 4 canopies. Their characteristics can be found in table 5.4, they are compared on the graph of figure 5.26 and their visual representations are on figure 5.25.

	Solution	X divisions	Y divisions	Height $[mm]$	Width $[mm]$	Angle $[°]$	Mass $[kg]$	Shaded Area $[m^2]$	Efficiency $[m^2/kg]$	Pattern
Lightest canopy	{8;128}	6	5	300	5	45	698	15	0.022	Diamond
Largest shaded area	{40;4}	12	13	400	7	30	2,967	29	0.010	Rectangular
Best efficiency	{12;75}	6	9	250	5	45	727	16	0.022	Diamond
Average of fitness ranks	{43;2}	12	13	400	5	45	1,703	28	0.016	Diamond

Table 5.4: Properties of the selected solutions for the 200-50 optimization of a 5x5m canopy

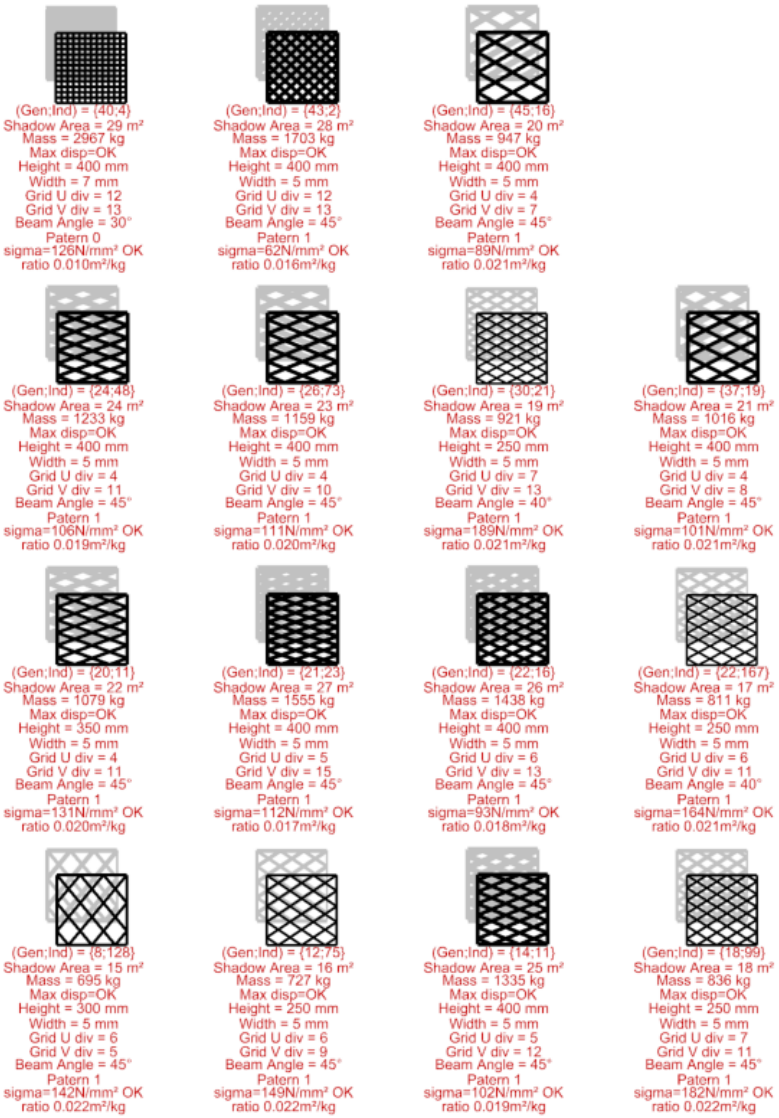
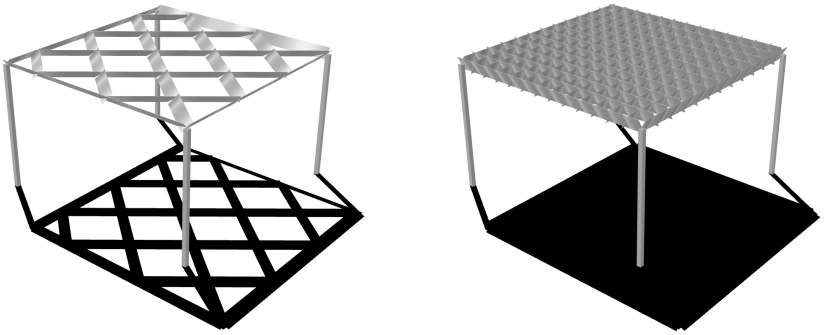
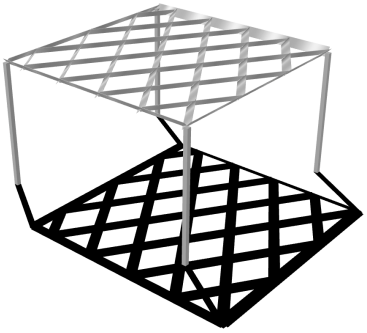


Figure 5.24: Top view of the results of the 200-50 optimization of a 5x5m canopy



(a) Lightest canopy

(b) Largest shaded area



(c) Best efficiency



(d) Best average of fitness ranks

Figure 5.25: Perspective view of the selected solutions for the 200-50 optimization of a 5x5m canopy

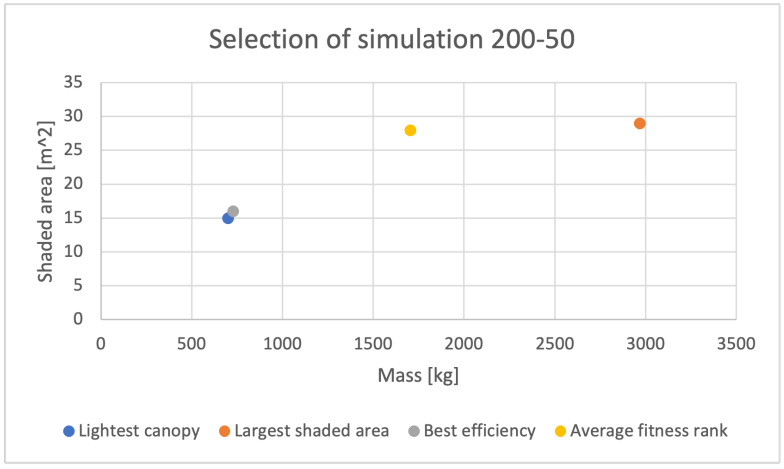


Figure 5.26: Graphical comparison of the selected solutions for the 200-50 optimization of a 5x5m canopy

1000-10

For this simulation, we will use a generation size of 1000 individuals over 10 generations. The simulation lasted for 1 hours 58 minutes and 49 seconds. We see on tab 2, see figure A.26 with only 10 generation it is impossible to tell if there is a real convergence in the trendlines.

From tab 3, see figure A.27, 15 Pareto solutions were found with cluster 3 (green) that respect the deflection constraint and the minimal shaded area. These solutions can be seen on figure 5.27. Solution {9;201} has to be rejected because its stress is above rupture limit of steel S235. We will use these 14 solutions in the conclusion.

From these solutions, we retrieve 3 canopies, their characteristics can be found in table 5.5, they are compared on the graph of figure 5.29 and their visual representations are on figure 5.28.

	Solution	X divisions	Y divisions	Height $[mm]$	Width $[mm]$	Angle $[°]$	Mass $[kg]$	Shaded Area $[m^2]$	Efficiency $[m^2/kg]$	Pattern
Lightest canopy & Best efficiency	{8;258}	4	5	350	5	40	715	15	0.021	Diamond
Largest shaded area	{6;151}	14	15	400	6	30	2,920	29	0.010	Rectangular
Average of fitness ranks	{9;269}	12	13	400	5	45	1,703	28	0.016	Diamond

Table 5.5: Properties of the selected solutions for the 1000-10 optimization of a 5x5m canopy

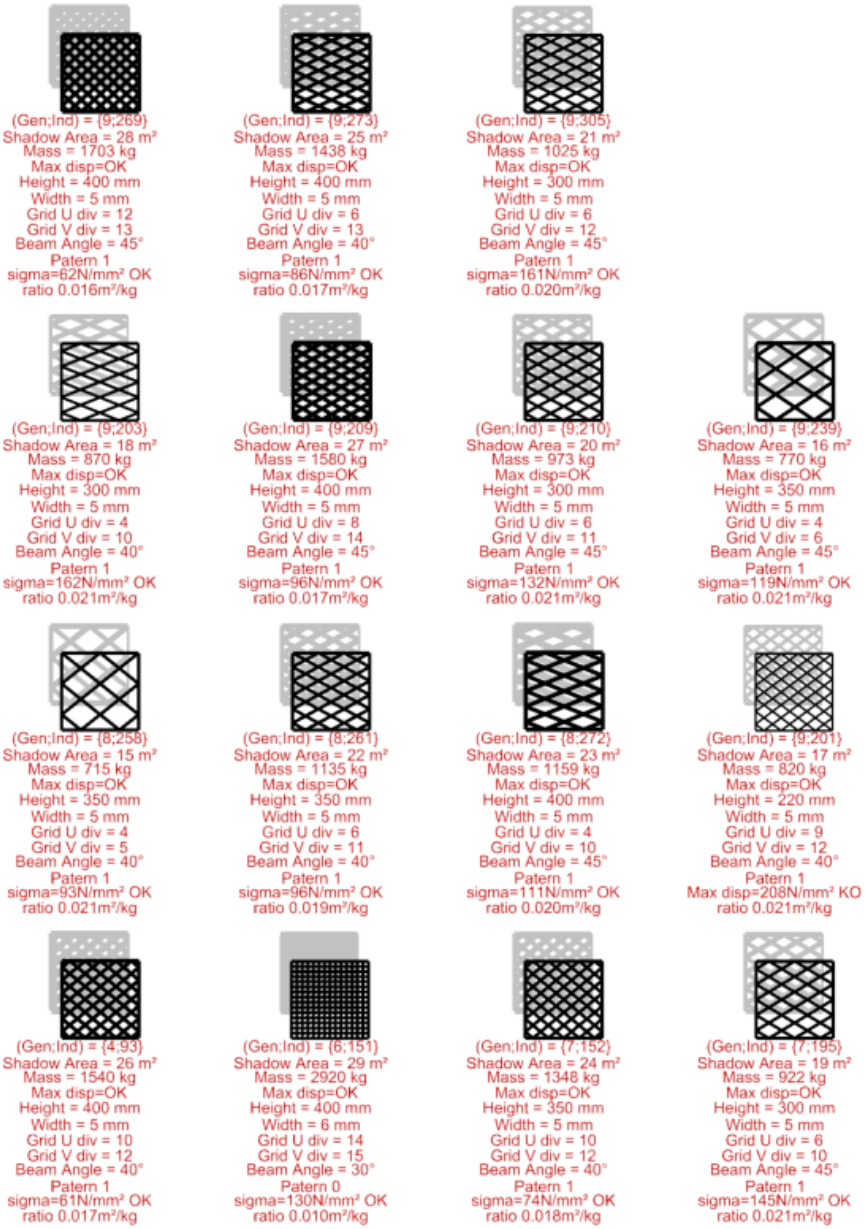
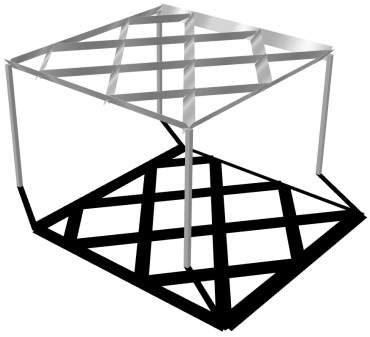
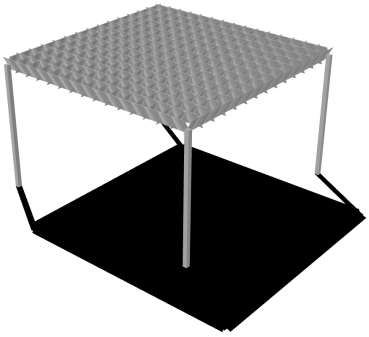


Figure 5.27: Top view of the results of the 1000-10 optimization of a 5x5m canopy



(a) Lightest canopy and best efficiency



(b) Largest shaded area



(c) Best average of fitness ranks

Figure 5.28: Perspective view of the selected solutions for the 1000-10 optimization of a 5x5m canopy

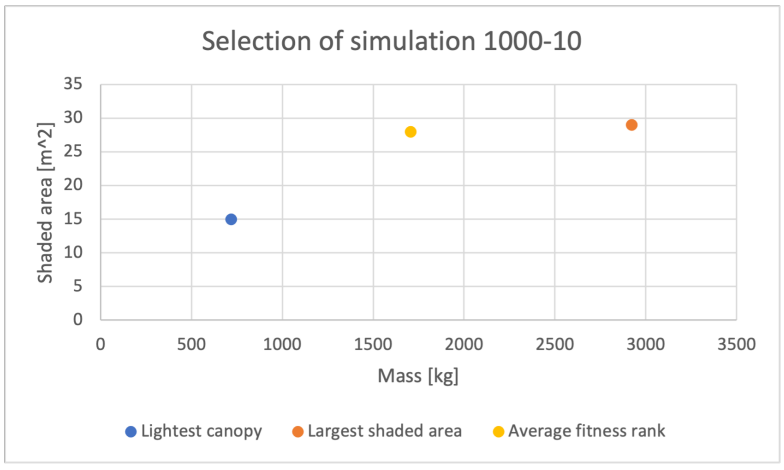


Figure 5.29: Graphical comparison of the selected solutions for the 1000-10 optimization of a 5x5m canopy

Conclusion

For a 5x5m canopy, we have 15 different shaded areas based on the maximal shaded area of 29 m^2 and therefore have a minimal shaded area of 15 m^2. In order to see which population parameters suits our canopy model best, we compared the 5 optimizations results. We have on table 5.6 the 15 available areas and their corresponding masses for each of the optimization. The data from the table are represented graphically on figure 5.30. From the table we determine the rank of each optimization for each of the areas. The optimization with the lightest canopy for a specific area has therefore a rank of 1 for that area and the heaviest canopy has a rank 5. We then give an average rank for each optimizations.

As we can see, the optimization 50-200 has the best average rank with a rank of 1.4, showing that its population parameters are the fittest for the optimization of our canopy model. It is closely followed by the optimization 200-50 with an average rank of 1.6. We then have optimizations 100-100, 1000-10, and 10-1000 with average ranks of respectively 2.5, 3.2 and 4.9. These results shows that there should be a good balance between the generation size and generation count. If the generation size is too small, the simulation will be able to optimize very few solution for each generation, if on the other hand there are few generation, the initial population will be large, but there won't be enough generations to properly optimize the solutions through crossovers and mutations.

We can also see that the most significant difference of mass for an area occurs for the area of 29 m^2 with almost a tonne of difference between the lightest solution and the four other solutions. This difference is achieved by selecting a diamond pattern instead of a rectangular pattern.

We will use the results from this analysis and base the population parameters of the optimizations of the dimensions and shade based analysis on the 50-200 population parameters. We will also use the four selected canopies from the 50-200 optimization.

	10-1000	50-200	100-100	200-50	1000-10
Shaded area $[m^2]$	Mass $[kg]$	Mass $[kg]$	Mass $[kg]$	Mass $[kg]$	Mass $[kg]$
15	/	695	715	695	715
16	/	727	760	727	770
17	842	791	795	811	/
18	872	829	836	836	870
19	1040	889	921	921	922
20	1068	947	989	947	973
21	1078	1015	1025	1016	1025
22	1289	1079	1105	1079	1135
23	1418	1159	1185	1159	1159
24	1424	1233	1269	1233	1348
25	1438	1341	1335	1335	1438
26	1582	1438	1424	1438	1540
27	1651	1555	1592	1555	1580
28	2543	1757	1703	1703	1703
29	2967	1979	2920	2967	2920
Average rank	4.9	1.4	2.5	1.6	3.2

Table 5.6: Numerical comparison of the canopy solutions from the different optimizations of a 5x5m canopy

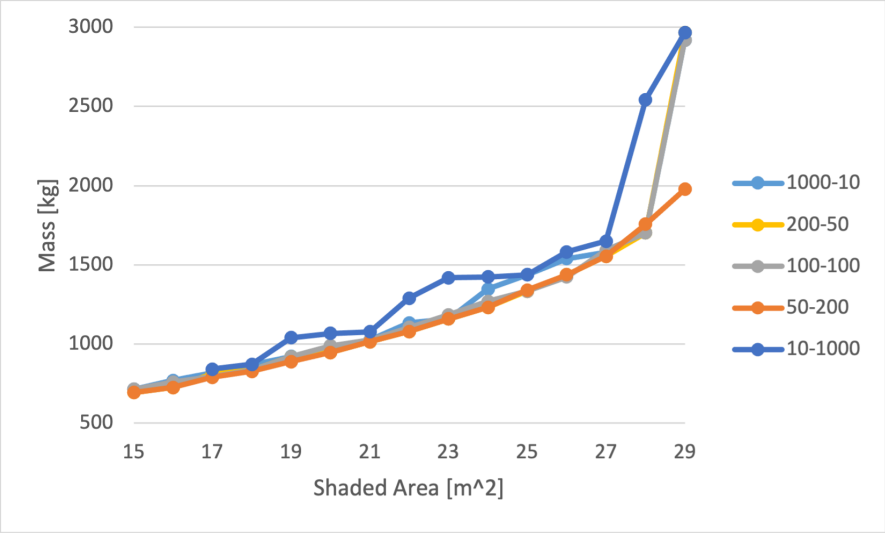


Figure 5.30: Graphical comparison of the canopy solutions from the different optimizations of a 5x5m canopy

5.2.3 Shade and dimension based analysis

In this section, we will analyse the impact of the dimensions of the canopy on the simulation and on the resulting solutions. We use the population parameters 50-200 found in the previous analysis. However in some cases the population was not sufficient, we therefore used a larger generation count.

10x5m

For a 10x5m canopy, the simulation has 6 genes, 104 values, 3 fitness objectives, and a search space with 4.7M solutions. With a generation size of 50 individuals and 800 generations resulting in a population of 40,000 individuals. The run time lasted for 18 hours 25 minutes and 59 seconds. We see on tab 2, see figure A.29, a general convergence for the mean values between 2,000 and 3,000 kg for the mass, between -30 and -40 m^2 for the shaded area. For the standard deviation, the values converged around 2,000 kg for the mass, 18 m^2 for the shaded area. Only the last objective shows no real sign of convergence. We can however see from figure 5.31 that no modification were made to the part of the Pareto front that respects the deflection constraint after the 652th generation. We therefore consider the Pareto front to be the true Pareto front or very close to it.

From tab 3, see figure A.30, 15 Pareto solutions were found from cluster 2 in blue that respect the deflection constraint and the minimal shaded area. These solutions can be seen on figure 5.31. All solutions respect the stress rupture limit of steel S235.

We retrieve 4 canopies. Their characteristics can be found in table 5.7, they are compared on the graph of figure 5.33 and their visual representations are on figure 5.32.

	Solution	X divisions	Y divisions	Height $[mm]$	Width $[mm]$	Angle $[°]$	Mass $[kg]$	Shaded Area $[m^2]$	Efficiency $[m^2/kg]$	Pattern
Lightest canopy	{308;47}	9	8	400	5	30	1,912	36	0.019	Diamond
Largest shaded area	{71;2}	26	14	400	8	30	7,159	56	0.008	Rectangular
Best efficiency	{78;6}	7	10	400	5	35	2,134	41	0.019	Diamond
Average of fitness ranks	{46;14}	18	15	400	5	40	3,217	53	0.016	Diamond

Table 5.7: Properties of the selected solutions for the optimization of a 10x5m canopy

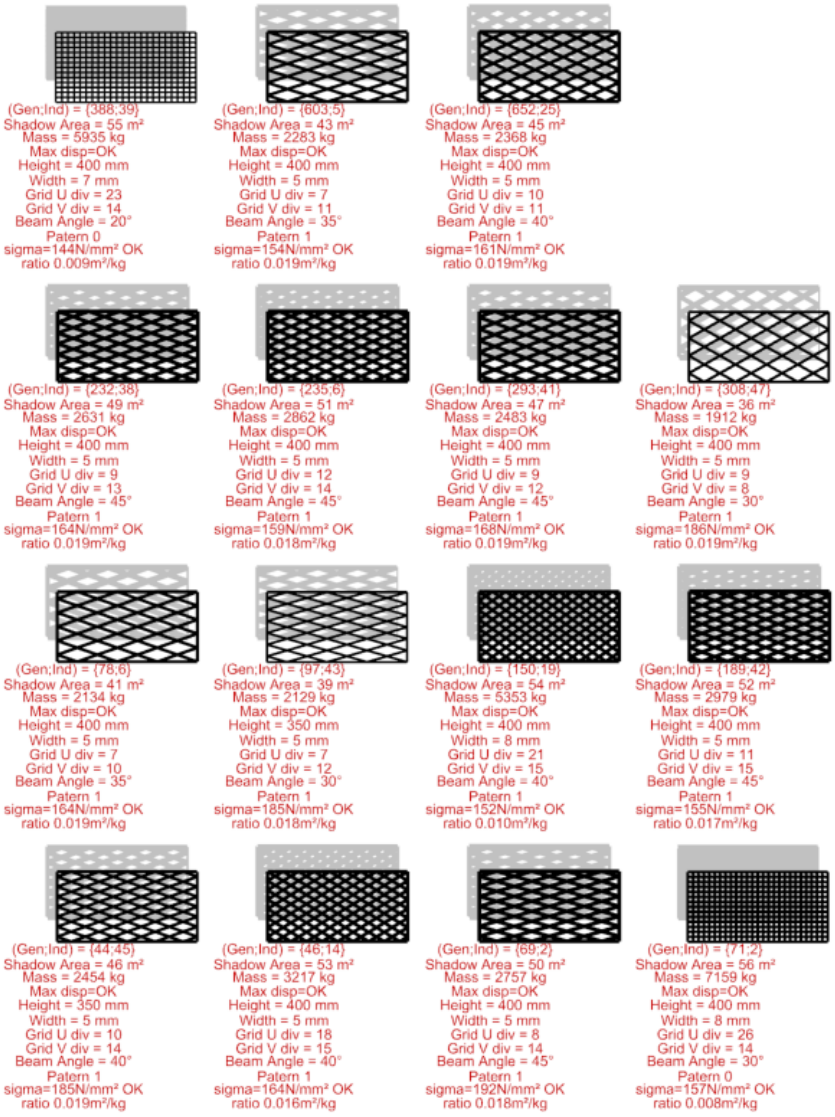
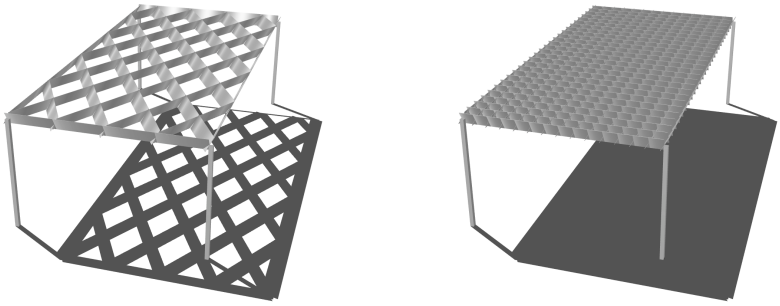
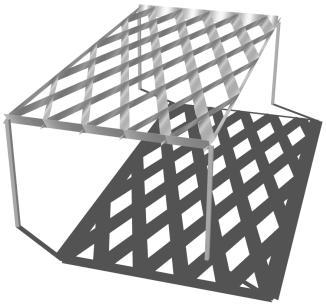


Figure 5.31: Top view of the results of the optimization of a 10x5m canopy

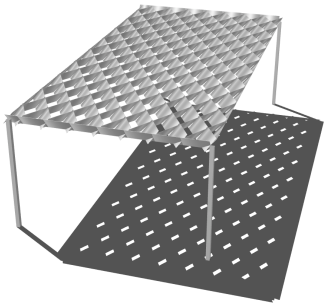


(a) Lightest canopy

(b) Largest shaded area



(c) Best efficiency



(d) Best average of fitness ranks

Figure 5.32: Perspective view of the selected solutions for the optimization of a 10x5m canopy

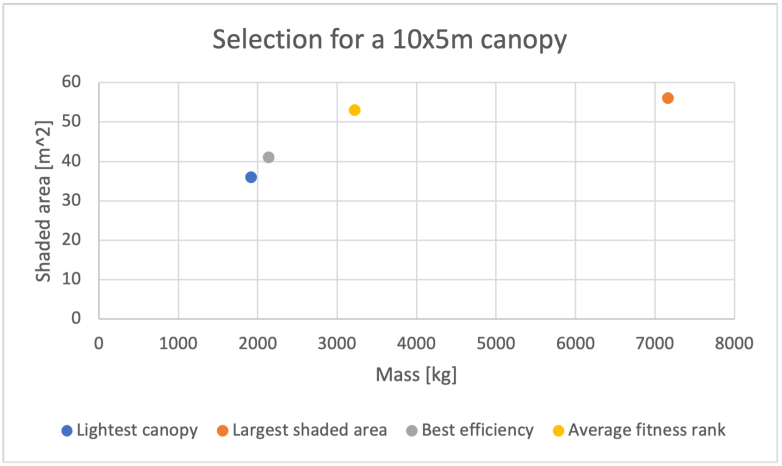


Figure 5.33: Graphical comparison of the selected solutions for the 50-800 optimization of a 10x5m canopy

20x2m

For a 20x2m canopy, the simulation has 6 genes, 129 values, 3 fitness objectives resulting in a search space of 3.8M solutions. For a population of 40,000 individuals with a generation size of 50 individuals and 800 generations. The run time is of 10 hour 46 minutes and 36 seconds. As we can see on figure A.32, trendlines of the two first objective stabilized between 8,000 and 12,000 kg for the average mass and its standard deviation, and between -35 an-30 m^2 for the mean shaded area and around 16 m^2 for its standard deviation. We still don't see stabilization for the third objective. We can see from figure 5.34 that a new modification was made to the part of the Pareto front that respects the deflection constraint on generation the 796th generation. Nevertheless, the previous modification occurred on generation 461, we therefore consider the Pareto front to be very close to the true Pareto front.

From tab 3, see figure A.33, 15 Pareto solutions were found in cluster 3 (green) that respect the deflection constraint and the minimal shaded area. These solutions can be seen on figure 5.34. All of the solutions respect the stress rupture limit of steel S235.

We retrieve 3 canopies. Their characteristics can be found in table 5.8, they are compared on the graph of figure 5.36 and their visual representations are on figure 5.35.

	Solution	X divisions	Y divisions	Height $[mm]$	Width $[mm]$	Angle $[°]$	Mass $[kg]$	Shaded Area $[m^2]$	Efficiency $[m^2/kg]$	Pattern
Lightest canopy & best efficiency	{87;33}	1	5	400	5	0	1,947	27	0.014	Rectangular
Largest shaded area	{178;0}	8	6	400	60	25	29,767	49	0.02	Rectangular
Average of fitness ranks	{70;1}	1	6	400	5	0	2,261	31	0.014	Rectangular

Table 5.8: Properties of the selected solutions for the optimization of a 20x2m canopy

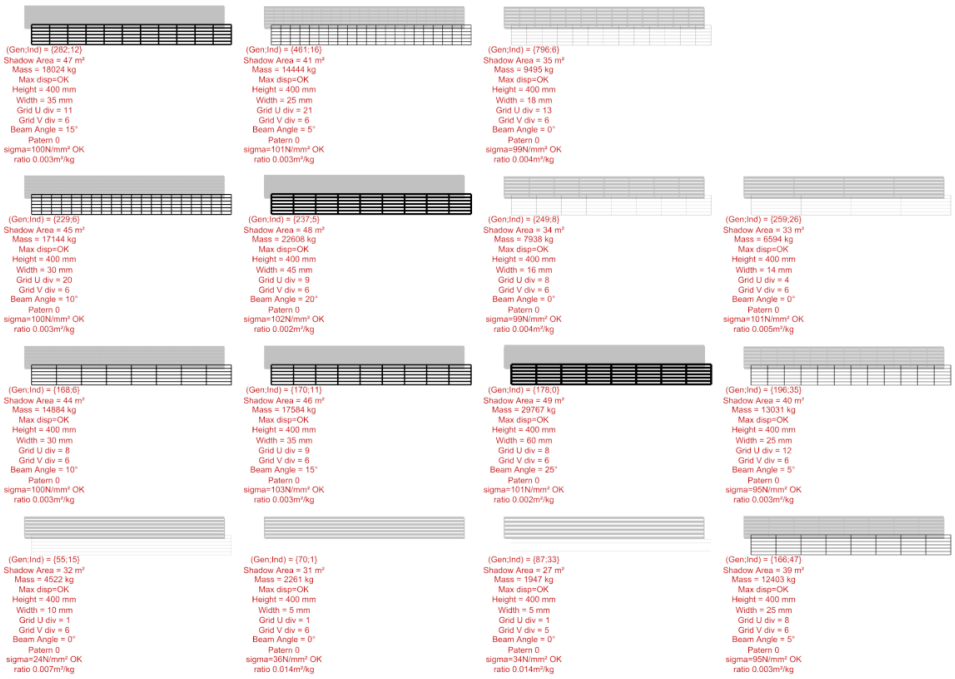
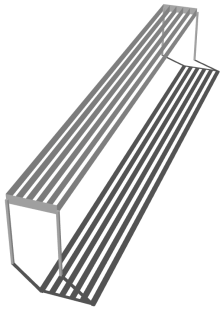
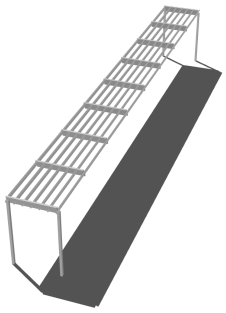


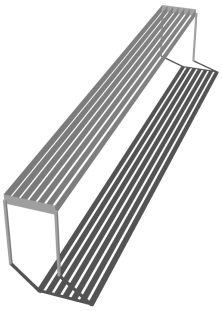
Figure 5.34: Top view of the results of the optimization of a 20x2m canopy



(a) Lightest canopy and best efficiency



(b) Largest shaded area



(c) Best average of fitness ranks

Figure 5.35: Perspective view of the selected solutions for the optimization of a 20x2m canopy

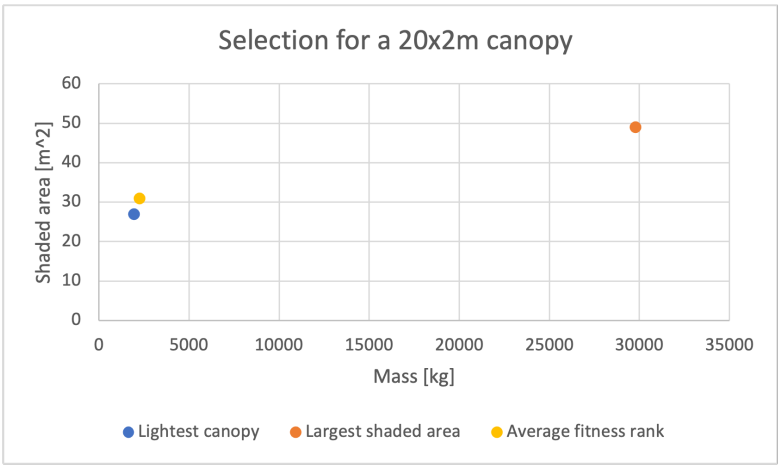


Figure 5.36: Graphical comparison of the selected solutions for the optimization of a 20x2m canopy

For the following canopy simulations, the solutions proposed were all exceeding the rupture stress limit of steel S235. For this reason, we had to add a fourth fitness objective. This fitness objective is to limit the stress to $235/1.15\ N/mm^2$. We therefore use two *Expression* components where we input the maximal stress and the following expressions: $if(x \leq 204, -1000, x)$ followed by $if(x < 1000, x, 1000)$. In order to facilitate the selection for the solution respecting the stress and deflection constraints, we rename the fitness objectives *wlc_4Minimize mass*, *wlc_1Maximize shaded area*, *wlc_2Limited displacement* and name the new fitness objective *wlc_3Limited stress*. This will permit us to have the two constrained objectives in the 3D space for the clustering and visualize the acceptable solutions easily.

10x10m

For a 10x10m canopy, the simulation has 6 genes, 119 values, 4 fitness objectives resulting in a search space of 9.4M solutions. For a population 10,000 individuals with a generation size of 50 individuals and 200 generations. The run time is of 6 hour 41 minutes and 31 seconds. As we can see on figure A.35, trendlines stabilized between 20,000 and 30,000 kg for the average mass, around 25,000 kg for its standard deviation, around -70 m^2 for the mean shaded area and around 35 m^2 for its standard deviation. We can now observe a stabilization of the mean displacement between -50 and -100 and around 110 for its standard deviation. However there is yet no stabilization for the limited stress. We can see from figure 5.37 that no modification were made to the part of the Pareto front that respects the deflection constraint after the 124th generation. We therefore consider the Pareto front to be the true Pareto front or very close to it.

From tab 3, see figure A.36, 7 Pareto solutions were found in cluster 11 (brown) that respect the deflection and stress constraints and the minimal shaded area. These solutions can be seen on figure 5.37. All of these solutions respect the stress rupture limit of steel S235.

However, we notice from those solutions that the maximal shaded area is of 107 m^2 while the maximal shaded area for such a canopy should be of 109 m^2. This shows that the constraints prevent the canopy to achieve its maximal shaded area.

We retrieve 3 canopies. Their characteristics can be found in table 5.9, they are compared on the graph of figure 5.39 and their visual representations are on figure 5.38.

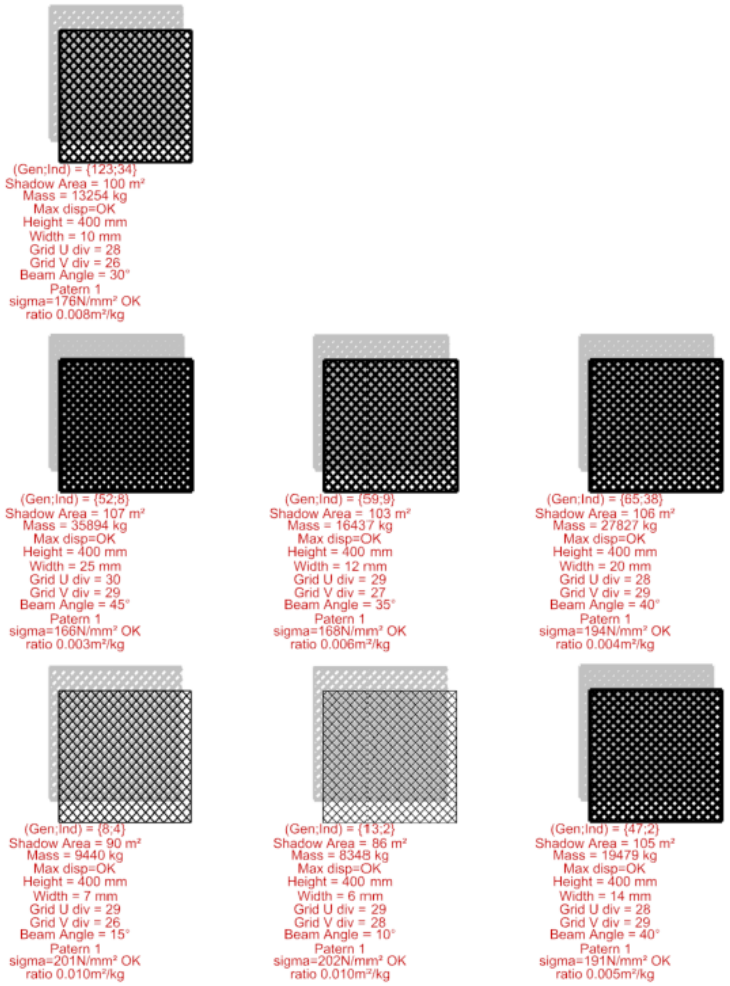
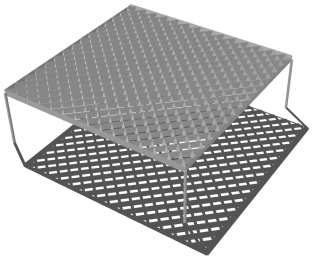


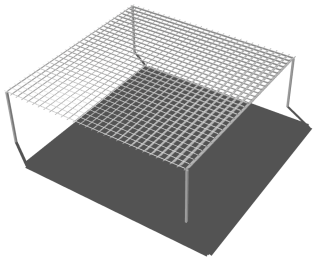
Figure 5.37: Top view of the results of the optimization of a 10x10m canopy

	Solution	X divisions	Y divisions	Height $[mm]$	Width $[mm]$	Angle $[°]$	Mass $[kg]$	Shaded Area $[m^2]$	Efficiency $[m^2/kg]$	Pattern
Lightest canopy & best efficiency	{13;2}	29	28	400	6	10	8,348	86	0.010	Diamond
Largest shaded area	{52;8}	30	29	400	25	45	35,894	107	0.003	Rectangular
Average of fitness ranks	{123;34}	28	26	400	10	30	13,254	100	0.008	Diamond

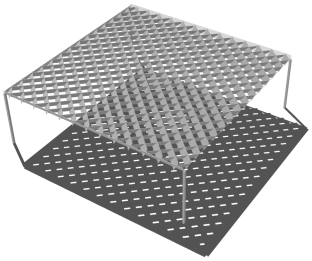
Table 5.9: Properties of the selected solutions for the optimization of a 10x10m canopy



(a) Lightest canopy and best efficiency



(b) Largest shaded area



(c) Best average of fitness ranks

Figure 5.38: Perspective view of the selected solutions for the optimization of a 10x10m canopy

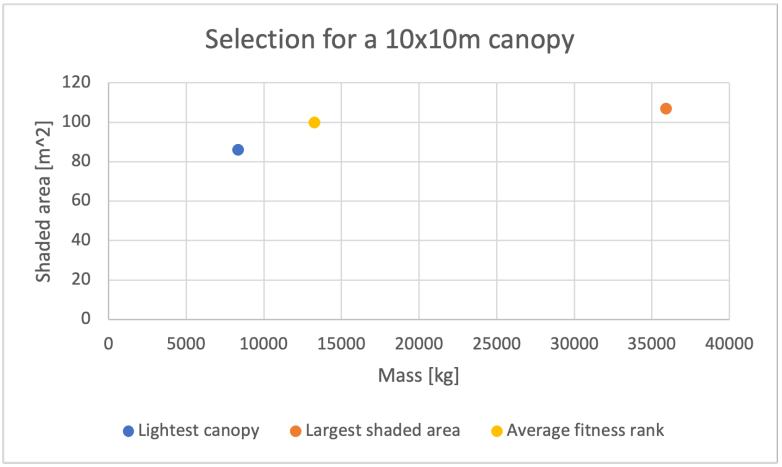


Figure 5.39: Graphical comparison of the selected solutions for the optimization of a 10x10m canopy

15x10m

For a 15x10m canopy, the simulation has 6 genes, 134 values, 4 fitness objectives resulting in a search space of 14M solutions. For generation size of 50 individuals and 400 generations resulting in a population of 20,000 individuals. The run time is of 28 hour 44 minutes and 12 seconds.

As we can see on figure A.38, trendlines stabilized around 60,000 kg for the average mass and and around 50,000 for its standard deviation, around -100 m^2 for the mean shaded area and between 50 m^2 for its standard deviation. We can't observe a stabilization of the mean displacement, however its standard deviation stabilized at 150. However there is yet no stabilization for the limited stress.

We can see from figure 5.37 that no modification were made to the part of the Pareto front that respects the deflection constraint after the 259th generation. We therefore consider the Pareto front to be the true Pareto front or very close to it.

From tab 3, see figure A.39, 11 Pareto solutions were found in cluster 1 (red) that respect the deflection and stress constraints and the minimal shaded area. These solutions can be seen on figure 5.40. All these solutions respect the stress rupture limit of steel S235.

However, we notice from those solutions that the maximal shaded area is of 133 m^2 while the maximal shaded area for such a canopy should be if 160 m^2. This shows that the constraints prevent the canopy to achieve its maximal shaded area.

We retrieve 3 canopies. Their characteristics can be found in table 5.10, they are compared on the graph of figure 5.42 and their visual representations are on figure 5.41.

	Solution	X divisions	Y divisions	Height $[mm]$	Width $[mm]$	Angle $[°]$	Mass $[kg]$	Shaded Area $[m^2]$	Efficiency $[m^2/kg]$	Pattern
Lightest canopy	{40;38}	14	19	400	16	0	18,465	71	0.004	Diamond
Largest shaded area	{229;2}	31	29	400	60	10	110,055	133	0.001	Diamond
Average of fitness ranks & best efficiency	{51;20}	24	29	400	14	0	24,038	98	0.004	Diamond

Table 5.10: Properties of the selected solutions for the optimization of a 15x10m canopy

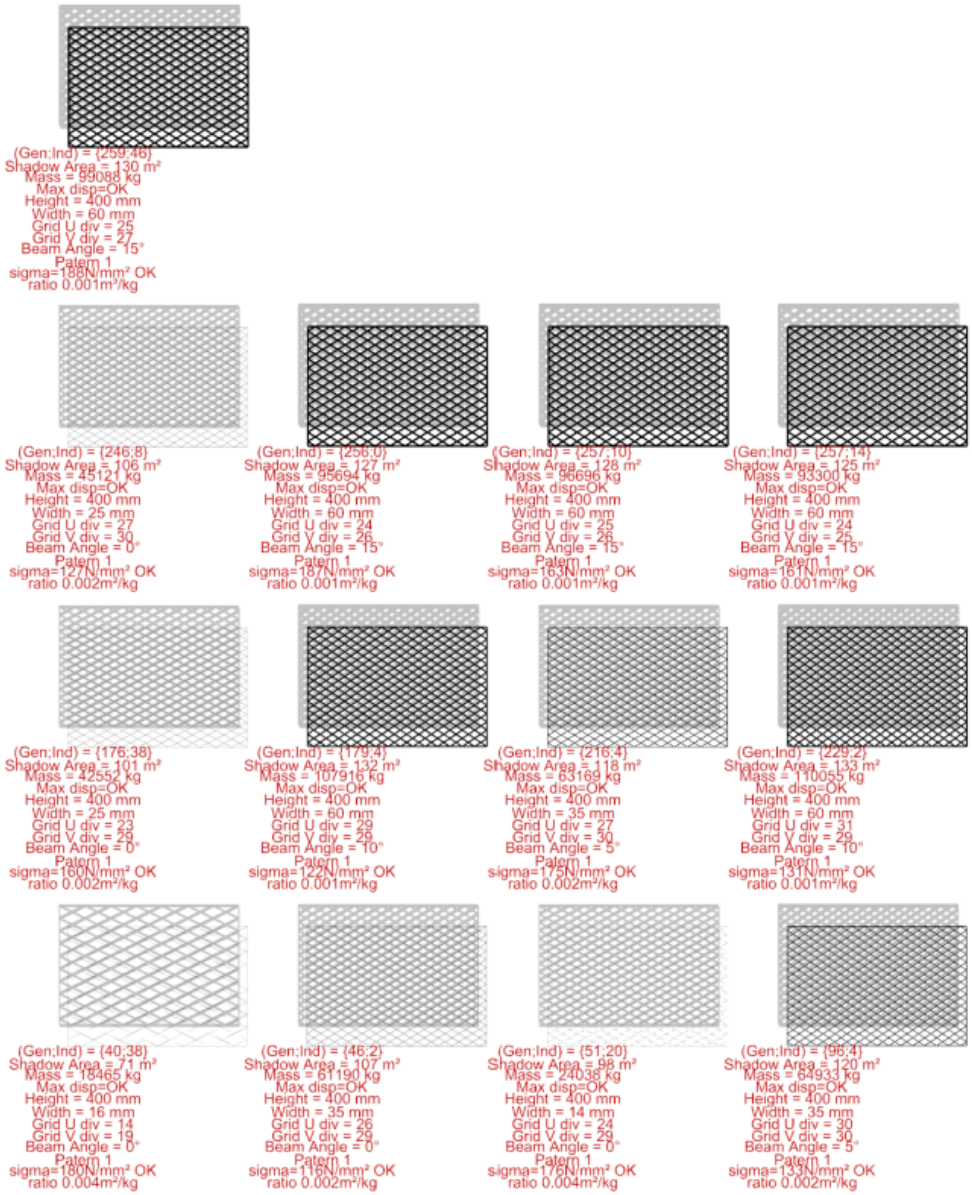
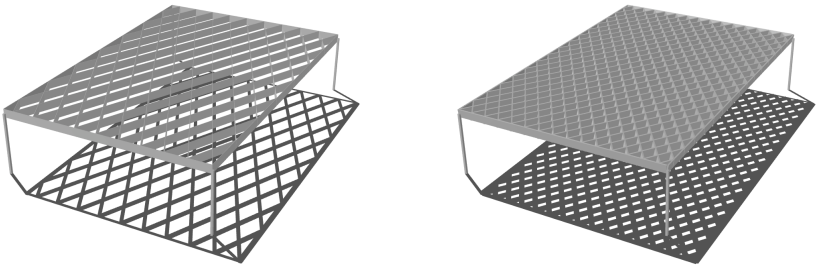
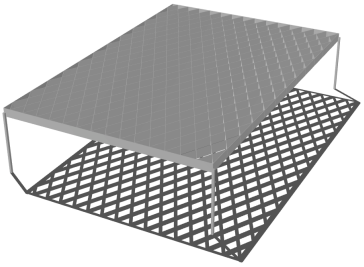


Figure 5.40: Top view of the results of the optimization of a 15x10m canopy



(a) Lightest canopy

(b) Largest shaded area



(c) Best average of fitness ranks and efficiency

Figure 5.41: Perspective view of the selected solutions for the optimization of a 15x10m canopy

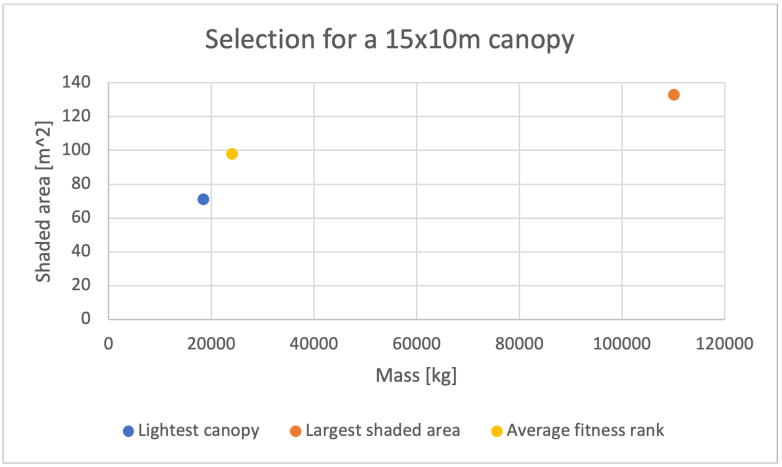


Figure 5.42: Graphical comparison of the selected solutions for the optimization of a 15x10m canopy

Conclusion

From these simulation we noticed that, when the area of the canopy increases:

- the search space increases
- the run time increases
- the stress and deflection increases
- the efficiency of the canopy decreases. When canopies are too large, the maximal stress and deflection get too big for the most efficient solutions to respect the constraint. The elements have to become larger with smaller inclination.

We notice that the diamond grid is most often preferred over the rectangular grid. The exception to this is for elongated canopies like the 20x2m canopy where the rectangular grid is always preferred or for the maximal shaded areas of some canopies. We also found that the most efficient solution is always very close or equal to the lightest solutions.

In order to minimize the mass and maximize the shaded area, the beam's height is most often at its maximal value of 400 mm and the width at its minimal value of 5 mm. The height can be smaller when we choose lighter solutions and the constraints permits it. The width can be larger when maximizing the shaded area and in order to respect the deflection and stress constraints.

The inclination angle is quickly limited by the stress and deflection constraints. This is often the cause of wider beams. The angle tends however to be as large as possible in order to maximize the shaded area if the constraints allows it without adding to much weight to the structure.

For the number of divisions, we note that when selecting the best average of fitness ranks, the number of divisions in the direction of the smallest side tends to be close to maximal. For the largest shaded area it is also true in both directions.

Because the efficiency of the canopies decreases the larger they get, we could combine multiple smaller canopies to create a larger one. With the canopies that we optimized:

If instead of a 10x5m canopy we use two 5x5m canopies:

- for the lightest canopy, the mass would decrease by 27% while the shaded area would decrease by 17% and the efficiency would increase by 16%.
- for the canopy with the largest shaded area, the mass would decrease by 45% while the shaded area would increase by 4% and the efficiency would increase by 88%.
- for the canopy with the best efficiency, the mass would decrease by 32% while the shaded area would decreased by 22% and the efficiency would increase by 16%.
- for the canopy with the best average of fitness ranks, the mass would decrease by 3% while the shaded area would increase by 2% and the efficiency would increase by 6%.

If instead of a 10x10m canopy we used two 10x5m canopies:

- for the lightest canopy, the mass would decrease by 54% while the shaded area would decreased by 16% and the efficiency would increase by 90%.
- for the canopy with the largest shaded area, the mass would decrease by 60% while the shaded area would increase by 5% and the efficiency would increase by 167%.
- for the canopy with the best efficiency, the mass would decrease by 49% while the shaded area would decrease by 5% and the efficiency would increase by 90%.
- for the canopy with the best average of fitness ranks, the mass would decrease by 51% while the shaded area would increase by 6% and the efficiency would increase by 100%.

If instead of a 15x10m canopy we used three 10x5m canopies:

- for the lightest canopy, the mass would decrease by 69% while the shaded area would increase by 52% and the efficiency would increase by 375%.
- for the canopy with the largest shaded area, the mass would decrease by 80% while the shaded area would increase by 26% and the efficiency would increase by 700%.

- for the canopy with the best efficiency, the mass would decrease by 73% while the shaded area would increase by 26% and the efficiency would increase by 375%.
- for the canopy with the best average of fitness ranks, the mass would decrease by 60% while the shaded area would increase by 62% and the efficiency would increase by 300%.

As we can see, combining canopies always results in an increase of efficiency. We get either lighter canopies producing larger shaded areas or lighter canopies with slightly smaller shaded areas.

The most significant gain in efficiency can always be observed when selecting the canopies with the largest shaded areas. The more canopies we combine the more efficient it gets. This is especially true for the canopies of 10x10m and 15x10m. Indeed, in those cases we can't use efficient genes otherwise the stress and deflection would be getting too important, therefore there is a great decrease of efficiency for larger canopies.

However, combining small canopies is not adapted to every environment, if it gets too small, it could become uncomfortable for the users. There could also be constraints for the location of the supports.

Chapter 6

Conclusion

This thesis has explored the concept of urban canopies as a structural solution to mitigate the heat island effect in cities by using multi-objective optimization. The city surfaces retain less heat thanks to the shade produced by urban canopies thus cooling down the city.

We started by defining the concept of urban canopy by researching remarkable examples of urban canopies in the world. We continued with a state of the art on multi-objective optimization and the different types of algorithms. We decided to use the multi-objective genetic algorithm NSGA-II for our optimization. We had to get familiar with Rhinoceros3D, Grasshopper, Karamba3D, Ladybug, and Wallacei that were necessary to model our canopy and optimize it.

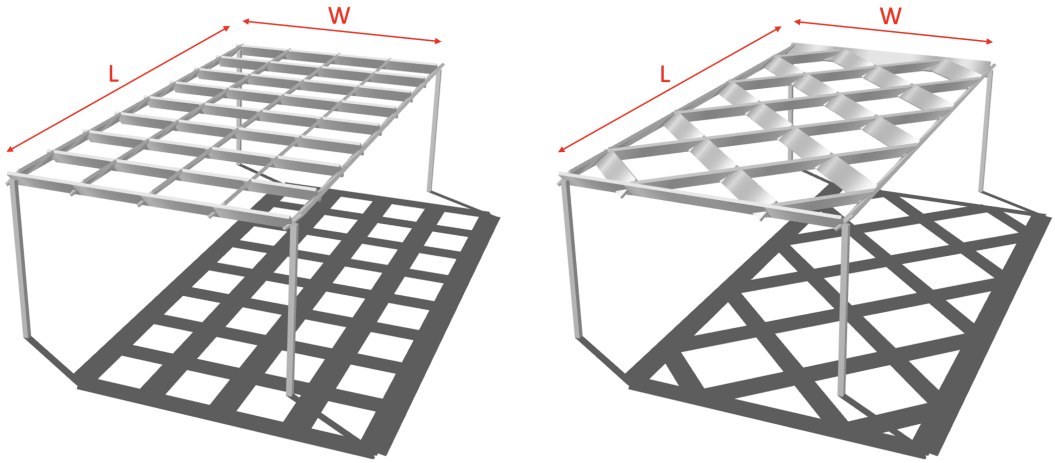
Modelization

For our model, we opted for a rectangular steel canopy with beams placed either in a rectangular grid pattern or a diamond grid pattern as can be seen on figure 6.1. The parameters that can be changed are the type of pattern, the beam spacing in the horizontal and vertical direction, the beam's heights and widths, and finally the inclination angle of the beams.

This model as the advantage to propose a light canopy that is not subject to the wind thanks to its aerated openings.

Optimization

We did three kind of optimizations: a structural optimization and two shade optimizations.



(a) Rectangular grid (b) Diamond grid

Figure 6.1: Perspective view of our canopy model

For the structural optimization, we minimized the mass of the canopy while respecting a deflection constraint of $L/200$. For the two shade optimizations we added an objective to maximize the shaded area produced by the canopy.

Structural optimization We structurally optimized canopies of different dimensions. The optimizations for the different canopy sizes resulted in the simplest canopies possible, the lightest canopies respecting the deflection constraint. The larger the canopy got, the larger the elements were.

Population based shade optimization We ran multiple optimization for a 5x5m canopy by changing the population parameters. All optimizations had a population of 10,000 individuals with the following generation size and counts: 10-1000, 50-200, 100-100, 200-50, and 1000-10. We then compared the resulting shaded areas and their corresponding weights. For each shaded area, we gave ranks from 1 to 5 to each optimization, 1 corresponding to the lightest solution. The population parameters 50-200 had the best average rank and had therefore the fittest generation size and count combination. It allows a sufficient initial population that is optimized by crossovers and mutation along sufficient generations. We used these parameters for the dimension based shade optimization. However, in some cases, the generation count was increased for better results.

Dimension based shade optimization We ran multiple optimization with canopies that have the following dimensions: 5x5m, 10x5m, 20x2m, 10x10m, and

15x10m. From these optimizations, we noted that:

- When the area of the canopy gets larger, the efficiency of the canopy decreases and the maximal deflection and stress increase.
- The diamond pattern is generally preferred over the rectangular pattern. We noted two exceptions to this statement, for elongated canopies like a canopy of 20x2m, the rectangular pattern is always chosen, and to achieve the largest shaded area of some canopies, the rectangular pattern is also chosen.
- Combining smaller canopies into a larger one, always result in significant gain in efficiency. This can result in lighter canopies producing larger shaded area or lighter canopies producing slightly smaller shaded areas. The largest increase can be observed when we select the canopies with the largest shaded area. We observed that the efficiency is increased by 700% when we combine three 10x5m canopies instead of a 15x10m canopy.
- When the constraints allows it, the beam's height and angle tend to have the maximal value of 400 mm and 45° and the beam's width tends to have the minimal value of 5 mm. The beam's height can be smaller if we select the lighter solutions. The beam's width is sometimes larger to maximize the shaded area and to respect the constraint.

6.1 Encountered difficulties & further developments

Modification to the model The simulations had to be redone many times due to issues encountered. An earlier model could incline the beams of 45° in both directions and have beams of different orientations to be inclined by the same angle or by opposite angles. We however simplified the model by making sure that all beam were oriented from the start so that when they were tilted from 0 to 45°, the shaded area would directly be maximized. This greatly reduced the size of the search space. However we later noticed that the point we chose to for the *X-Orientation* of the *Orientate Elem* component was faulty in some specific case. We therefore add to relaunch all the simulations with a better adapted point.
We also had to round the shaded area, because the mass of the canopy was ever increasing to add less than 1 m^2 of shaded area making the canopy three to four time heavier than necessary. We later went from using the total shaded area to the average shaded area in order to have less solutions in the Pareto front.

Computational power To be able to use Wallacei, I had to create a Windows partition on my mac. This resulted in a low computational power. With a more adapted computer, the optimization would be much quicker. We could therefore analyse even larger population in order to be 100% sure to have the true Pareto front.

Wallacei The issue with Wallacei was that it is not yet possible to set real constraint nor to add weight to an objective. Therefore, most of the solutions found were not respecting the constraints and Wallacei kept exploring inadequate solutions. If we were able to add weight to the constraint objective or even add a real constraint, it would greatly shorten the run time of the optimization and require smaller populations to find the true Pareto front. It would therefore be best to find a multi-objective optimization plugin that takes constraint or at least weight of objectives into account.

Shape variation The canopy should be able to have a wide range of possible shape in order to adapt best to its environment.

Supports A next model should be able to take the supports into account and add them at the required location. This would enable us to make canopies of any size with a maximum of efficiency. With this we would be sure not to have any issues of constraint or deflection.

Appendix A

A.1 Structural analysis

10x5

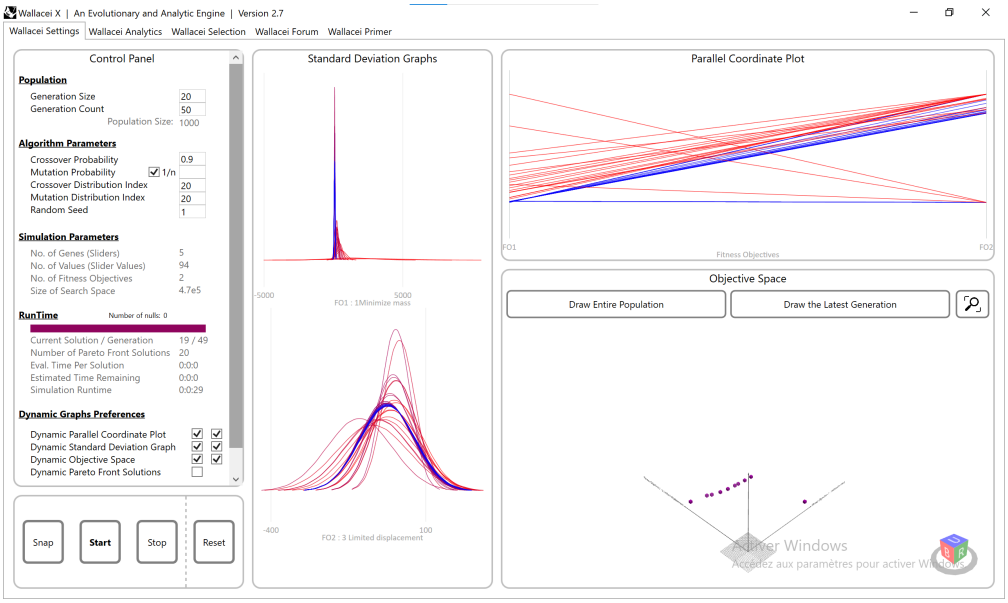


Figure A.1: Wallacei Settings for the structural optimization of a 10x5m canopy with 50 generations and 20 individuals per generations

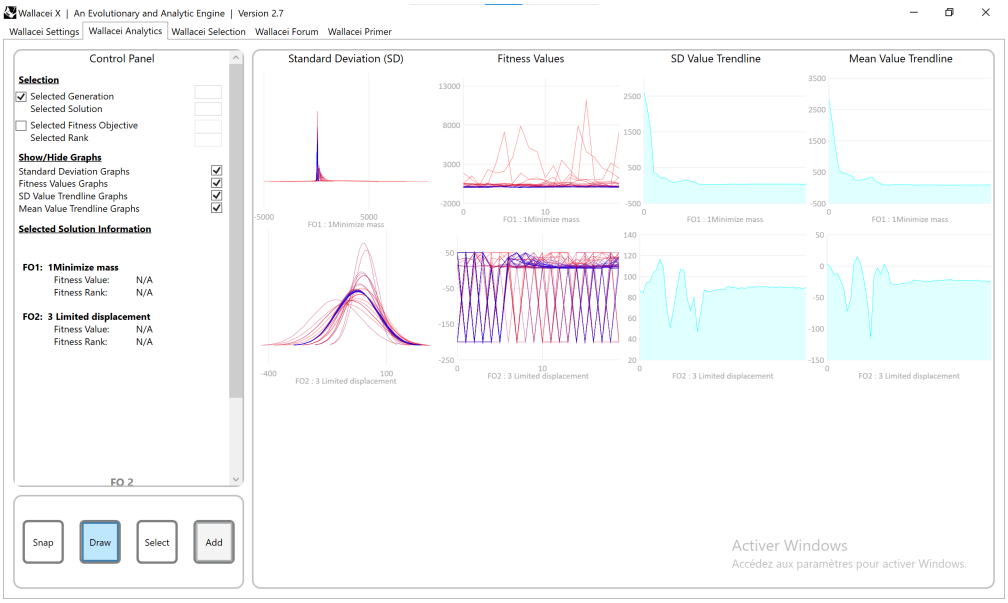


Figure A.2: Wallacei Analytics for the structural optimization of a 10x5m canopy with 50 generations and 20 individuals per generations

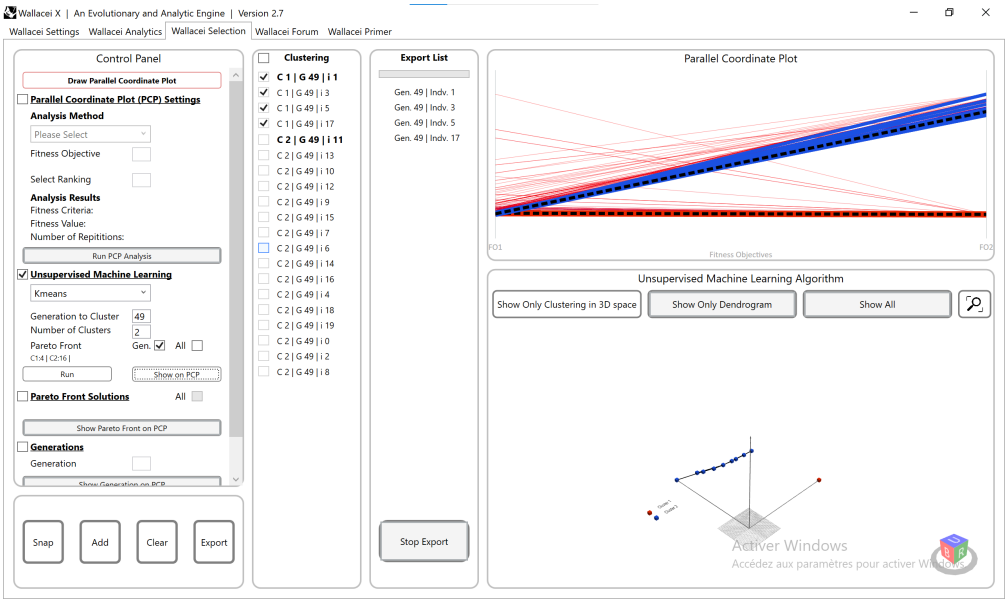


Figure A.3: Wallacei Selection for the structural optimization of a 10x5m canopy with 50 generations and 20 individuals per generations

5x5m

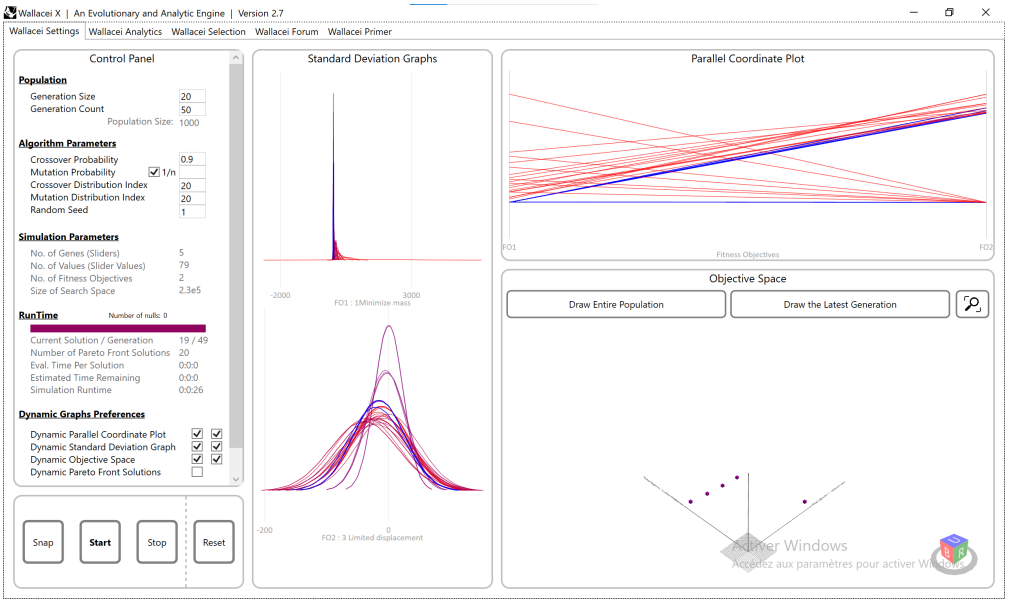


Figure A.4: Wallacei Settings for the structural optimization of a 5x5m canopy with 50 generations and 0 individuals per generations

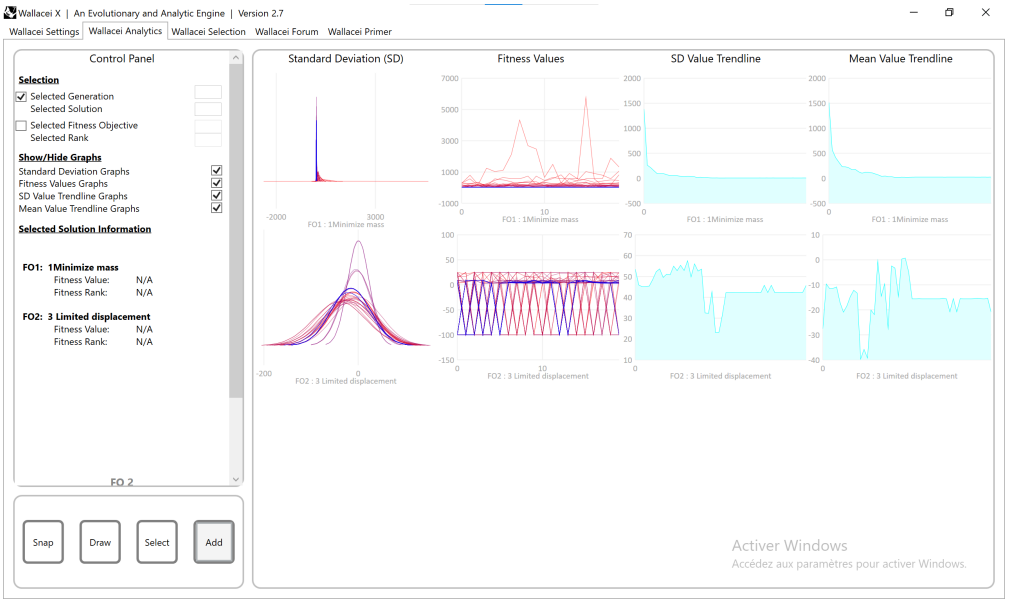


Figure A.5: Wallacei Analytics for the structural optimization of a 5x5m canopy with 50 generations and 20 individuals per generations

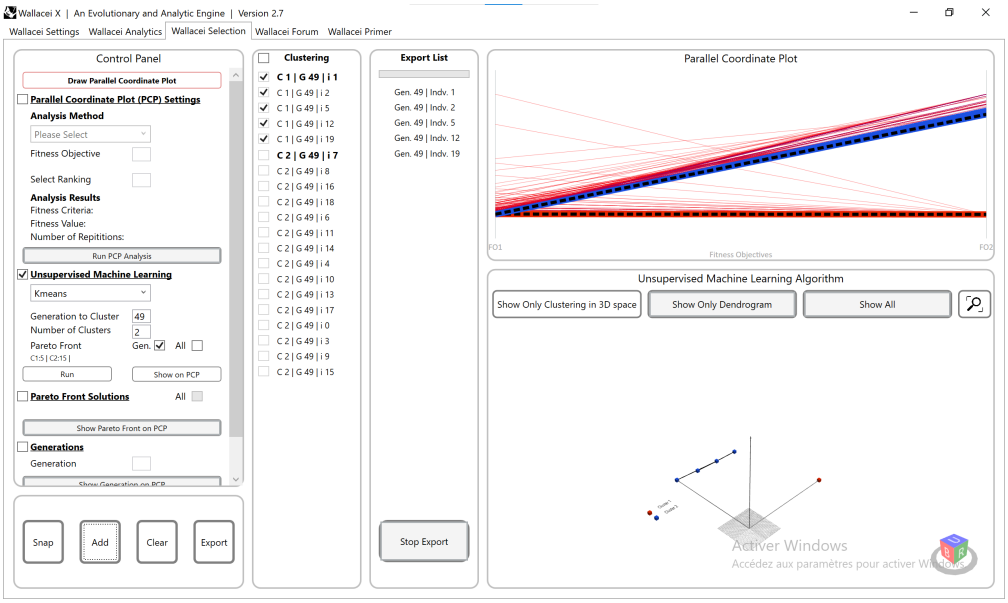


Figure A.6: Wallacei Selection for the structural optimization of a 5x5m canopy with 50 generations and 20 individuals per generations

15x10m

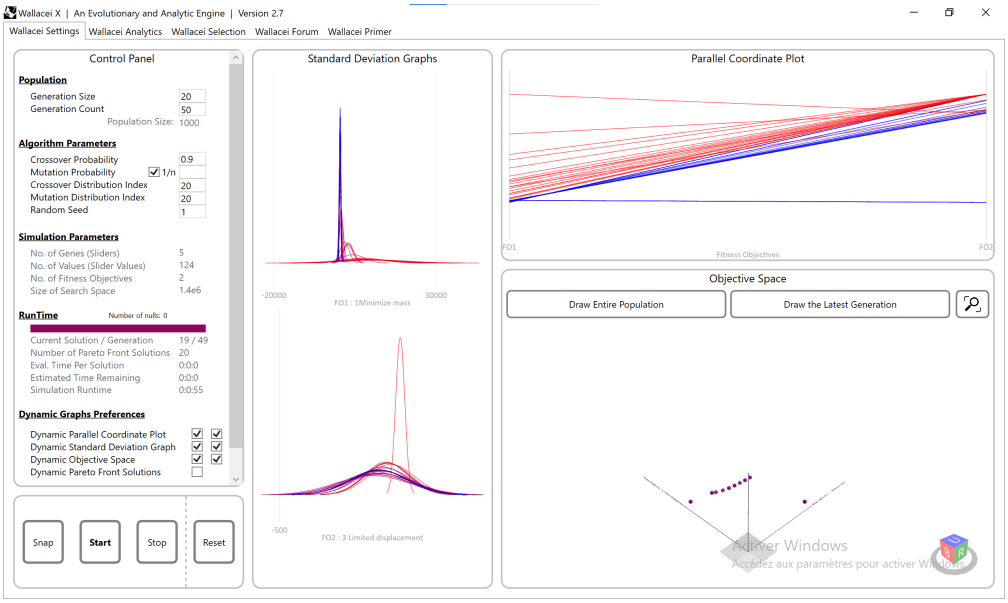


Figure A.7: Wallacei Settings for the structural optimization of a 15x10m canopy with 50 generations and 20 individuals per generations

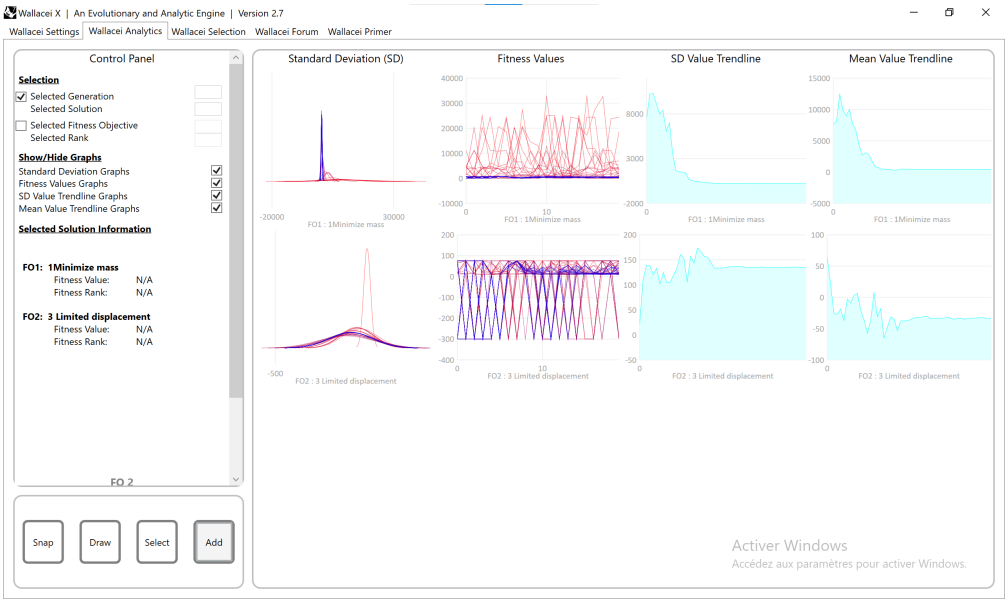


Figure A.8: Wallacei Analytics for the structural optimization of a 15x10m canopy with 50 generations and 20 individuals per generations

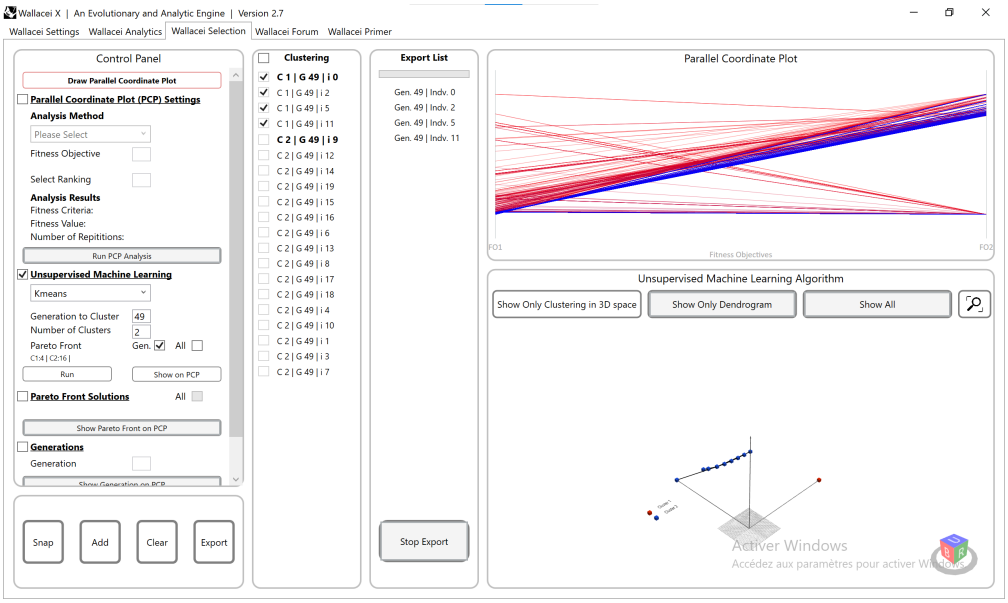


Figure A.9: Wallacei Selection for the structural optimization of a 15x10m canopy with 50 generations and 20 individuals per generations

20x2m

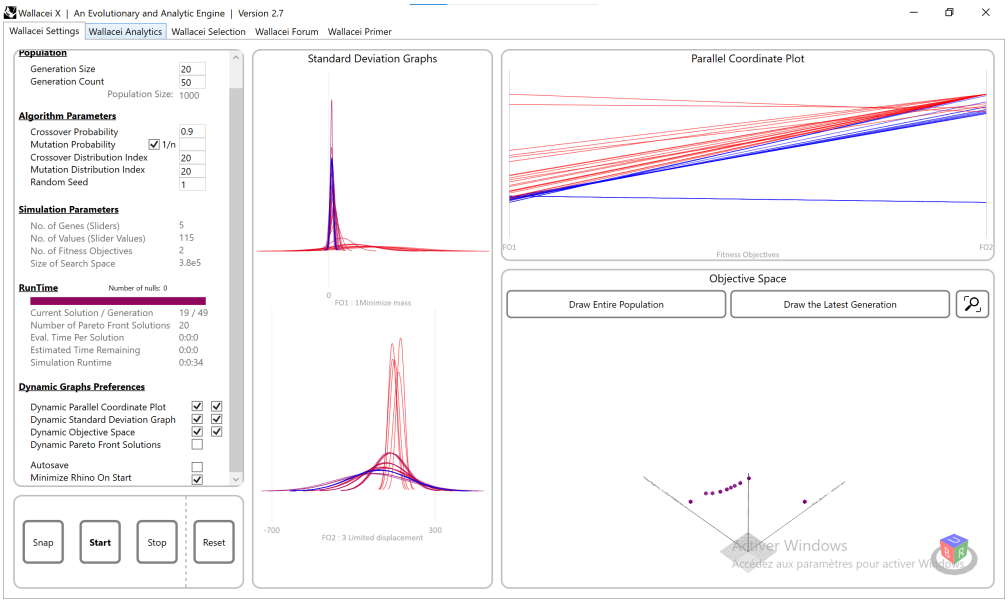


Figure A.10: Wallacei Settings for the structural optimization of a 20x2m canopy with 50 generations and 20 individuals per generations

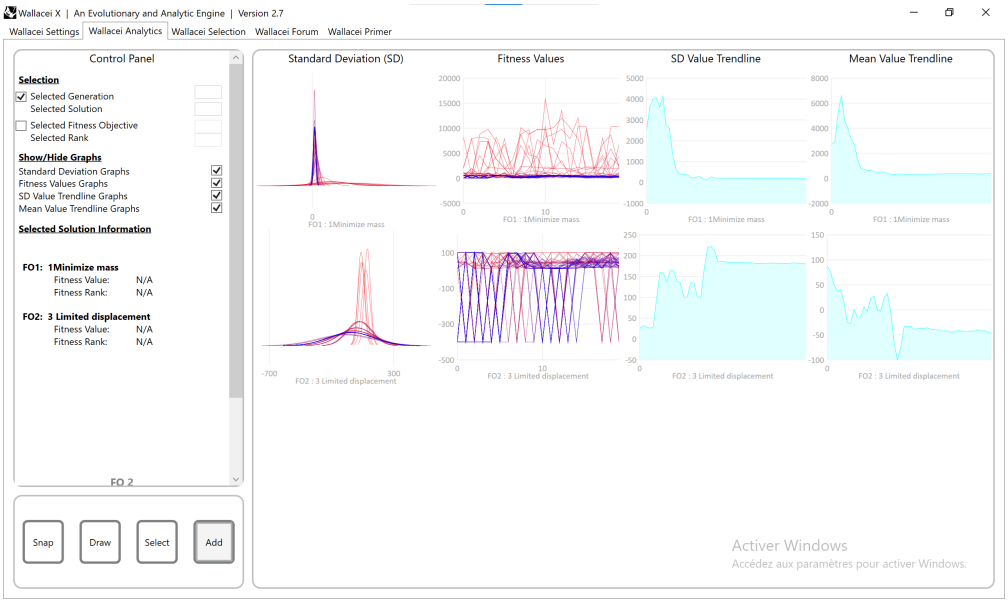


Figure A.11: Wallacei Analytics for the structural optimization of a 20x2m canopy with 50 generations and 20 individuals per generations

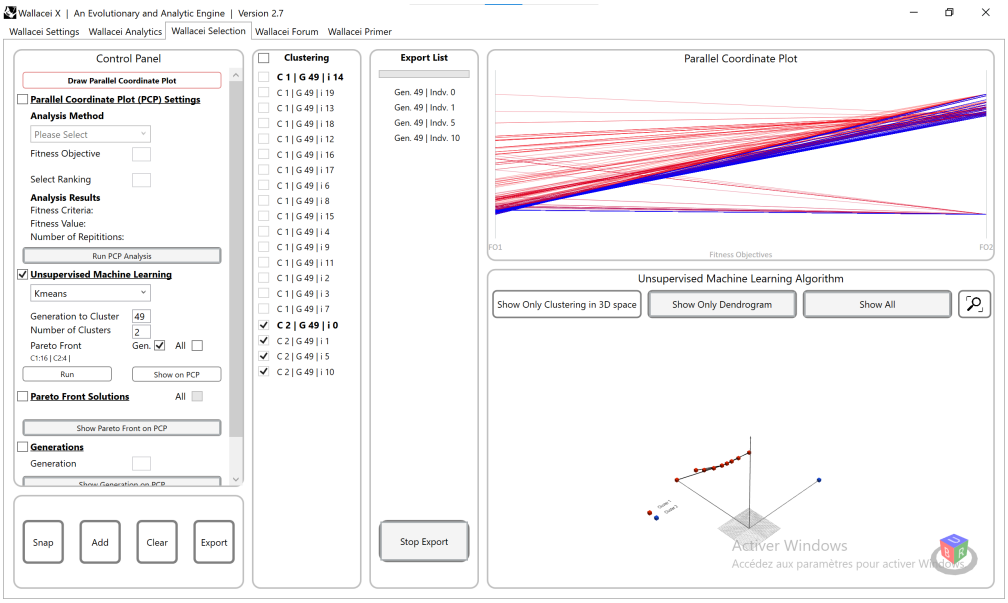


Figure A.12: Wallacei Selection for the structural optimization of a 20x2m canopy with 50 generations and 20 individuals per generations

A.2 Shade and population based analysis

10-1000

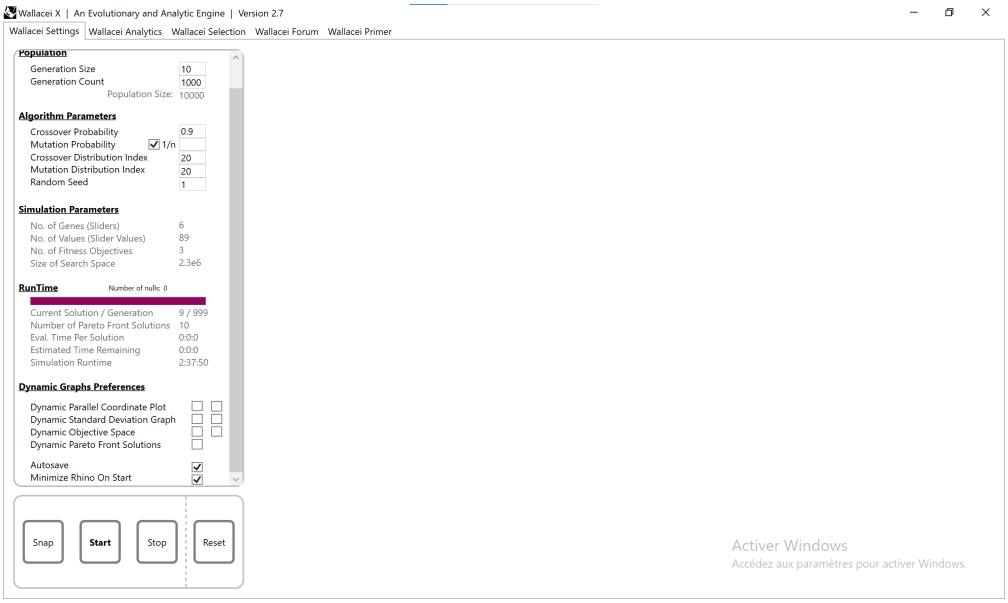


Figure A.13: Wallacei Settings for the shade optimization of a 5x5m canopy with 50 generations and 20 individuals per generations

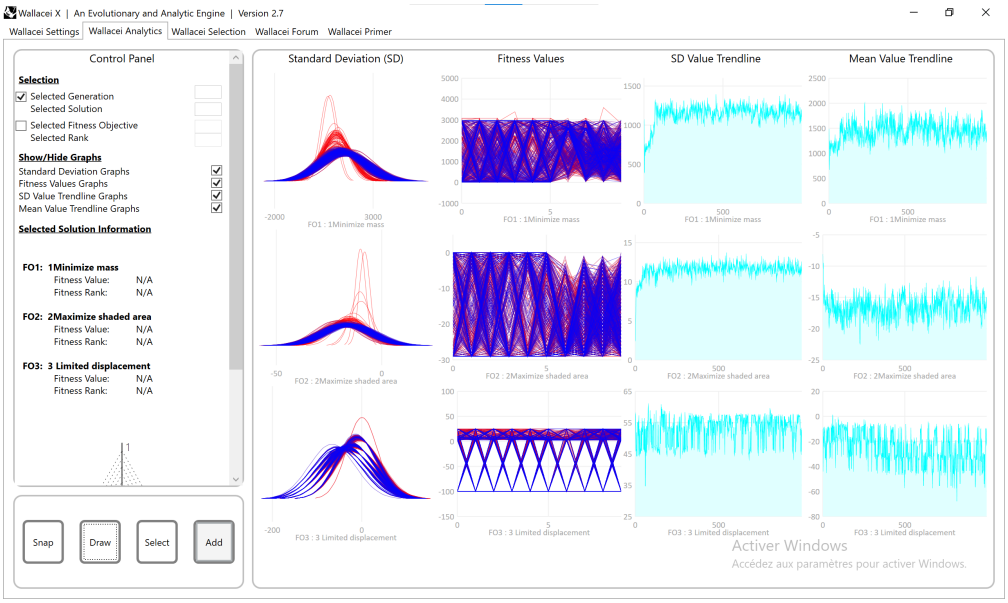


Figure A.14: Wallacei Analytics for the shade optimization of a 5x5m canopy with 50 generations and 20 individuals per generations

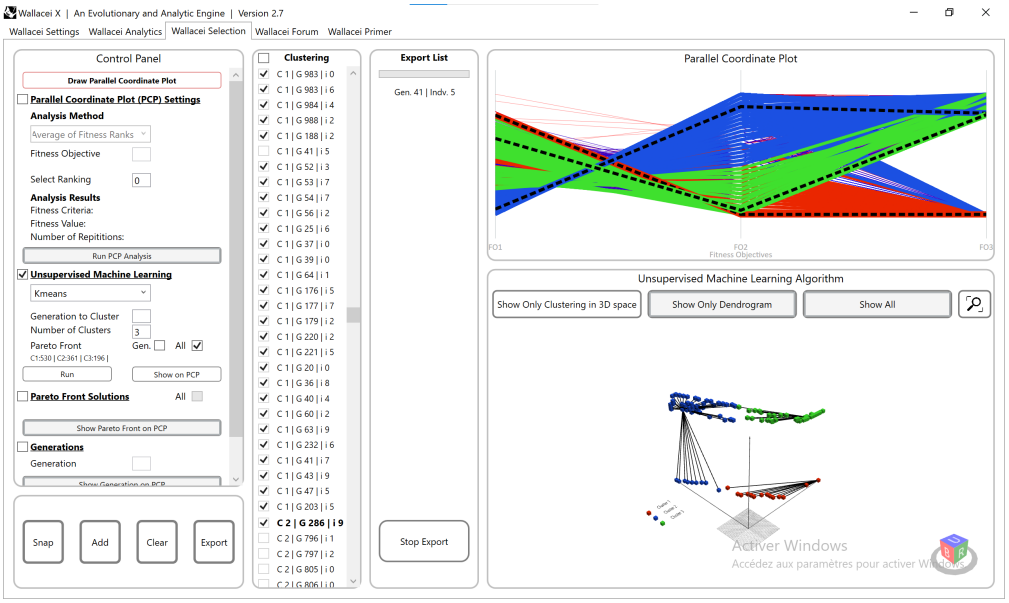


Figure A.15: Wallacei Selection for the shade optimization of a 5x5m canopy with 50 generations and 20 individuals per generations

50-200

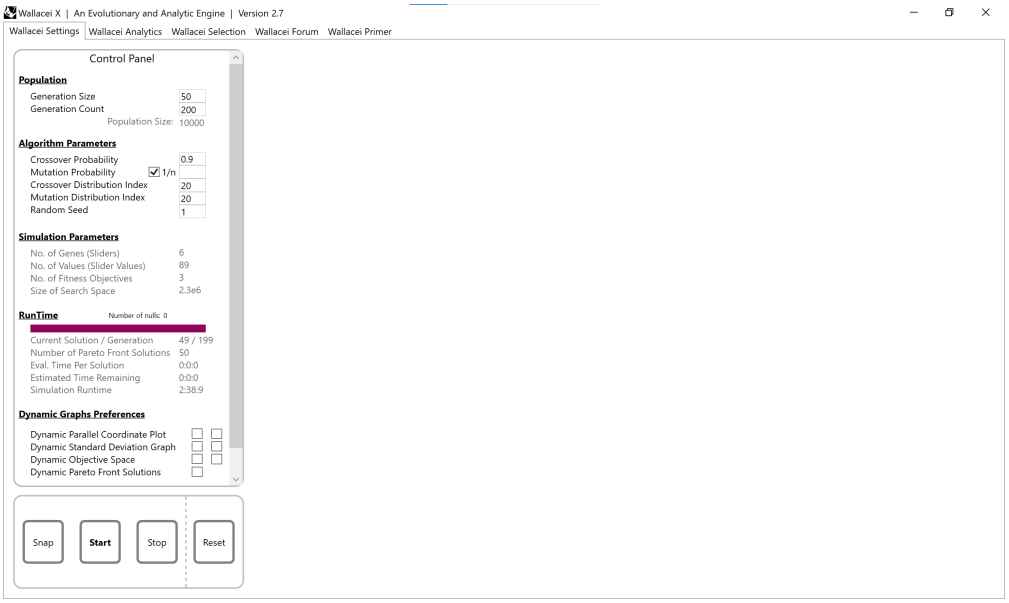


Figure A.16: Wallacei Settings for the shade optimization of a 5x5m canopy with 200 generations and 50 individuals per generations

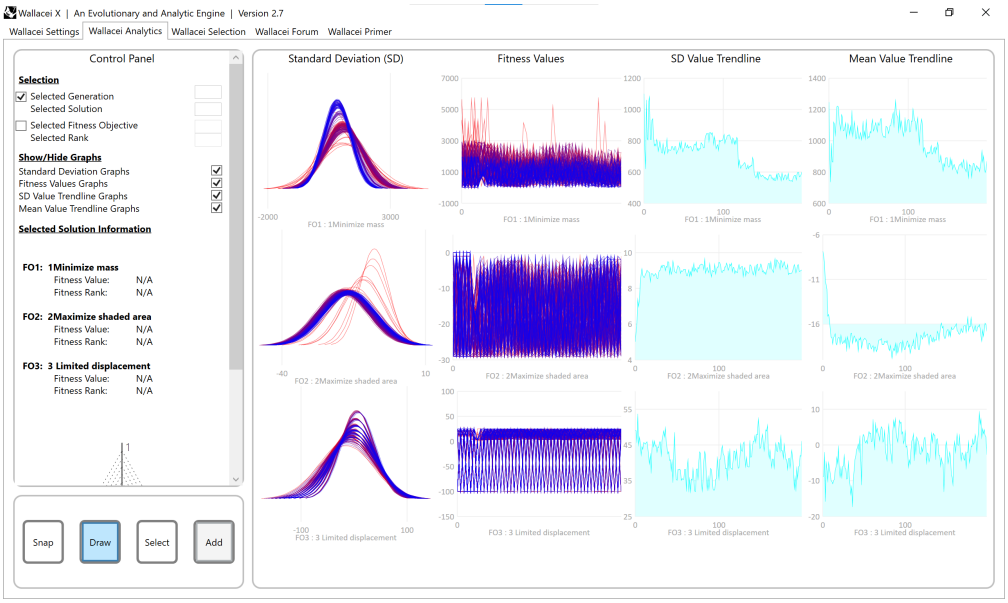


Figure A.17: Wallacei Analytics for the shade optimization of a 5x5m canopy with 200 generations and 50 individuals per generations

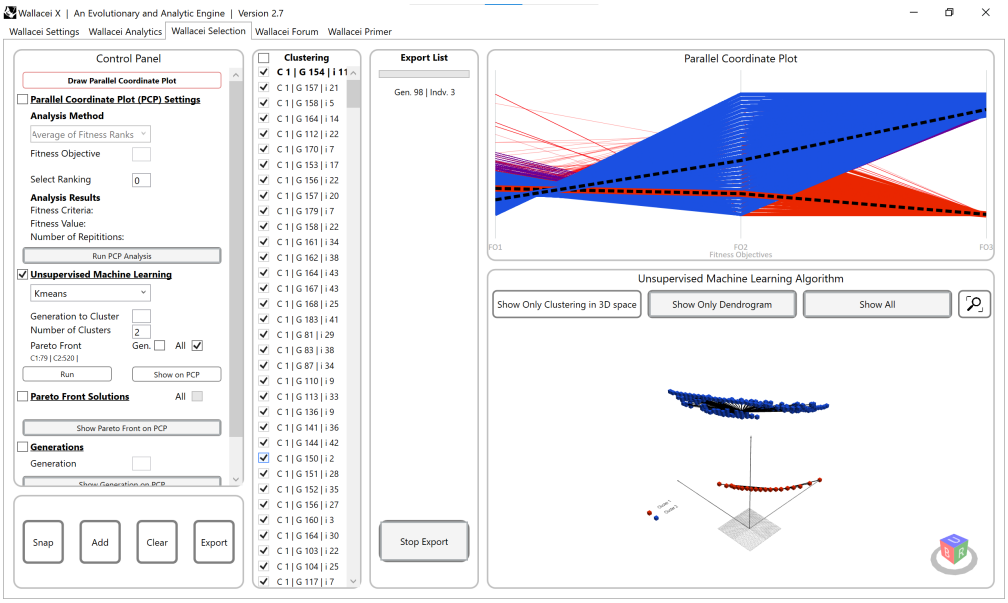


Figure A.18: Wallacei Selection for the shade optimization of a 5x5m canopy with 200 generations and 50 individuals per generations

100-100

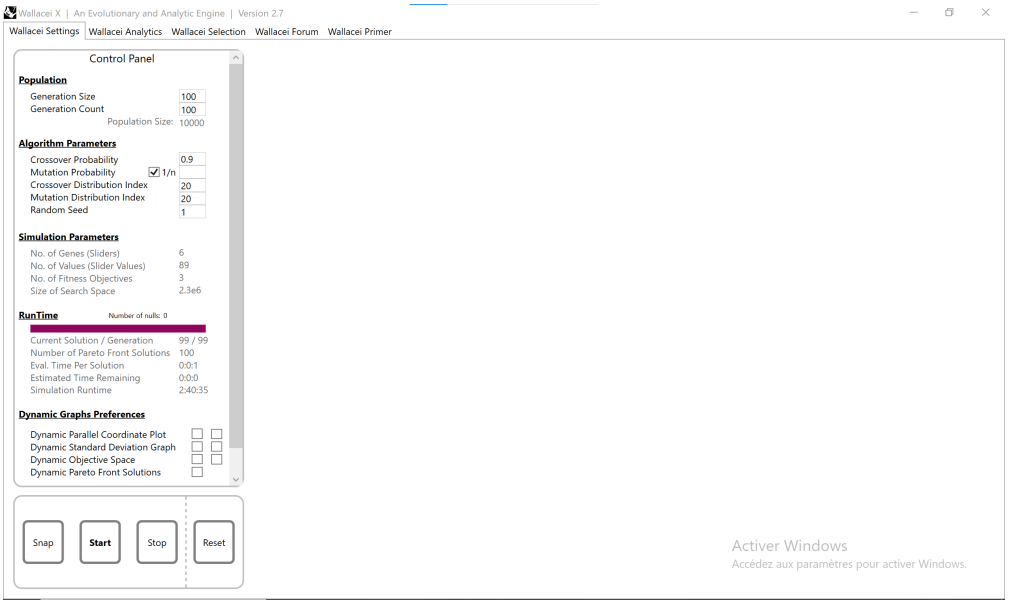


Figure A.19: Wallacei Settings for the shade optimization of a 5x5m canopy with 20 generations and 50 individuals per generations

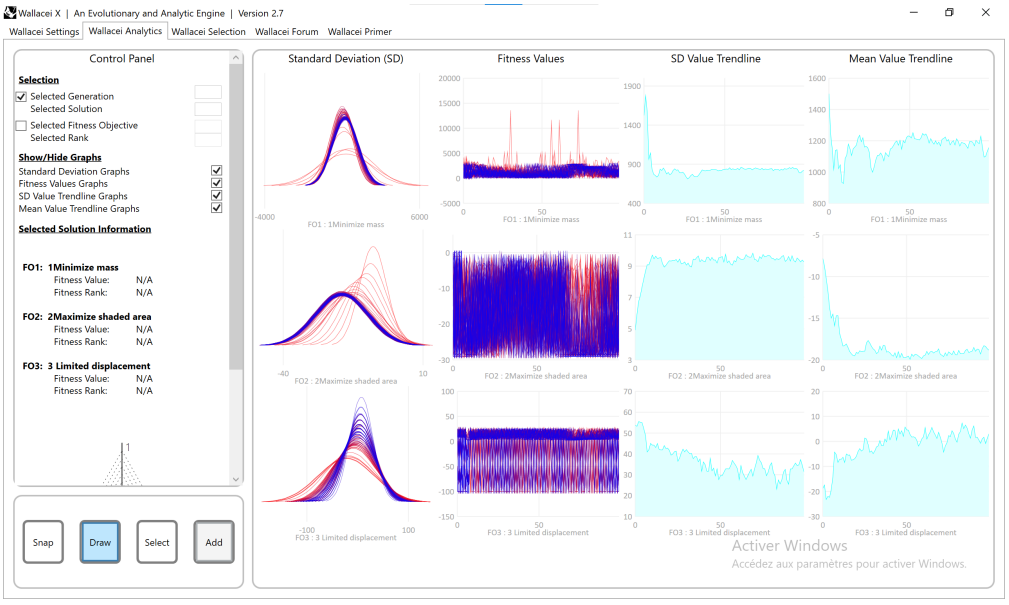


Figure A.20: Wallacei Analytics for the shade optimization of a 5x5m canopy with 20 generations and 50 individuals per generations

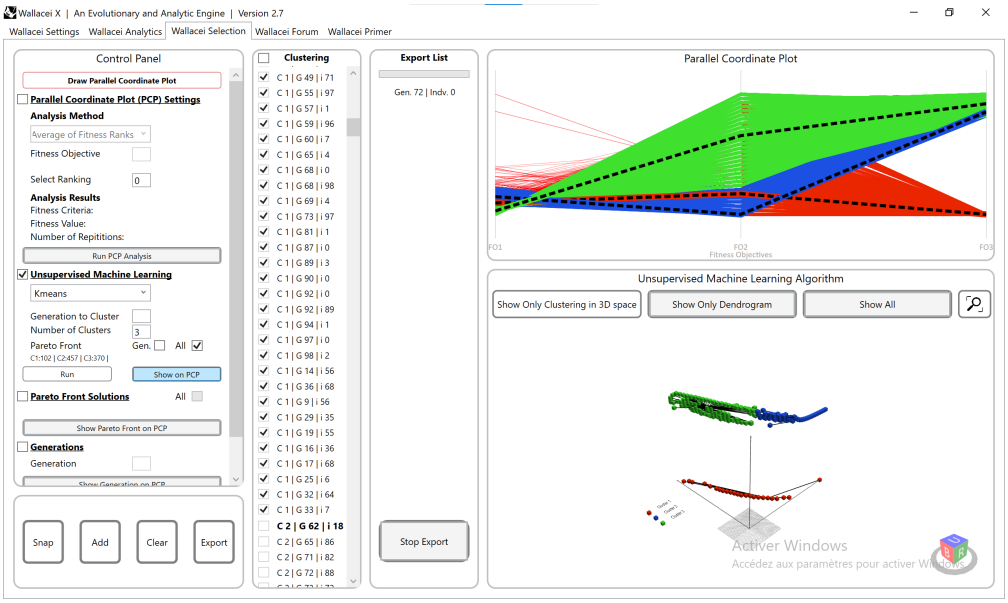


Figure A.21: Wallacei Selection for the shade optimization of a 5x5m canopy with 20 generations and 50 individuals per generations

200-50

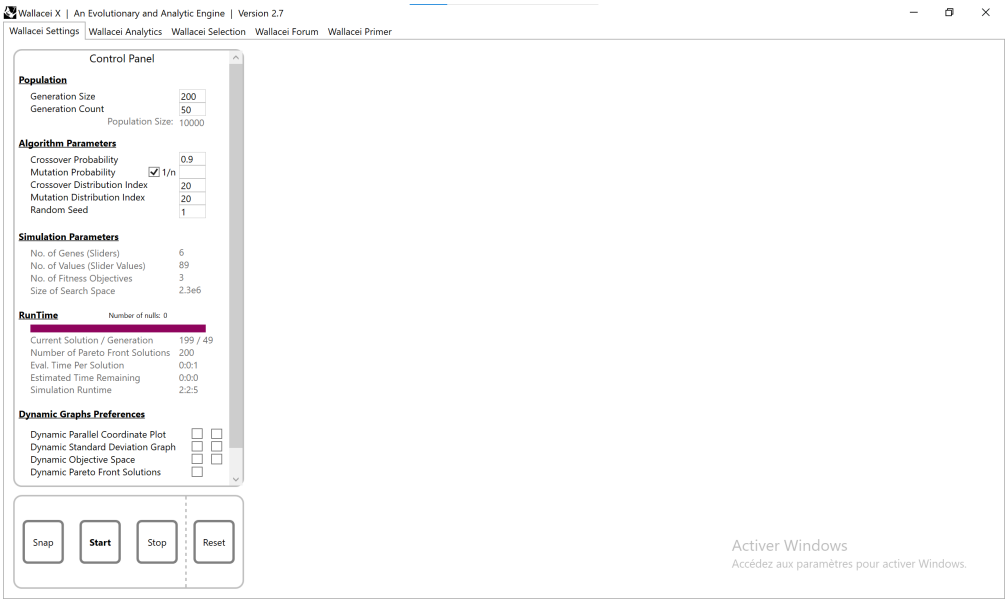


Figure A.22: Wallacei Settings for the shade optimization of a 5x5m canopy with 10 generations and 100 individuals per generations

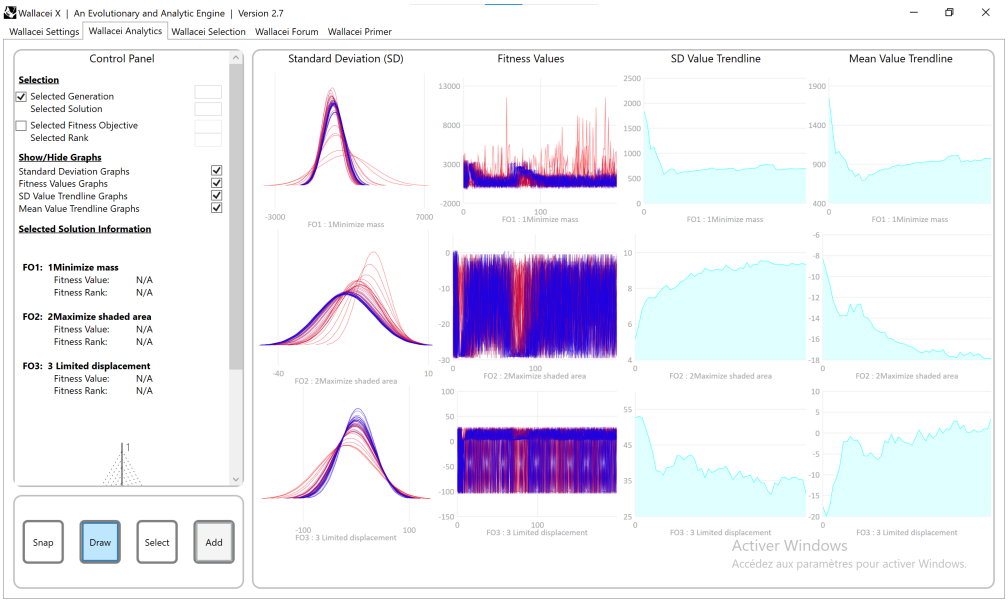


Figure A.23: Wallacei Analytics for the shade optimization of a 5x5m canopy with 10 generations and 100 individuals per generations

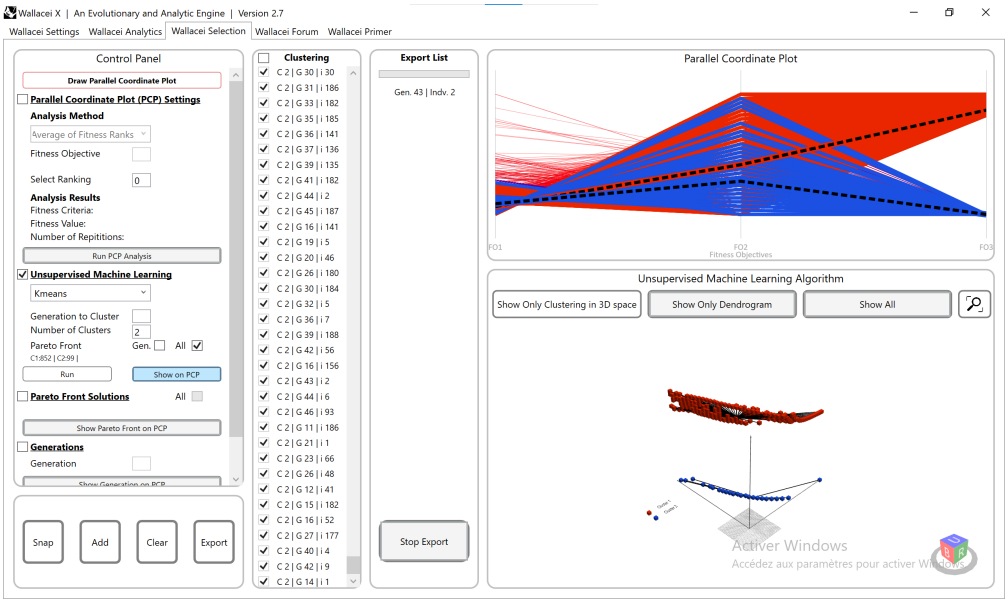


Figure A.24: Wallacei Selection for the shade optimization of a 5x5m canopy with 10 generations and 100 individuals per generations

1000-10

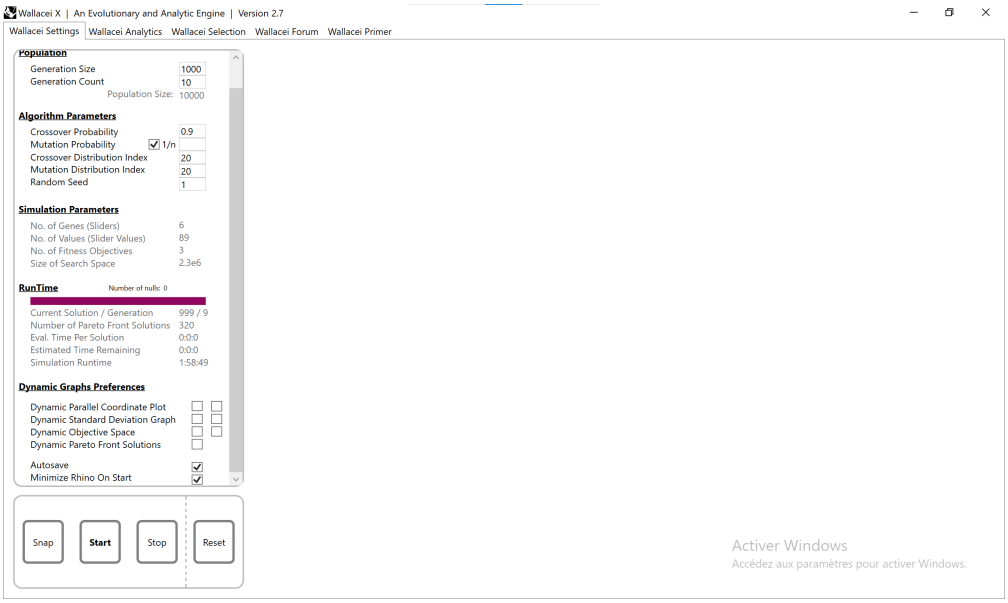


Figure A.25: Wallacei Settings for the shade optimization of a 5x5m canopy with 100 generations and 10 individuals per generations

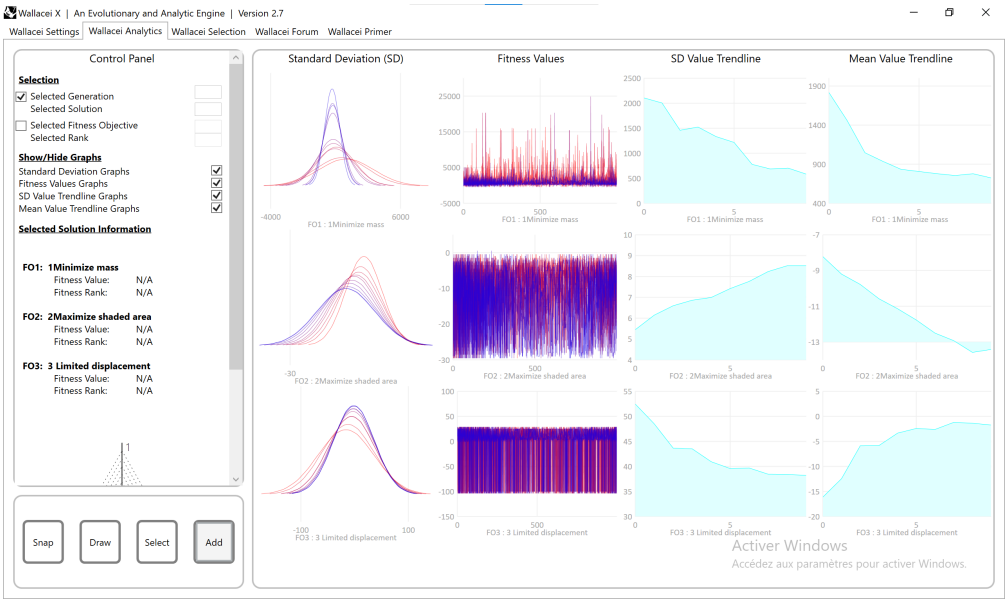


Figure A.26: Wallacei Analytics for the shade optimization of a 5x5m canopy with 100 generations and 10 individuals per generations

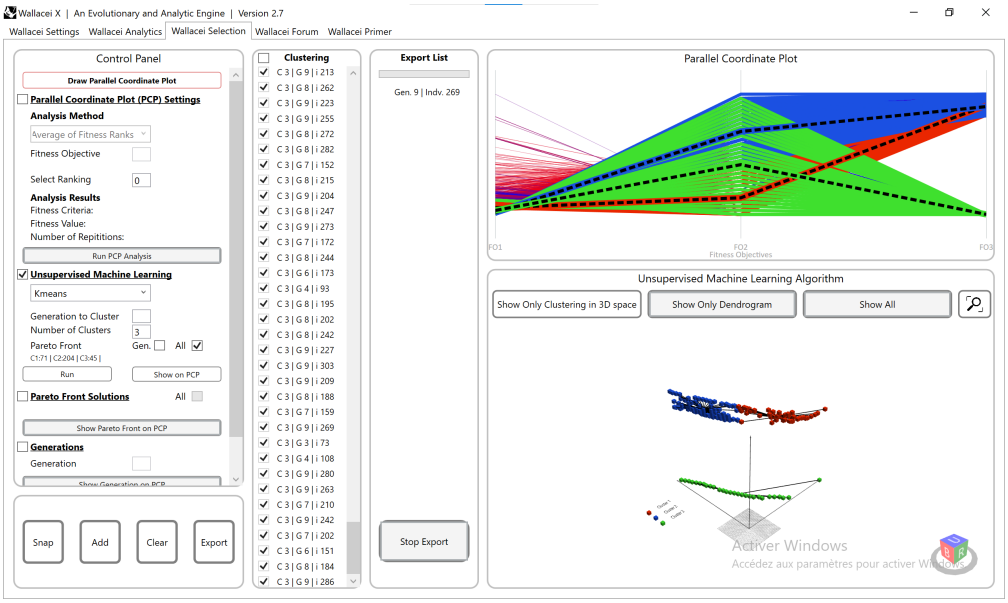


Figure A.27: Wallacei Selection for the shade optimization of a 5x5m canopy with 100 generations and 10 individuals per generations

A.3 Shade and size based analysis

10x5m

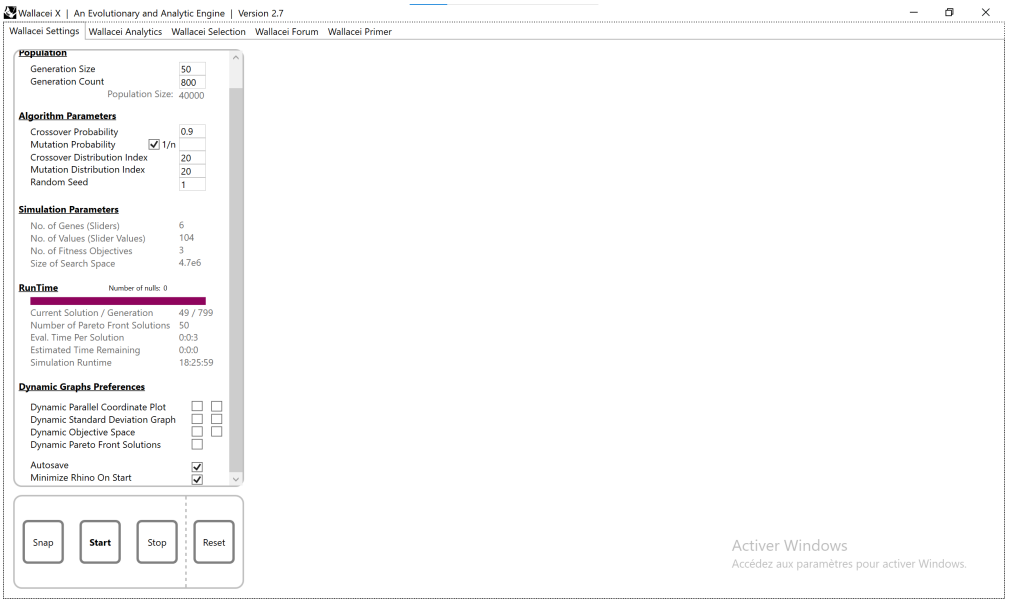


Figure A.28: Wallacei Settings for the shade optimization of a 10x5m canopy with 200 generations and 50 individuals per generations

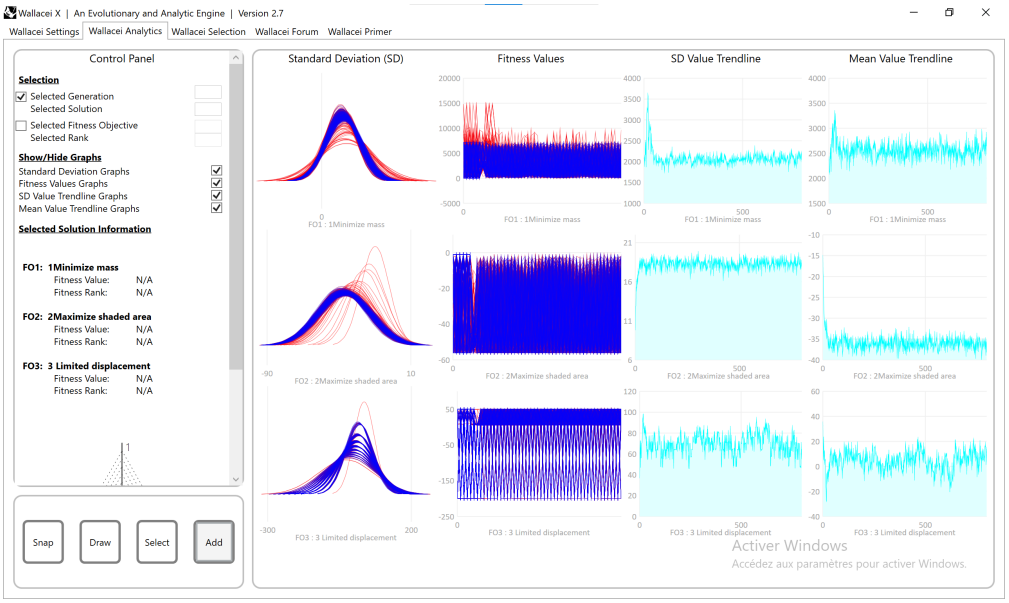


Figure A.29: Wallacei Analytics for the shade optimization of a 10x5m canopy with 200 generations and 50 individuals per generations

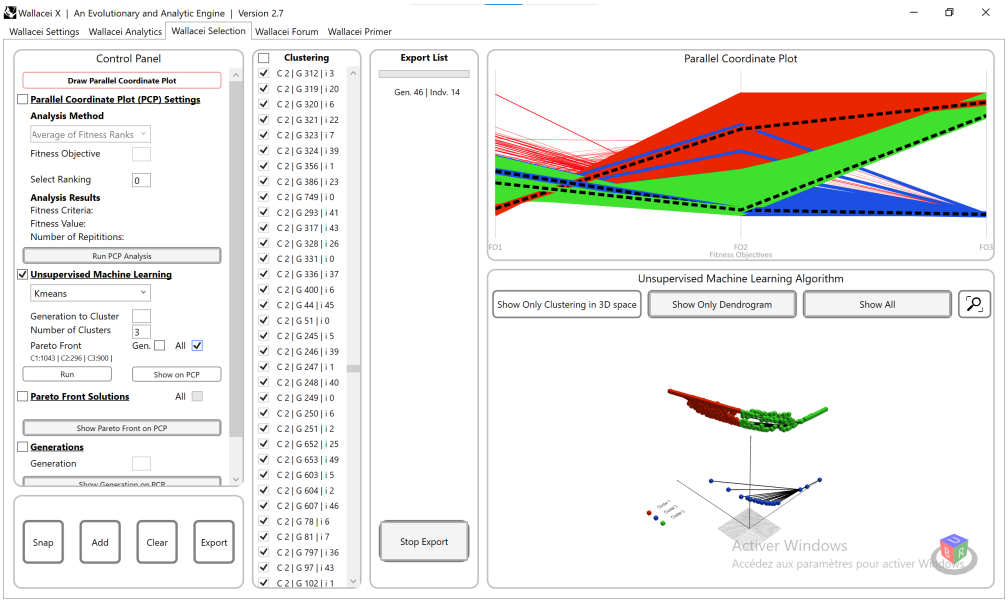


Figure A.30: Wallacei Selection for the shade optimization of a 10x5m canopy with 200 generations and 50 individuals per generations

20x2m

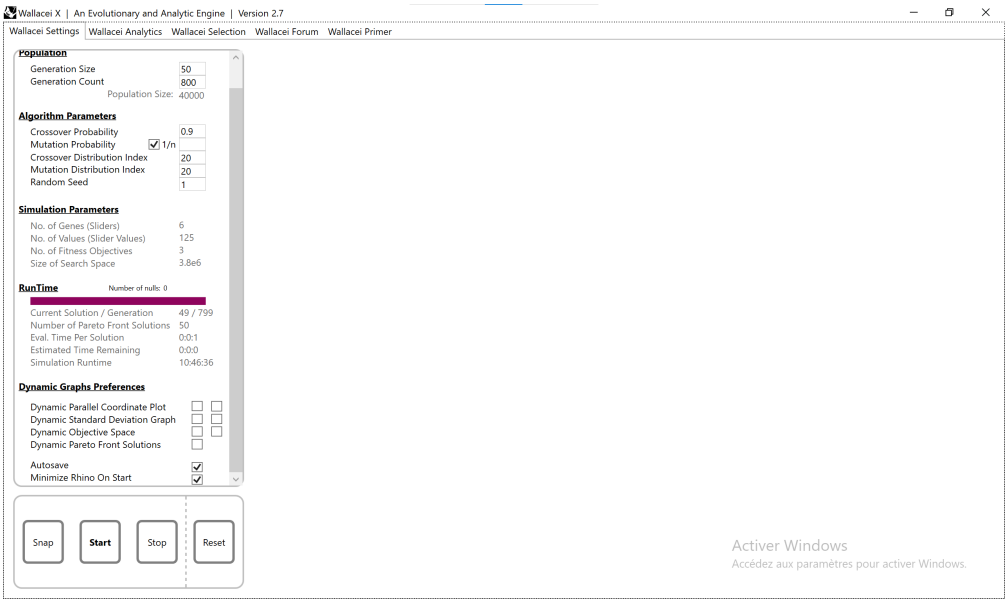


Figure A.31: Wallacei Settings for the shade optimization of a 20x2m canopy with 800 generations and 50 individuals per generations

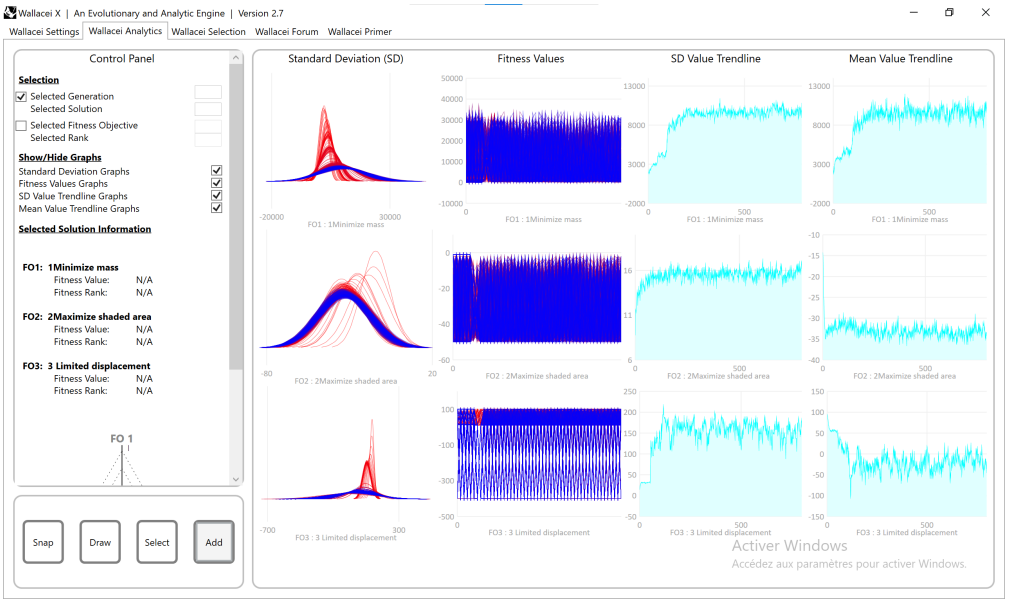


Figure A.32: Wallacei Analytics for the shade optimization of a 20x2m canopy with 800 generations and 50 individuals per generations

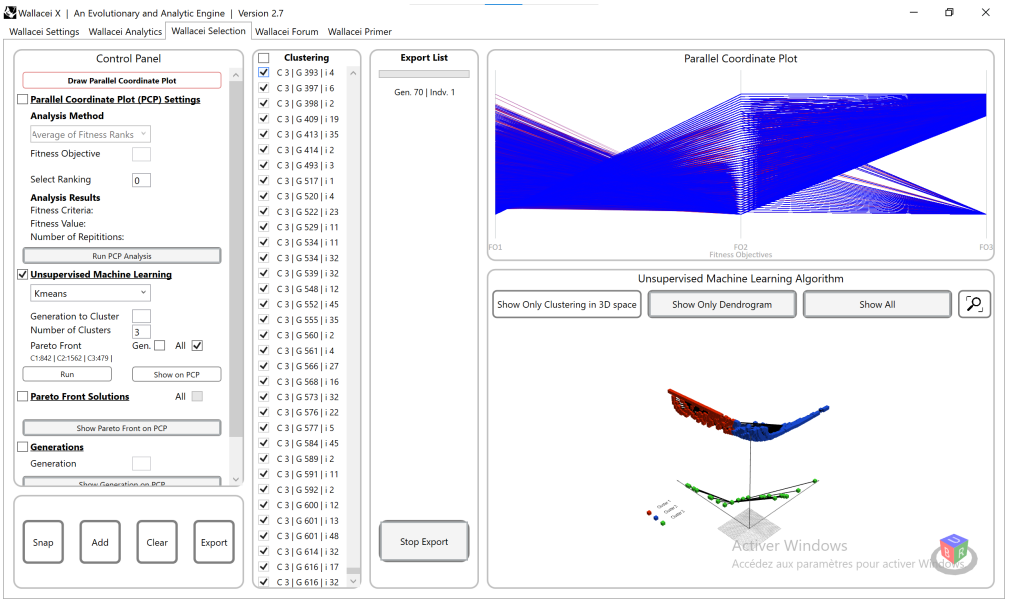


Figure A.33: Wallacei Selection for the shade optimization of a 20x2m canopy with 800 generations and 50 individuals per generations

10x10m

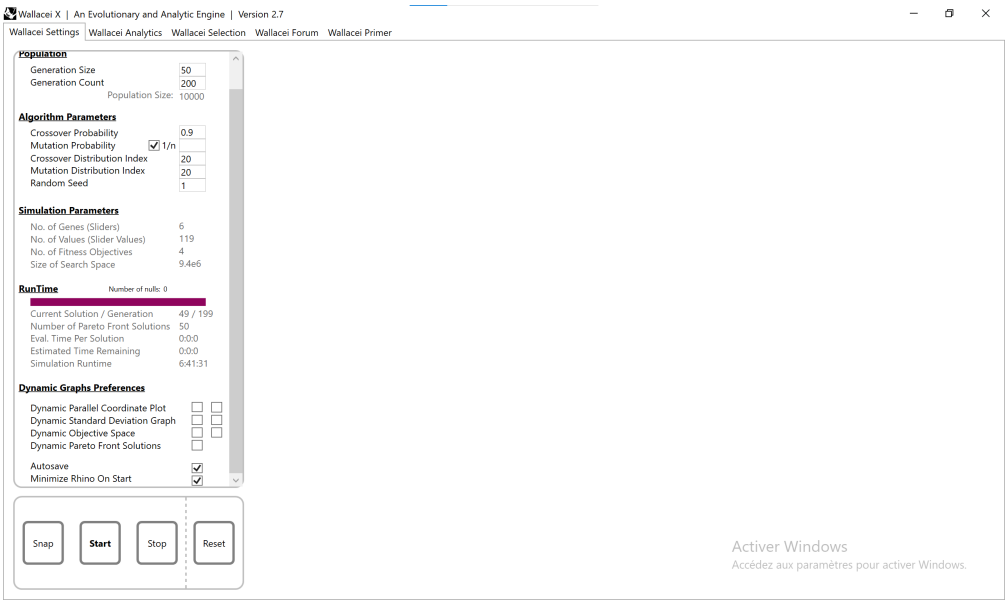


Figure A.34: Wallacei Settings for the shade optimization of a 10x10m canopy with 200 generations and 50 individuals per generations

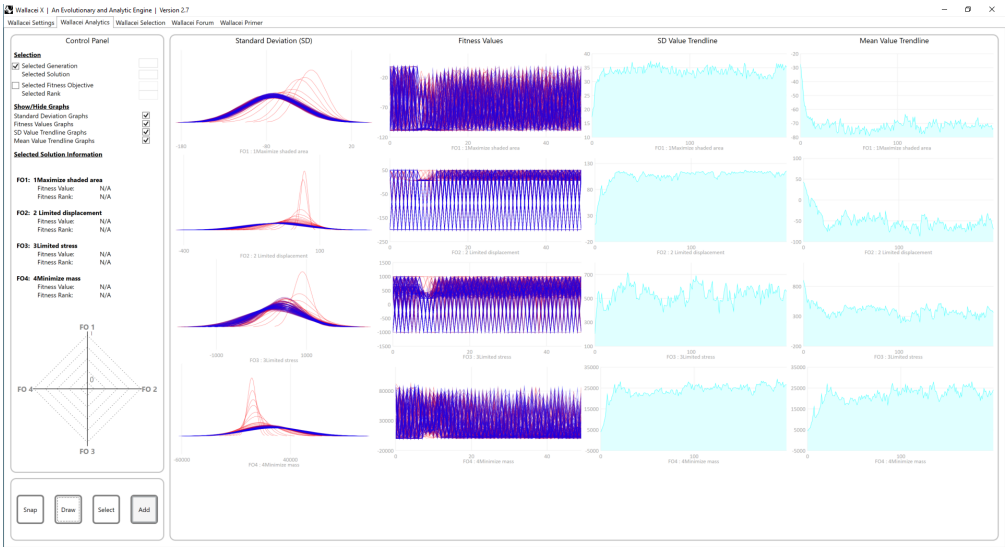


Figure A.35: Wallacei Analytics for the shade optimization of a 10x10m canopy with 200 generations and 50 individuals per generations

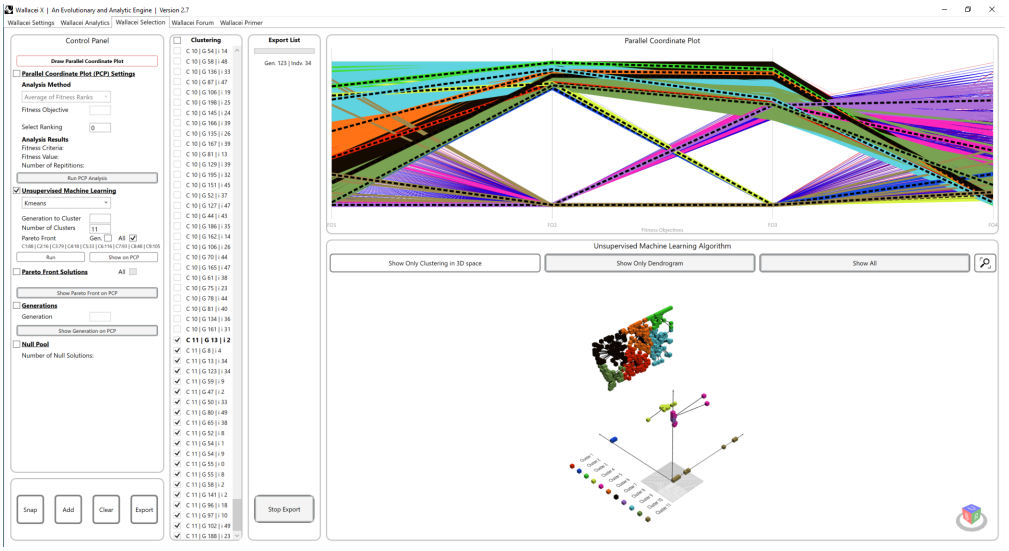


Figure A.36: Wallacei Selection for the shade optimization of a 10x10m canopy with 200 generations and 50 individuals per generations

15x10m

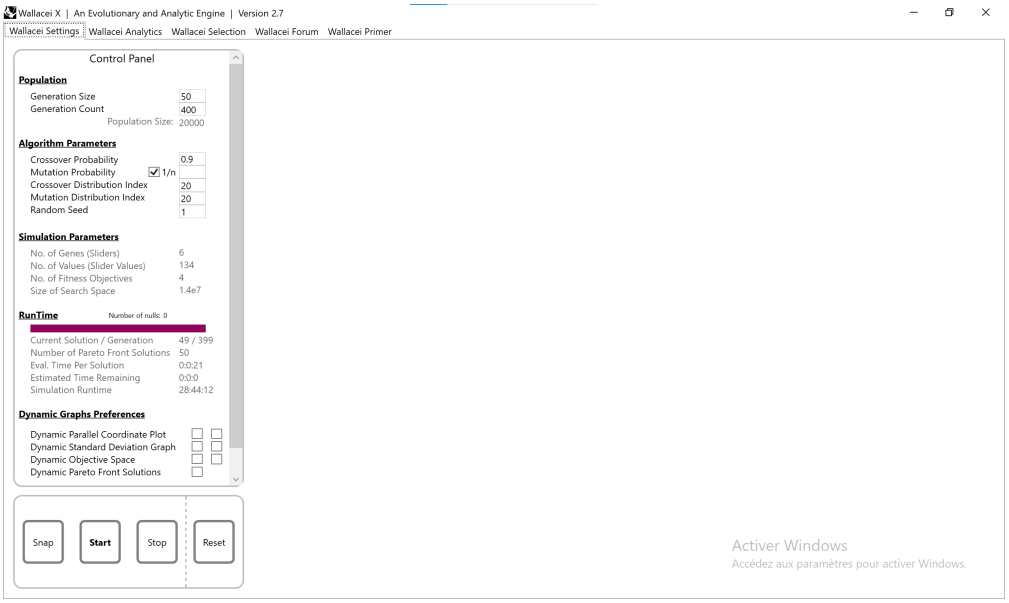


Figure A.37: Wallacei Settings for the shade optimization of a 15x10m canopy with 400 generations and 50 individuals per generations

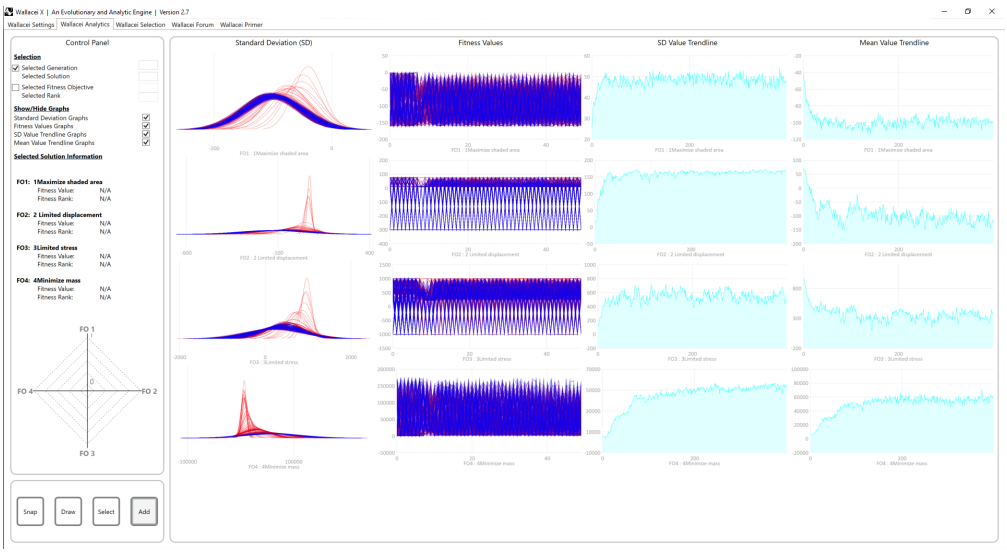


Figure A.38: Wallacei Analytics for the shade optimization of a 15x10m canopy with 400 generations and 50 individuals per generations

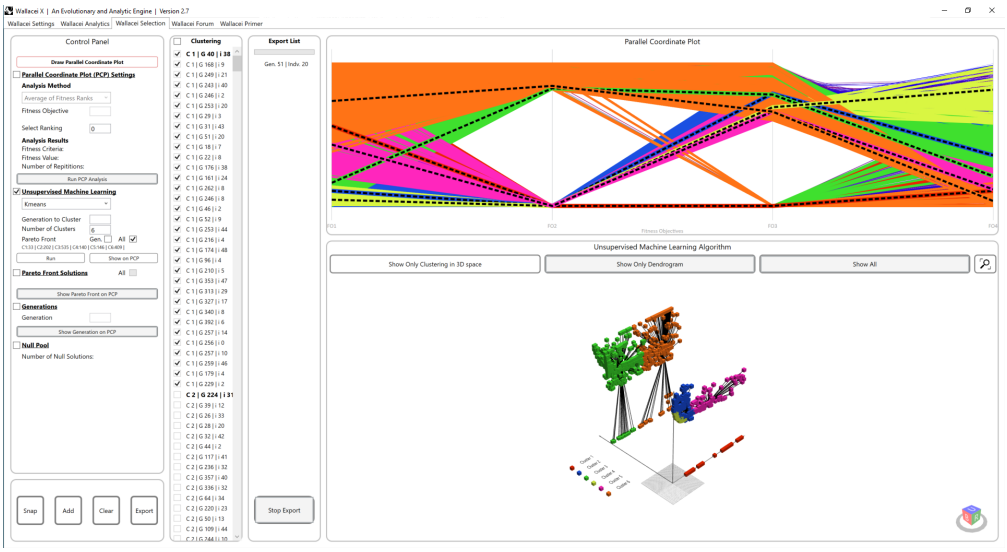


Figure A.39: Wallacei Selection for the shade optimization of a 15x10m canopy with 400 generations and 50 individuals per generations

List of Figures

1.1 Urban canopy model 1
1.2 Perspective view of our canopy model 3

2.2 Canopy of ancient Egypt[7] 5
2.3 The canopy - images by Sergio Grazia[11] 6
2.4 Cityscape[12] 7
2.5 Guillemins station - images by fredlarebiere (a,b,d)[16] and (c)[15] . 8
2.6 Kiel canopy - images by Filip Dujardin (a,b,c)[18] and Nicolas Janberg (d)[19] 9
2.7 Market Hall - images by Dienst Toerisme (a)[20], Tim Van de Velde(b,d)[23], and Hufton + Crow (c)[22] 10
2.8 Metropol Parasol - images by Fernando Alda (a)[26], Léon de Séjournet (b,c), and David Franck (d)[26] 11
2.9 Oostende station - images by David Boureau[28] 12
2.10 Perdana Canopy- images by (a)[29] and Ryan Chin (b,c,d)[31] . . . 13
2.11 Solar Trees Marketplace - images by ZY Photography[32] 14
2.12 Theaterplein - images by Teresa Cos[34] 15
2.13 Tree-Structure Canopy - images by Eibe Sönnecken (a,c)[36] and (b,d)[37] 16
2.14 Wooden Canopy - image by Erik Giudice Architecture[39] 17

3.1 The general evolutionary algorithm[48] 23
3.2 Genetic programming process[49] 24
3.3 Flow chart of NSGA 27
3.4 Schematic procedure for NSGA-II[45] 29
3.5 Crowding distance calculation 29

4.1 Parameter Components 34
4.2 Construct Point Component 35
4.3 Line Component 35
4.4 Assemble Model Component 35
4.5 Line to Beam Component 36

4.6 Support components . . . 36
4.7 Beam Loads components . . . 37
4.8 Loads components . . . 37
4.9 Unit Vectors components . . . 37
4.10 Cross Section components . . . 38
4.11 Analyse component . . . 38
4.12 View components . . . 39
4.13 Internal loads[68] . . . 39
4.14 Load Case 1 . . . 42
4.15 Load Case 2 . . . 42
4.16 Load Case 3 . . . 43
4.17 Load Case 4 . . . 44
4.18 Load Case 5 . . . 44
4.19 LB components . . . 46
4.20 Hoy components . . . 46
4.21 Mesh Shadow . . . 47
4.22 Area . . . 47
4.23 Shadow Case 1 . . . 48
4.24 Shadow Case 2 . . . 48
4.25 Wallacei X Component . . . 49
4.26 Wallacei Settings[72] . . . 52
4.27 Wallacei Analytics[72] . . . 53
4.28 Wallacei Selection[72] . . . 54
4.29 Distribute to Grid . . . 58
4.30 Wallacei Settings for the structural optimization of an IPE beam . . 61
4.31 Wallacei Analytics for the structural optimization of an IPE beam . 62
4.32 Wallacei Selection for the structural optimization of an IPE beam . 62
4.33 Result of the structural optimization of an IPE beam . . . 63
4.34 Perspective view of the selected solutions for the shade optimization of an IPE beam . . . 64
4.35 Wallacei Settings for the shade optimization of an IPE beam . . . 65
4.36 Wallacei Analytics for the shade optimization of an IPE beam . . . 65
4.37 Wallacei Selection for the shade optimization of an IPE beam . . . 66
4.38 Perspective view of the selected solution for the structural optimization of an rectangular beam . . . 68
4.39 Wallacei Settings for the structural optimization of a rectangular beam 68
4.40 Wallacei Analytics for the structural optimization of a rectangular beam . . . 69
4.41 Wallacei Selection for the structural optimization of a rectangular beam . . . 69

4.42 Top view of the result of the shade optimization of a rectangular beam 71
4.43 Perspective view of the selected solutions for the shade optimization of an rectangular beam 72
4.44 Wallacei Settings for the shade optimization of a rectangular beam . 72
4.45 Wallacei Analytics for the shade optimization of a rectangular beam 73
4.46 Wallacei Selection for the shade optimization of a rectangular beam 73

5.1 Perspective view of our canopy model 75
5.2 Top view of our canopy model 76
5.3 Sectional view of our canopy model 76
5.4 Diamond Panels component 77
5.5 Load distribution on a canopy 78
5.6 ArcelorMittal flat bars catalog 79
5.7 Orientate Elem component 80
5.8 Normal stress of a beam subject to bending and compression[68] . . 81
5.9 Normal stress and shear stress when bending is applied to a beam[68] 82
5.10 Top view of the canopy with the maximal shear stress 83
5.11 Perspective view of the structural optimization of a 10x5m urban canopy 85
5.12 Perspective view of the structural optimization of a 5x5m urban canopy 85
5.13 Result of the structural optimization of a 20x2m beam structure with 50 generations and 20 individuals per generations 86
5.14 Perspective view of the structural optimization of a 15x10m urban canopy 87
5.15 Top view of the results of the 10-1000 optimization of a 5x5m canopy 89
5.16 Perspective view of the selected solutions for the 10-1000 optimization of a 5x5m canopy 90
5.17 Graphical comparison of the selected solutions for the 10-1000 optimization of a 5x5m canopy 90
5.18 Top view of the results of the 50-200 optimization of a 5x5m canopy 92
5.19 Perspective view of the selected solutions for the 50-200 optimization of a 5x5m canopy 93
5.20 Graphical comparison of the selected solutions for the 50-200 optimization of a 5x5m canopy 93
5.21 Top view of the results of the 100-100 optimization of a 5x5m canopy 95
5.22 Perspective view of the selected solutions for the 100-100 optimization of a 5x5m canopy 96
5.23 Graphical comparison of the selected solutions for the 100-100 optimization of a 5x5m canopy 96
5.24 Top view of the results of the 200-50 optimization of a 5x5m canopy 98

5.25 Perspective view of the selected solutions for the 200-50 optimization of a 5x5m canopy 99
5.26 Graphical comparison of the selected solutions for the 200-50 optimization of a 5x5m canopy 99
5.27 Top view of the results of the 1000-10 optimization of a 5x5m canopy 101
5.28 Perspective view of the selected solutions for the 1000-10 optimization of a 5x5m canopy 102
5.29 Graphical comparison of the selected solutions for the 1000-10 optimization of a 5x5m canopy 102
5.30 Graphical comparison of the canopy solutions from the different optimizations of a 5x5m canopy 104
5.31 Top view of the results of the optimization of a 10x5m canopy . . . 106
5.32 Perspective view of the selected solutions for the optimization of a 10x5m canopy 107
5.33 Graphical comparison of the selected solutions for the 50-800 optimization of a 10x5m canopy 107
5.34 Top view of the results of the optimization of a 20x2m canopy . . . 109
5.35 Perspective view of the selected solutions for the optimization of a 20x2m canopy 110
5.36 Graphical comparison of the selected solutions for the optimization of a 20x2m canopy 110
5.37 Top view of the results of the optimization of a 10x10m canopy . . 112
5.38 Perspective view of the selected solutions for the optimization of a 10x10m canopy 113
5.39 Graphical comparison of the selected solutions for the optimization of a 10x10m canopy 113
5.40 Top view of the results of the optimization of a 15x10m canopy . . 115
5.41 Perspective view of the selected solutions for the optimization of a 15x10m canopy 116
5.42 Graphical comparison of the selected solutions for the optimization of a 15x10m canopy 116

6.1 Perspective view of our canopy model 121

A.1 Wallacei Settings for the structural optimization of a 10x5m canopy with 50 generations and 20 individuals per generations i
A.2 Wallacei Analytics for the structural optimization of a 10x5m canopy with 50 generations and 20 individuals per generations ii
A.3 Wallacei Selection for the structural optimization of a 10x5m canopy with 50 generations and 20 individuals per generations ii

A.4 Wallacei Settings for the structural optimization of a 5x5m canopy with 50 generations and 0 individuals per generations iii
A.5 Wallacei Analytics for the structural optimization of a 5x5m canopy with 50 generations and 20 individuals per generations iii
A.6 Wallacei Selection for the structural optimization of a 5x5m canopy with 50 generations and 20 individuals per generations iv
A.7 Wallacei Settings for the structural optimization of a 15x10m canopy with 50 generations and 20 individuals per generations iv
A.8 Wallacei Analytics for the structural optimization of a 15x10m canopy with 50 generations and 20 individuals per generations v
A.9 Wallacei Selection for the structural optimization of a 15x10m canopy with 50 generations and 20 individuals per generations v
A.10 Wallacei Settings for the structural optimization of a 20x2m canopy with 50 generations and 20 individuals per generations vi
A.11 Wallacei Analytics for the structural optimization of a 20x2m canopy with 50 generations and 20 individuals per generations vi
A.12 Wallacei Selection for the structural optimization of a 20x2m canopy with 50 generations and 20 individuals per generations vii
A.13 Wallacei Settings for the shade optimization of a 5x5m canopy with 50 generations and 20 individuals per generations viii
A.14 Wallacei Analytics for the shade optimization of a 5x5m canopy with 50 generations and 20 individuals per generations viii
A.15 Wallacei Selection for the shade optimization of a 5x5m canopy with 50 generations and 20 individuals per generations ix
A.16 Wallacei Settings for the shade optimization of a 5x5m canopy with 200 generations and 50 individuals per generations ix
A.17 Wallacei Analytics for the shade optimization of a 5x5m canopy with 200 generations and 50 individuals per generations x
A.18 Wallacei Selection for the shade optimization of a 5x5m canopy with 200 generations and 50 individuals per generations x
A.19 Wallacei Settings for the shade optimization of a 5x5m canopy with 20 generations and 50 individuals per generations xi
A.20 Wallacei Analytics for the shade optimization of a 5x5m canopy with 20 generations and 50 individuals per generations xi
A.21 Wallacei Selection for the shade optimization of a 5x5m canopy with 20 generations and 50 individuals per generations xii
A.22 Wallacei Settings for the shade optimization of a 5x5m canopy with 10 generations and 100 individuals per generations xii
A.23 Wallacei Analytics for the shade optimization of a 5x5m canopy with 10 generations and 100 individuals per generations xiii

A.24 Wallacei Selection for the shade optimization of a 5x5m canopy with 10 generations and 100 individuals per generations xiii
A.25 Wallacei Settings for the shade optimization of a 5x5m canopy with 100 generations and 10 individuals per generations xiv
A.26 Wallacei Analytics for the shade optimization of a 5x5m canopy with 100 generations and 10 individuals per generations xiv
A.27 Wallacei Selection for the shade optimization of a 5x5m canopy with 100 generations and 10 individuals per generations xv
A.28 Wallacei Settings for the shade optimization of a 10x5m canopy with 200 generations and 50 individuals per generations xvi
A.29 Wallacei Analytics for the shade optimization of a 10x5m canopy with 200 generations and 50 individuals per generations xvi
A.30 Wallacei Selection for the shade optimization of a 10x5m canopy with 200 generations and 50 individuals per generations xvii
A.31 Wallacei Settings for the shade optimization of a 20x2m canopy with 800 generations and 50 individuals per generations xvii
A.32 Wallacei Analytics for the shade optimization of a 20x2m canopy with 800 generations and 50 individuals per generations xviii
A.33 Wallacei Selection for the shade optimization of a 20x2m canopy with 800 generations and 50 individuals per generations xviii
A.34 Wallacei Settings for the shade optimization of a 10x10m canopy with 200 generations and 50 individuals per generations xix
A.35 Wallacei Analytics for the shade optimization of a 10x10m canopy with 200 generations and 50 individuals per generations xix
A.36 Wallacei Selection for the shade optimization of a 10x10m canopy with 200 generations and 50 individuals per generations xx
A.37 Wallacei Settings for the shade optimization of a 15x10m canopy with 400 generations and 50 individuals per generations xx
A.38 Wallacei Analytics for the shade optimization of a 15x10m canopy with 400 generations and 50 individuals per generations xxi
A.39 Wallacei Selection for the shade optimization of a 15x10m canopy with 400 generations and 50 individuals per generations xxi

List of Tables

4.1 Load Case 1 . . . 41
4.2 Load Case 2 . . . 42
4.3 Load Case 3 . . . 43
4.4 Load Case 4 . . . 44
4.5 Load Case 5 . . . 45
4.6 Shadow Case 1 . . . 47
4.7 Shadow Case 2 . . . 48
4.8 Verification of beam optimization . . . 61
4.9 Properties of the selected solutions for the shade optimization of an IPE beam . . . 64
4.10 Properties of the selected solutions for the shade optimization of an rectangular beam . . . 71

5.1 Properties of the selected solutions for the 10-1000 optimization of a 5x5m canopy . . . 88
5.2 Properties of the selected solutions for the 50-200 optimization of a 5x5m canopy . . . 91
5.3 Properties of the selected solutions for the 100-100 optimization of a 5x5m canopy . . . 94
5.4 Properties of the selected solutions for the 200-50 optimization of a 5x5m canopy . . . 97
5.5 Properties of the selected solutions for the 1000-10 optimization of a 5x5m canopy . . . 100
5.6 Numerical comparison of the canopy solutions from the different optimizations of a 5x5m canopy . . . 104
5.7 Properties of the selected solutions for the optimization of a 10x5m canopy . . . 105
5.8 Properties of the selected solutions for the optimization of a 20x2m canopy . . . 108
5.9 Properties of the selected solutions for the optimization of a 10x10m canopy . . . 112

5.10 Properties of the selected solutions for the optimization of a 15x10m canopy 114

Bibliography

[1] Lindita Bande et al. "Evaluation of Smart Shading Structures in Mitigating Urban Heat Island in a District of a Hot Arid Climate City (Abu Dhabi)." In: ().

[2] United States Environmental Protection Agency. *Reduce Urban Heat Island Effect*. https://www.epa.gov/green-infrastructure/reduce-urban-heat-island-effect. Overviews and Factsheets. Oct. 2015.

[3] *Canopy Definition and Meaning | Collins English Dictionary*. https://www.collinsdictionary.com

[4] *Urban Definition and Meaning | Collins English Dictionary*. https://www.collinsdictionary.com/

[5] "Keeping Cool in the Sizzling Summer: The Covered Streets of Granada, Spain". In: *Washington Post* (Dec. 2021). ISSN: 0190-8286.

[6] *Umbrella Sky Project | Lighter Quicker Cheaper*. https://www.pps.org/places/umbrella-sky-project.

[7] *Hall of State in the Palace of an Egyptian Nomarch*. https://digitalcollections.nypl.org/items/510 37e0-a3d9-e040-e00a18064a99. (Visited on 06/04/2023).

[8] *Les Halles in Paris: The 'Canopy' Marks the Forum's Renovation*. https://ww.fashionnetwork.co halles-in-paris-the-canopy-marks-the-forum-s-renovation,678131.html.

[9] Oliver Wainwright. "A Custard-Coloured Flop: The €1bn Revamp of Les Halles in Paris". In: *The Guardian* (Apr. 2016). ISSN: 0261-3077.

[10] Angelique Chrisafis. "Paris Hopes €1bn Revamp of Les Halles Can Become City's 'Beating Heart'". In: *The Guardian* (Feb. 2016). ISSN: 0261-3077.

[11] *Les Halles – Arch Journey*. https://archjourney.org/projects/leshalles/.

[12] *https://www.arnequinze.com/art-and-exhibitions/Marie Ingelbeen*. https://www.arnequinze.com and-exhibitions/Marie Ingelbeen.

[13] *Cityscape Wooded Sculpture by Arne Quinze | BrusselsPictures.Com*. https://www.brusselspictur wooded-sculpture-by-arne-quinze/.

[14] *Guillemins TGV Railway Station / Liège (Overview) - Santiago Calatrava – Architects & Engineers*. https://calatrava.com/projects/guillemins-tgv-railway-station-liege.html.

[15] *Liège - Gare des Guillemins*. https://www.wust.be/fr/projects/liege-gare-des-guillemins.

[16] fredlarebiere. *La gare de Liège par Santiago Calatrava*. July 2017.

[17] *Kiel Canopy by Ney & Partners*. https://architizer.com/projects/kiel-canopy/.

[18] *Canopy - Kiel*. https://b-architecten.be/projects/canopy-kiel?cat=offices.

[19] *Kiel Canopy (Antwerp, 2005)*. https://structurae.net/en/structures/kiel-canopy.

[20] *City Pavilion*. https://visit.gent.be/en/see-do/city-pavilion.

[21] Tom Holbrook. *Ghent Market Hall by Robbrecht En Daem and Marie-José van Hee*. Jan. 2013.

[22] *Market Hall by Robbrecht En Daem and Marie-José Van Hee*. https://www.dezeen.com/2013/04/ hall-by-robbrecht-en-daem-architecten-and-marie-jose-van-hee-architecten/. Apr. 2013.

[23] *Market Hall in Ghent / Marie-José Van Hee + Robbrecht & Daem*. https://www.archdaily.com/3 hall-in-ghent-marie-jose-van-hee-robbrecht-and-daem. Apr. 2013.

[24] Rowan Moore. "Metropol Parasol, Seville by Jürgen Mayer H – Review". In: *The Observer* (Mar. 2011). ISSN: 0029-7712.

[25] Karen Cilento. *Metropol Parasol / J. Mayer H + Arup*. https://www.archdaily.com/201961/metr parasol-j-mayer-h-arup. Jan. 2012.

[26] Marcia Argyriades. *Metropol Parasol // The World's Largest Wooden Structure*. http://www.yatzer.com/Metropol-Parasol-The-World-s-Largest-Wooden-Structure-J-MAYER-H-Architects. Apr. 2011.

[27] Philip Stevens. *Dietmar Feichtinger Unites Ostend Railway Station with Giant Roof Canopy*. https://www.designboom.com/architecture/dietmar-feichtinger-ostend-railway-station-giant-roof-canopy-belgium-12-15-2019/. Dec. 2019.

[28] Paula Pintos. *Oostende Station / Dietmar Feichtinger Architectes*. https://www.archdaily.com/9 station-dietmar-feichtinger-architectes. Dec. 2019.

[29] *Perdana Canopy - GDP*. July 2020.

[30] Ryan Chin. *Perdana Canopy @ Perdana Botanic Garden | LinkedIn*. https://www.linkedin.com/p canopy-botanic-garden-ryan-chin/. May 2022.

[31] *Perdana Canopy*. https://www.klinteriorphotography.com/new-page/.

[32] *Solar Trees Marketplace - Koichi Takada Architects*.

[33] *Theatreplein, Antwerp - International Competition*. http://secchi-vigano.eu/atS04/at%20S04_th

[34] *Theaterplein by Studio Bernardo Secchi & Paola Viganò | The Strength of Architecture | From 1998*. https://www.metalocus.es/en/news/theaterplein-studio-bernardo-secchi-paola-vigano.

[35] Asterios Agkathidis and André Brown. "Tree-Structure Canopy: A Case Study in Design and Fabrication of Complex Steel Structures Using Digital Tools". In: *International Journal of Architectural Computing* 11.1 (Mar. 2013), pp. 87–104. ISSN: 1478-0771, 2048-3988. DOI: 10.1260/1478-0771.11.1.87.

[36] a3lab. *Tree-Structure Canopy*. Apr. 2011.

[37] *WestendGate / Just Burgeff Architekten + A3lab*. https://www.archdaily.com/175519/westendga just-burgeff-architekten-a3lab. Oct. 2011.

[38] Juliana Neira. *Erik Giudice Architects Proposes Wooden Canopy for Jonkoping Station in Sweden*. https://www.designboom.com/architecture/erik-giudice-architects-wooden-canopy-jonkoping-station-sweden-09-21-2016/. Sept. 2016.

[39] Marco Rinaldi. *Wooden Canopy for Jönköping Station by Erik Giudice Architecture – Aasarchitecture*. Sept. 2016.

[40] Vineet Kumar et al. "State-of-the-Art Optimization and Metaheuristic Algorithms". In: *Handbook of Intelligent Computing and Optimization for Sustainable Development*. Ed. by Mukhdeep Singh Manshahia et al. First. Wiley, Feb. 2022, pp. 509–536. ISBN: 978-1-119-79182-9 978-1-119-79264-2. DOI: 10.1002/9781119792642.ch25.

[41] Kalyanmoy Deb. *Multi-Objective Optimization Using Evolutionary Algorithms*. 1st ed. Wiley-Interscience Series in Systems and Optimization. Chichester ; New York: John Wiley & Sons, 2001. ISBN: 978-0-471-87339-6.

[42] Abdullah Konak, David W. Coit, and Alice E. Smith. "Multi-Objective Optimization Using Genetic Algorithms: A Tutorial". In: *Reliability Engineering & System Safety* 91.9 (Sept. 2006), pp. 992–1007. ISSN: 09518320. DOI: 10.1016/j.ress.2005.11.018.

[43] Laurent Magnier and Fariborz Haghighat. "Multiobjective Optimization of Building Design Using TRNSYS Simulations, Genetic Algorithm, and Artificial Neural Network". In: *Building and Environment* 45.3 (Mar. 2010), pp. 739–746. ISSN: 03601323. DOI: 10.1016/j.buildenv.2009.08.016.

[44] K. Deb et al. "A Fast and Elitist Multiobjective Genetic Algorithm: NSGA-II". In: *IEEE Transactions on Evolutionary Computation* 6.2 (Apr. 2002), pp. 182–197. ISSN: 1089778X. DOI: 10.1109/4235.996017.

[45] Kalyanmoy Deb. "Multi-Objective Optimization Using Evolutionary Algorithms: An Introduction". In: *Multi-objective Evolutionary Optimisation for Product Design and Manufacturing* (Feb. 2011), pp. 3–34. DOI: 10.1007/978-0-85729-652-8_1.

[46] Aimin Zhou et al. "Multiobjective Evolutionary Algorithms: A Survey of the State of the Art". In: *Swarm and Evolutionary Computation* 1.1 (Mar. 2011), pp. 32–49. ISSN: 22106502. DOI: 10.1016/j.swevo.2011.03.001.

[47] Adam Slowik and Halina Kwasnicka. "Evolutionary Algorithms and Their Applications to Engineering Problems". In: *Neural Computing and Applications* 32.16 (Aug. 2020), pp. 12363–12379. ISSN: 0941-0643, 1433-3058. DOI: 10.1007/s00521-020-04832-8.

[48] Hans-Georg Beyer. *The Theory of Evolution Strategies*. Berlin, Heidelberg: Springer Berlin Heidelberg, 2001. ISBN: 978-3-662-04378-3.

[49] John R. Koza and Riccardo Poli. "Genetic Programming". In: *Search Methodologies*. Ed. by Edmund K. Burke and Graham Kendall. Boston, MA: Springer US, 2005, pp. 127–164. ISBN: 978-0-387-23460-1. DOI: 10.1007/0-387-28356-0_5. (Visited on 04/04/2023).

[50] Rainer Storn and Kenneth Price. "Differential Evolution – A Simple and Efficient Heuristic for Global Optimization over Continuous Spaces." In: *Journal of Global Optimization* 11.4 (1997), pp. 341–359. ISSN: 09255001. DOI: 10.1023/A:1008202821328. (Visited on 04/04/2023).

[51] Swagatam Das and Ponnuthurai Nagaratnam Suganthan. "Differential Evolution: A Survey of the State-of-the-Art". In: *IEEE Transactions on Evolutionary Computation* 15.1 (Feb. 2011), pp. 4–31. ISSN: 1089-778X, 1941-0026. DOI: 10.1109/TEVC.2010.2059031. (Visited on 04/05/2023).

[52] Wei Yu et al. "Application of Multi-Objective Genetic Algorithm to Optimize Energy Efficiency and Thermal Comfort in Building Design". In: *Energy and Buildings* 88 (Feb. 2015), pp. 135–143. ISSN: 03787788. DOI: 10.1016/j.enbuild.2014.11.063.

[53] *Food4Rhino*. https://www.food4rhino.com/en. Text. (Visited on 04/11/2023).

[54] N. Srinivas and Kalyanmoy Deb. "Muiltiobjective Optimization Using Nondominated Sorting in Genetic Algorithms". In: *Evolutionary Computation* 2.3 (Sept. 1994), pp. 221–248. ISSN: 1063-6560, 1530-9304. DOI: 10.1162/evco.1994.2.3.221.

[55] Eckart Zitzler, Marco Laumanns, and Lothar Thiele. "SPEA2: Improving the Strength Pareto Evolutionary Algorithm". In: *TIK Report* 103 (July 2001). DOI: 10.3929/ethz-a-004284029.

[56] Shifali Bhargava. “A Note on Evolutionary Algorithms and Its Applications”. In: 8 (2013).

[57] Yun Kyu Yi et al. “Multi-Objective Optimization (MOO) of a Skylight Roof System for Structure Integrity, Daylight, and Material Cost”. In: *Journal of Building Engineering* 34 (Feb. 2021), p. 102056. ISSN: 23527102. DOI: 10.1016/j.jobe.2020.102056. (Visited on 03/08/2023).

[58] C.P. Quaglia et al. “Balancing Energy Efficiency and Structural Performance through Multi-Objective Shape Optimization: Case Study of a Rapidly Deployable Origami-Inspired Shelter”. In: *Energy and Buildings* 82 (Oct. 2014), pp. 733–745. ISSN: 03787788. DOI: 10.1016/j.enbuild.2014.07.063.

[59] Jeroen van Ameijde et al. “Data-Driven Placemaking: Public Space Canopy Design through Multi-Objective Optimisation Considering Shading, Structural and Social Performance”. In: *Frontiers of Architectural Research* 11.2 (Apr. 2022), pp. 308–323. ISSN: 20952635. DOI: 10.1016/j.foar.2021.10.007.

[60] Luca Sgambi, Konstantinos Gkoumas, and Franco Bontempi. “Genetic Algorithms for the Dependability Assurance in the Design of a Long Span Suspension Bridge”. In: *Computer-Aided Civil and Infrastructure Engineering* 27.9 (Oct. 2012), pp. 655–675. ISSN: 10939687. DOI: 10.1111/j.1467-8667.2012.00780.x. (Visited on 05/03/2023).

[61] Luca Sgambi. “Artificial Intelligence for the Analysis and Design of Complex Bridge Structures”. In: *Proceedings of the 9th International Conference on Structural Safety and Reliability*. Rome, Italy, June 2005. ISBN: 90-5966-040-4.

[62] Luca Sgambi. “Genetic Algorithm Approach for Performances Evaluation of Long Span Suspension Bridge”. In: *The Tenth International Conference on Civil, Structural and Environmental Engineering Computing*. Rome, Italy, Sept. 2005. ISBN: 1-905088-02-7.

[63] Luca Sgambi, Konstantinos Gkoumas, and Franco Bontempi. “Genetic Algorithm Optimization of Precast Hollow Core Slabs”. In: *Computers and Concrete* 13.3 (Mar. 2014), pp. 389–409. DOI: 10.12989/CAC.2014.13.3.389.

[64] *Rhinoceros 3D*. https://www.rhino3d.com/.

[65] *Grasshopper*. https://www.grasshopper3d.com/.

[66] *Karamba3D*. https://karamba3d.com/.

[67] Clemens Preisinger. “Linking Structure and Parametric Geometry”. In: *Architectural Design* 83 (2013), pp. 110–113. DOI: 10.1002/ad.1564..

[68] Pierre Latteur. *Mecanique Des Structures*. Sept. 2017.

[69] *Ladybug Tools*. https://www.ladybug.tools/index.html#header-slide-show.

[70] *EnergyPlus Weather File (EPW) Format*. https://designbuilder.co.uk/cahelp/Content/EnergyP

[71] *Wallacei*. https://www.wallacei.com/.

[72] M. Makki, M. Showkatbakhsh, and Y. Song. "Wallacei Primer 2.0". In: (2019).

[73] *Catalogue Des Profilés et Aciers Marchands Arcelor Mittal*.

UNIVERSITÉ CATHOLIQUE DE LOUVAIN
École polytechnique de Louvain
Rue Archimède, 1 bte L6.11.01, 1348 Louvain-la-Neuve, Belgique | **www.uclouvain.be/epl**